# DEVELOPMENT OF A SHOCK-CAPTURING METHOD USING AN ENTROPY-CONSISTENT FIRST ORDER SYSTEMS APPROACH FOR THE NAVIER-STOKES EQUATIONS

by

# AKMAL NIZAM MOHAMMED

Thesis submitted in fulfillment of the requirements for the degree of Doctor of Philosophy

July 2014

#### ACKNOWLEDGMENTS

First of all, I want to give my humble gratitude to Dr. Farzad Ismail for his guidance and advice throughout this study.

I am profoundly grateful to my wife, my son, my parents and my family for all the support they have given.

I would also like to thank University Sains Malaysia (USM) and its staff, my friends and all of my colleagues at the School of Mechanical Engineering, the School of Aerospace Engineering, and the Institute of Postgraduate Studies. Special thanks to my research group members Tarmizi, Nisa, Nadihah, and Hossein, my lab mates Fauzy, Ikhsan, Kok Hwa, Najmi, Vizy, and Zubair, and to lab administrator Mr. Najib, all of whom are also my dear friends.

I am deeply indebted to Universiti Tun Hussein Onn Malaysia, especially the Faculty of Mechanical and Manufacturing Engineering and its Dean for the opportunity to pursue this endeavor. I am thankful as well to all my colleagues at the faculty for all their advice and encouragement.

To Dr. Nishikawa, thank you for the assistance and comments that immensely helped with my understanding of this subject.

Lastly, thanks to Dr. Rand Alfaris and Dr. Hailiza Kamarulhaili at the School of Mathematical Researches, USM, for providing the PhD thesis latex template.

# TABLE OF CONTENTS

			Page	
ACK	NOV	LEDGMENTS	ii	
LIST	OF	TABLES	v	
LIST	OF	FIGURES	vi	
LIST	OF.	ABBREVIATIONS	viii	
NON	<b>MENC</b>	CLATURE	ix	
	TRA		xii	
	TRA		xiv	
ADS	LICA		XIV	
CHA	PTE	${f R}$		
1 II	INTRODUCTION			
1.	1 Sir	nulating the Shockwave	1	
1.	2 Ad	vancements in Numerical Analysis	3	
1.	3 Mc	·		
1.	.4 Research Objective, Methodology and Scope			
1.	5 Th	5 Thesis Organization		
2 L	LITERATURE REVIEW		10	
2.	1 En	Entropy Consistency		
2.	2 Fir	First Order Systems		
2.	3 Cu	•		
3 S	CALA	R EQUATIONS	22	
		•		
0.		.1 Burgers' Equation	$\begin{array}{c} 22 \\ 25 \end{array}$	
		.2 Roe's Entropy Conserving Flux	26	
		.3 Stability, Production, and Consistency	30	
3.		perbolic First Order Systems	33	
	•	.1 Burgers' First Order System	34	
	3.2	•	38	
	3.2	_	39	
	3.2		41	
	3.2	_	43	
	3.2		45	
		.7 Flux Update	45	

4	$\mathbf{F}\mathbf{R}$	OM E	ULER TO NAVIER-STOKES	46
	4.1	Entro	py Consistency for the Euler Equations	47
		4.1.1	Discrete Entropy Conservative Fluxes	49
		4.1.2	Entropy Production and the Dissipative Flux	51
	4.2	Conse	ervation Laws for the Navier-Stokes Equations	54
	4.3	Entro	py Consistent Fluxes for the First-Order System of Navier-	
		Stokes	s Equations	59
	4.4	Secon	d Order Accuracy	68
	4.5	Exten	sion to Two Dimensions	70
		4.5.1	Upwind flux via entropy conservation approach	76
		4.5.2	Upwind flux via abbreviated system approach	85
5	RESULTS AND DISCUSSION			
	5.1	Introd	luction	87
	5.2	Burge	ers' Equation	87
		5.2.1	Stationary shock	88
		5.2.2	The square wave initial condition	91
	5.3	Navie	r-Stokes Equations	94
		5.3.1	Stationary shock	96
		5.3.2	Sod's shock tube problem	104
	5.4	The T	Two Dimensional Case	111
		5.4.1	Flow over a flat plate	111
		5.4.2	Flow over a forward facing step	114
		5.4.3	Flow over a cylinder	117
		5.4.4	Flow over an airfoil	127
	5.5	Summ	nary	130
6	CONCLUSIONS AND FUTURE WORK			
	6.1	Concl	usion	141
	6.2	2 Future Work		
$\mathbf{R}$	e <b>fe</b> j	RENC	EES/BIBLIOGRAPHY	144
		NDIC	•	150
	J.		<del></del>	100
			OF STUDENT	154
LI	ST	OF PU	JBLICATIONS	155

## LIST OF TABLES

Table		Page
5.1	Tests matrix for the steady shock problem	96
5.2	Initial conditions for Sod's problem	109
5.3	Initial conditions for flow over a cylinder	117
5.4	Comparison of L1, L2 and infinity norms between different grid	
	sizes for the ECS flux <sup>a</sup>	120

## LIST OF FIGURES

Figure Pa		
1.1	The amount of iteration required to reduce the variable residuals by five orders of magnitude according to node count for the first order system flux (FOS), the discontinuous galerkin method at $Re = 1000$ (Galerkin1), and the discontinuous galerkin method at $Re = 100$ (Galerkin2).	6
3.1	Grid representation of the finite volume method from (a) LeVeque (2002) and (b) Ismail and Roe (2009).	24
4.1	Grid representation of the finite volume method from Ismail (2006).	75
5.1 5.2	Steady state shock solution with low viscosity terms for the tested fluxes in terms of (a) velocity, and (b) velocity difference.  Steady state shock solution with medium viscosity terms for the	90
J.Z	tested fluxes in terms of (a) velocity, and (b) velocity difference.	92
5.3	Steady state shock solution with high viscosity terms for the tested fluxes in terms of (a) velocity, and (b) velocity difference.	93
5.4	ECS2 flux compared to EC flux and exact solution, with (a) low viscosity, and (b) viscosity coefficient set at 0.1.	95
<ul><li>5.5</li><li>5.6</li></ul>	Steady state shock solution of density at Mach number 1.5 with viscosity coefficient of (a) $1.0 \times 10^{-7}$ , (b) $10^{-4}$ , (c) $10^{-3}$ , and (d) $10^{-2}$ . Steady state shock solution of density at Mach number 7.0 with	98
	viscosity coefficient of (a) $1.0 \times 10^{-7}$ , (b) $10^{-4}$ , (c) $10^{-3}$ , and (d) $10^{-2}$ .	101
5.7	Steady state shock solution of density at Mach number 20.0 with viscosity coefficient of (a) $1.0 \times 10^{-7}$ , (b) $10^{-4}$ , (c) $10^{-3}$ , and (d)	
5.8	$10^{-2}$ . Second order density plot of steady shock for the EC fluxes in the case of (a) $Ma = 1.5, \nu = 1e - 7$ , (b) $Ma = 1.5, \nu = 1e - 2$ , (c)	103
5.9	$Ma = 20.0$ , $\nu = 1e - 7$ , and (d) $Ma = 20.0$ , $\nu = 1e - 2$ . Second order viscous stress plot of steady shock for the EC fluxes	106
5.10	in the case of (a) $Ma = 1.5$ , $\nu = 1e - 7$ , (b) $Ma = 1.5$ , $\nu = 1e - 2$ , (c) $Ma = 20.0$ , $\nu = 1e - 7$ , and (d) $Ma = 20.0$ , $\nu = 1e - 2$ . Results of Sod's problem with viscosity coefficient of 0.01 for different system cases showing data of (a) density, (b) velocity, and	108
P 11	(c) pressure.	110
5.11	Sample grid of the flat plate.	112

5.12	Simulation result for flow over a flat plate showing (a) Mach number contour, and (b) comparison of velocity magnitude with Blasius	
	solution.	113
5.13	Sample grid of the forward facing step.	114
5.14	Results for flow over forward facing step using (a) EC1, (b) EC2, and (c) Roe, (d) ECS.	116
5.15	Grid used for flow over cylinder with node counts of (a) $80 \times 160$ , (b) $161 \times 160$ with growth factor 3.2, and (c) $161 \times 160$ with growth	
	factor 5.0.	119
5.16	Flow over cylinder at Mach numbers 0.3 for fluxes of (a) EC1, (b) ECS, (c) EC1 zoomed in, and (d) ECS zoomed in.	122
5.17	X-Velocity contour at low Reynolds number for (a) ECS flux at Re = 40, (b) ECS flux at Re = 2000, (c) Fluent result at Re = 40, (d)	
	Fluent result at $Re = 2000$ .	124
5.18	Pressure data for the ECS flux showing pressure coefficient $(C_p)$	
	distribution at (a) $Re = 40$ , and (b) $Re = 2000$ , compared to	
	available experimental data.	126
	Contour plot at Mach 3.0 for (a) EC1 flux, (b) ECS flux.	128
5.20	Mesh of NACA0012 airfoil using quadrilateral cells.	129
5.21	Flow over airfoil at Mach numbers 0.2 for fluxes of (a) Roe, (b)	
	EC1, and (c) ECS.	132
5.22	Zoomed in view of flow over airfoil at Mach numbers 0.2 for fluxes	
	of (a) Roe, (b) EC1, and (c) ECS.	134
5.23	Flow over airfoil at Mach numbers 0.63 for fluxes of (a) Roe, (b)	
	EC1, and (c) ECS.	136
5.24	Flow over airfoil at Mach numbers 0.9 for fluxes of (a) Roe, (b)	100
- 0-	EC1, and (c) ECS.	138
5.25	Flow over airfoil at Mach numbers 1.5 for fluxes of (a) Roe, (b) EC1, (c) ECS, and coefficients of pressure for $Re = 9.7 \times 10^4$ .	140
B.1	Flow chart of the solver algorithm.	153

#### LIST OF ABBREVIATIONS

CFL Courant-Friedrichs-Lewy number

CIR Courant, Isaacson and Rees scheme

ECS Entropy Conservative System

ES Entropy Stable Scheme

EC1 Entropy Consistent Scheme 1

EC2 Entropy Consistent Scheme 2

NS The Navier-Stokes Equations

ODEs Ordinary Differential Equations

PDEs Partial Differential Equations

RK2 Second-order Runge-Kutta Method

RK4 Fourth-order Runge-Kutta Method

#### NOMENCLATURE

Symbol Description

a Speed of sound

A Cell area

A Jacobian matrix

 $C_p$  Pressure coefficient

D Dissipation matrix

e Fluids internal energy

E Total energy

 $E_{exact}$  L1-Norm between numerical and analytical solution

 $E_{exp}$  L1-Norm between numerical and experimental solution

 $f = (f_x, f_y)$  Conservative flux vectors

F Net flux at cell interface

H Total enthalpy

L Left eigenvector matrix

Mach number

 $\mathbf{n} = (n_x, n_y)$  Normal vector

q Normal velocity

r Tangential velocity

R Right eigenvector matrix

S Physical entropy

ix

S Diagonal scaling matrix

 $\mathbf{t} = (t_x, t_y)$  Tangent vector

u Conservative variables-vector

U Entropy function

v Entropy variable-vector

w Primitive variables-vector

 $\nabla \mathbf{W}$  Slope gradient

#### Greek

 $\gamma$  Fluids specific heat ratios

 $\delta$  Percentage difference of L1-Norm at ( $\Delta x = \text{zero}$ ) w.r.t. the

reference value (origin)

 $\phi$  Slope Limiter

 $\lambda$  Fluids wave speeds

 $\Delta s$  Cell face length

 $\Delta t$  Time step

 $\Delta x$ ,  $\Delta y$  Mesh increment in (x, y)-axis

Λ Diagonal eigenvalue matrix

### Subscripts

c (x, y) coordinates of cell centroid

f (x, y) coordinates of cell interface

i Index of computed cell

j Index of neighouring cells

L Left cell interface

R Right cell interface

# Superscripts

n Discrete time level

- Arithmetic mean

ln Logarithmic mean

# PEMBANGUNAN KAEDAH 'SHOCK-CAPTURING' MENGGUNAKAN PENDEKATAN SISTEM TERTIB PERTAMA BERENTROPI TEKAL UNTUK PERSAMAAN NAVIER-STOKES

#### **ABSTRAK**

Disebabkan faktor praktikal, gelombang kejutan biasanya dikaji secara berangka melalui Simulasi Bendalir Dinamik (CFD). Simulasi ini menggunakan teknik berangka seperti skim menangkap kejutan, yang mana dengannya ketidakselanjaran boleh diramalkan dengan baik. Walau bagaimanapun, masih terdapat beberapa masalah di mana kaedah sedia ada tidak mampu untuk menghasilkan keputusan yang diingini, sebagai contoh fenomena 'carbuncle'. Skini berkejituan tinggi dengan kos pengkomputeran yang mahal tidak menjamin keputusan yang boleh dipercayai sepenuhnya, manakala skim kos rendah memberi tumpuan kepada kecekapan pengiraan dengan mengorbankan ketepatan. Walau bagaimanapun, keseimbangan yang baik antara kedua-duanya boleh didapati dengan fluks berentropi konsisten. Sungguhpun fluks ini agak tepat dan agak cekap, tetapi ia masih boleh diperbaiki, terutamanya dalam mengendalikan aspek kelikatan dan pemindahan haba yang secara semulajadi bersifat parabola. Untuk memenuhi keperluan tersebut, satu penyelesaian telah dibangunkan dengan pendekatan sistem hiperbola peringkat pertama. Dalam tesis ini, idea-idea ketepatan entropi dan sistem tertib pertama telah disintesis untuk mewujudkan satu skim baru yang mendapat faedah daripada kedua-dua falsafah. Kaedah ini diuji dengan persamaan Burgers, dan kemudian diperluaskan kepada sistem persamaan Navier-Stokes, dengan menggunakan kes-kes ujian standard seperti kejutan malar, kejutan berkembang, dan masalah Sod. Keputusan yang didapati menunjukkan bahawa skim ini dapat memberikan hasil yang setanding dengan skim entropi konsisten sedia ada; ini memberikan peluang untuk penambah-baikan jika ianya diperhalusi. Konsep ini berpotensi untuk dilanjutkan kepada tiga dimensi supaya faedah sebenar skim ini boleh diterokai sepenuhnya.

# APPROACH FOR THE NAVIER-STOKES EQUATIONS

#### ABSTRACT

For practical reasons, shock waves are usually studied numerically through Computational Fluid Dynamics (CFD) simulations. These simulations employ numerical techniques such as the shock capturing scheme, with which discontinuities can be reasonably predicted. However, there remain a number of problems where existing methods fall short of delivering the desired results, for example the carbuncle phenomenon. High-order accurate schemes with high computational costs do not guarantee reliable results, whilst low-cost schemes focus on efficiency of calculation at the expense of accuracy. Incidentally, a good balance between the two can be found in the entropy consistent flux approach. This method is fairly accurate and relatively efficient, but it can still be improved upon, particularly in handling terms of viscosity and heat transfer that are parabolic in nature. To resolve these terms, a possible solution comes in the form of the first order hyperbolic system approach. In this thesis, the ideas of entropy-consistency and the first-order system are synthesized to create a new scheme that enjoys the benefits of both philosophies. The method is firstly tested with Burgers' equation as the governing equation, and then extended to the Navier-Stokes system of equations using standard test cases. Results herein show that the scheme is able to provide comparable results to existing entropy-consistent schemes which present an avenue for its further refinement. A distinct possibility is to extend this concept to three dimensions so that the true benefit of the scheme can be fully explored.

# CHAPTER 1

#### INTRODUCTION

#### 1.1 Simulating the Shockwave

In the natural world, movement of any kind is usually thought of being smooth and continuous, such as the trickling of water in a stream or the fluttering of leaves blowing in the wind. However, at the high end of speed, there exist phenomena in which sudden changes and discontinuities can occur. Amongst them is the shockwave, a propagating wave of disturbance across which flow parameters such as density, pressure, and temperature vary abruptly. With the advent of modern supersonic transportation and projectiles, studying flow discontinuities has turned from purely an academic interest to a more practical perspective (Anderson, 2004). A complete understanding of shockwave is required in order to design vehicles and vehicular components that can operate safely and efficiently under its influence. In the bigger picture, discontinuities of flow is applicable to a broad range of subjects with far reaching significance. For example in the study of detonations, a working knowledge is needed to predict the effects of explosives, to prevent knocking in internal combustion engines, or even to harness the shockwave energy transfer capability as in the wave disk engine. In the realm of astrophysics and magnetohydrodynamics, different kinds of shockwave are observed in association with phenomena such as the formation of stars and collision between galactic entities.

However, the shockwave itself is a notoriously demanding challenge to study empirically; a major obstacle in the examination of the shockwave is the difficulty of recreating it in a controlled environment. One could imagine the enormous resources and effort it would take to build a wind tunnel or any other set-up

that is powerful enough to generate high wind velocities, while at the same time having measurement equipment that can reliably operate under the extreme conditions. Considering this fact, scientists and researchers often turn to the tried and tested alternative of Computational Fluid Dynamics (CFD). CFD is a field of knowledge in which fluid flow problems are resolved numerically using model equations that represent the governing laws of conservation. Instead of solving these equations analytically, approximations are iteratively calculated to simulate and predict the solution as closely to real-world results as possible. These numerical methods are classified into the major categories of finite difference, finite volume, and finite element methods (LeVeque, 2002). Other methods include the point difference, residual-distribution, spectral, and panel method. Amongst all the available methods, the most widely used is arguably the finite volume method of discretization.

In the finite volume method, we define a flow domain, or a control volume, in which we study the particular physical phenomenon of interest. This control volume is divided into a discrete number of cells that form a grid. Information passes through the domain (and most probably changes) according to how the boundaries and initial conditions are set up, and a change that occur across a cell will affect all other cells in the wake of the direction of flow. In order for the information to make sense, it is required that any changes that occur inside the domain to be coherent in terms of its physics, and this is achieved by way of enforcing conservation laws. As information travels from cell to cell along the domain, we can track the changes from the domain inlet to its outlet, and recover the data transferred between cells, in the same manner as if we are solving a series of Riemann problems. Thus, the set of solution equations that perform such calculations are often deemed as Riemann solvers (Toro, 1999), and the

equations themselves are called flux functions. A special category of solution methods have the ability to perform calculations and remain numerically stable even when discontinuities are encountered; these methods are designated as shock capturing schemes (Hirsch, 2000). Within the discussion of shock capturing, one of the most important class of methods is the entropy conservative scheme, where the conservation law of flow is supported by an additional constraint that follows the second law of thermodynamics. An example of this can be found in the research that have been presented in the Ph.D. thesis by Ismail (2006).

The benefit of such a scheme is that the flux function would be able to pick up the physically relevant solutions from those that are unphysical, such as the rarefaction shock. When the flux is producing just the right amount of entropy to turn a rarefaction shock into a fan, or to diffuse a total discontinuity into a more physical shock profile, then the scheme is acknowledged to be entropy consistent. Entropy consistency is achieved through entropy control, a strategy utilized in numerical schemes to either generate or limit diffusion in the solution. One of the ways to do this is through physical viscosity, as introduced by Tadmor (1987). Alternatively, control could also be acquired by employing concepts of entropy conservation, entropy stability, and entropy production, resulting in an entropy consistent flux, (Ismail and Roe, 2009). In any case, the control of entropy is indeed an important facet of the shock capturing method, with an active field of research continuing for the foreseeable future.

#### 1.2 Advancements in Numerical Analysis

The goal of a numerical scheme is always to provide solutions and predictions as accurately as the method allows, in a manner that is as computationally cheap as possible. Some schemes, particularly those with high order of accuracy, con-

centrate on getting a close representation of the physical behavior of flow whilst sacrificing the speed of iterative convergence. In today's world of parallel processors and high-powered computing, this may not be such a bad choice, but the issue is usually more about the amount of time and resources that one is willing to spend to get the desired result. Hence, there is still a need for schemes that can get the job done quickly, cheaply, and reliably. These affordable schemes may not necessarily be less accurate than the more sophisticated ones given the particular problem to be solved. An example of a reliable low-cost scheme is found in Roe (unpublished) and Ismail and Roe (2009), using the concept of entropy conservation and consistency to obtain physically relevant solutions in the presence of shock. The value in using this approach is not only in its relative accuracy and cost-effectiveness, but also in the fact that it is based on solid physical interpretations and not just heuristics or improvisations.

Having said that, the whole concept of entropy consistency is yet to be fully explored, and is yet in the developmental stages. Thus, its proponents are continually looking for ways to refine the technique, through optimizations or even by synthesizing it with other approaches. One particular niche of interest is the new approach of using first-order hyperbolic system of equations to construct the governing law of flow, as introduced initially in Nishikawa (2007) and other subsequent works. The main idea for this method is to resolve higher order terms of an equation into its equivalent set of first-order expressions, with the intention of getting every term in the governing law to have a hyperbolic characteristic. This would enable the use of one unified discretization strategy for the whole equation, which would in turn ensure uniform order of accuracy for each component. This method is typically used in system dynamics and control (Kitamura et al., 2009). The biggest benefit of reconstructing higher order equations into first order sys-

tems is the reduced amount of iterations required for convergence. Calculations of first order equations are usually simpler than second order ones, and thus the advantage of doing so could more than offset the requirement of solving a larger number of equations during the course of one iteration. A demonstration of this is shown in Figure 1.1.

In this figure, the aforementioned first-order system of flux functions (FOS) is compared to the well-established discontinuous Galerkin method in terms of its iterative efficiency. As evidenced by the result, the hyperbolic first order system approach promises a substantial benefit in the reduction of computational cost as the mesh of the simulated flow domain becomes more refined. This result can be seen as a good motivation to explore the potential of this method, particularly in having it incorporated into the realm of shock capturing.

#### 1.3 Motivation and Problem Statement

It is a known fact that even the state of the art softwares that solve Navier-Stokes and other flow equations are known to have issues of accuracy. Furthermore, most accurate solvers incur high costs in terms of computing power and time. These challenges are being slowly overcome with ongoing researches in the CFD field, by acquiring more understanding in the fundamental nature of the flow phenomena, and also in the behavior of the numerical schemes themselves. Despite the continuous advances, there are still a lot of gains to be made in the improvement of shock capturing, even at its most basic level. With this angle in mind, the intent of this research is not to create something that exceeds the capability of any modern CFD codes available out there, but merely to take a step back and consider the possibility of building a good basis for a future multi-dimensional CFD solver. From amongst a host of other options, we see two major avenues

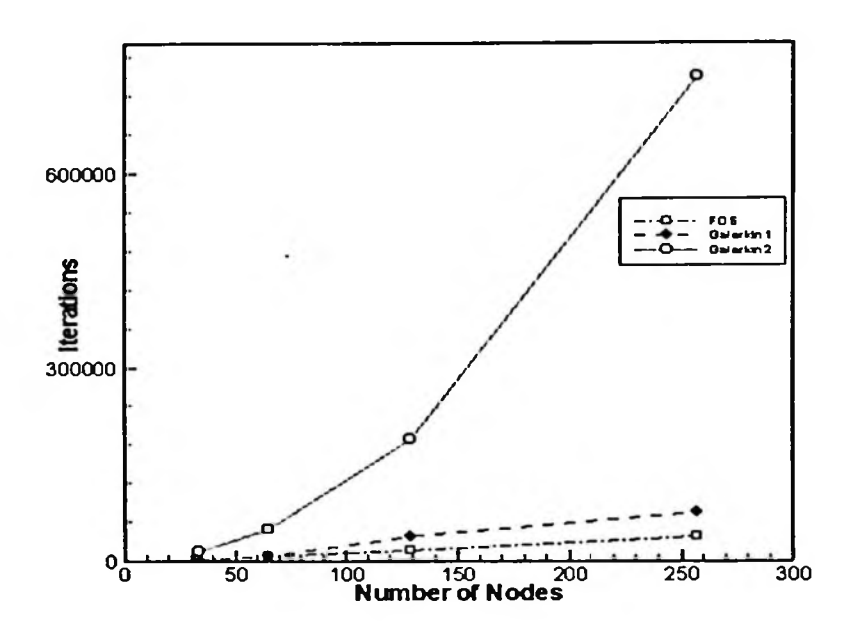


Figure 1.1: The amount of iteration required to reduce the variable residuals by five orders of magnitude according to node count for the first order system flux (FOS), the discontinuous galerkin method at Re = 1000 (Galerkin1), and the discontinuous galerkin method at Re = 100 (Galerkin2).

of development: firstly in the topic of entropy consistency, and secondly in the approach of using first order hyperbolic equations.

The problem is to find a way to successfully synergize both concepts into one coherent strategy that would enable us to construct a new numerical scheme; to our knowledge this endeavor has never been undertaken before. The flux functions should ideally be able to extract the advantages of the first-order system, and reinforce it with the sound physical basis of the entropy consistent flux formulation. Achieving this will require a re-examination of entropy consistency, and a reconstruction of the existing methods in terms of its numerical discretization. It is acknowledged that the task of combining the two concepts is in itself a big challenge, but a well-worth one considering the possible benefits of faster and more accurate fluxes.

#### 1.4 Research Objective, Methodology and Scope

This research is centered around two main objectives:

- To develop entropy consistent flux functions based on combining the concepts of entropy consistency and the first order hyperbolic system of equations.
- To study the effects of utilizing physical viscosity instead of the artificial numerical viscosity in creating diffusion for the numerical scheme.

For the purpose of fulfilling first objective, the plan is to create an entropy consistent first-order system of flux functions, initially based on Burgers' equation as a proof of concept. Should the flux prove to be viable solution, the research will continue with development of the first-order entropy consistent flux functions for the Navier-Stokes system of equations in one-dimension. From there, the Navier-Stokes system fluxes can be extended to two-dimension. Meanwhile, to satisfy the second objective, the newly created Burgers' system flux will be compared with the available exact solutions. Also, the new Navier-Stokes system flux will be contrasted with the existing entropy-consistent fluxes and experimental data to ascertain its characteristics.

For its contribution to knowledge, this thesis offers an advancement in the field of the shock-capturing numerical method by way of:

- An understanding of how the concept of entropy consistency can be extended to linear hyperbolic systems.
- New flux functions based on the Burgers' equation and the Navier-Stokes equation that are entropy consistent and fully hyperbolic in nature.

• Extensions of these fluxes to higher-order accuracy and multi-dimensional problems that could pave the way for practical use.

As mentioned earlier, the study will focus on two equation models, namely the Burgers' equation and the Navier-Stokes equation discretized using the finite volume method. Fluid flow is assumed to be compressible, and moving at the transonic and supersonic regions. Therefore, flow will have laminar characteristics and considerations regarding turbulence is minimal, so as to concentrate on the actual behavior of the developed fluxes without bringing up the separate issue of turbulence modelling. Furthermore, the study focuses more on the viscous characteristic in the model equation, whilst heat transfer is not focused upon. The fluxes are developed for one and two dimensions, with accuracy of only up to second-order. Since the formulation of the equation model utilizes relatively new concepts, the work concentrates on lower order accuracy to ensure its practicality before higher-orders can be considered. This is also the reason the development of the fluxes is concentrated on one dimension, with some result also shown for two dimensions to demonstrate their viability. Since the fluxes are specifically developed to be shock-capturing, flow regimes for one dimension is concentrated on high velocity, while the two dimensional simulations also touch upon moderate velocity flows at limited Reynolds number.

#### 1.5 Thesis Organization

Chapter 2 will discuss the history and current state of progress for the two main concepts in question which are entropy consistency and linear hyperbolic systems. Then in Chapter 3, a numerical scheme is developed based on the Advection-Diffusion and the Burgers' equation model. This work is continued in Chapter 4, where the Euler and Navier-Stokes equations are discussed. A one-dimensional

flux function is developed based on these equations, and is then extended to two dimensions. Next, the results of simulations using these flux functions are compiled in Chapter 5, and their merits are discussed therein. Finally, the study is concluded in Chapter 6, and the possibilities for future continuation of this work is highlighted.

#### CHAPTER 2

#### LITERATURE REVIEW

#### 2.1 Entropy Consistency

Given that complexities in Fluid Dynamics prevent most problems of flow from being solved analytically, it makes sense that the numerical alternatives to getting the solutions are usually based on vastly simpler equation models. These models are stripped down versions of the full flow equations, and carry with it only the fundamental behavior of the flow variables as they change across the pre-defined domain. One example of a widely used model equation is the linear advection equation:

$$\frac{\partial u}{\partial t} + a \frac{\partial u}{\partial x} = 0 \quad \text{or} \tag{2.1a}$$

$$u_t + au_x = 0 (2.1b)$$

As suggested by its name, this equation models the propagation of fluid or waves along a particular trajectory, and thus is qualitatively classified as a hyperbolic type of partial differential equation (PDE); this is as opposed to the parabolic type that is diffusive in nature, or the elliptic PDE with solutions that are typically smooth functions in steady state. The partial differential equation can be numerically evaluated by choosing from amongst several classes of methods, the established classes of which include the finite difference (Courant et al., 1952; Lax, 1954; Friedrich, 1954; Lax and Wendroff, 1960; MacCormack, 2003), finite element (Reed and Hill, 1973; Patera, 1984; Babuska and Guo, 1992; Mos et al., 1999), and finite volume (Godunov, 1959; Van Leer, 1979; Harten, 1983a; Liou and Steffen, 1993). One could easily come up with a valid justification for picking any of

these methods, but in compressible flow applications, the finite volume method remains the sensible choice for being conservative, flexible (allowing unstructured meshes), and robust.

In finite volume discretization, an array of control volumes, or cells, is defined throughout the flow domain, and changes in the behavior of the flow can be described by the interaction of the fluid at the interface (which are the boundaries that distinguish the limits between adjacent cells) in the form of a flux function. Evaluating these flux functions is conceptually akin to solving multiple Riemann problems, hence solution methods are called Riemann solvers (Toro, 1999; LeVeque, 2002). The Godunov flux solves these Riemann problems exactly, whilst others are approximate or linearized solvers (Roe, 1981; Einfeldt, 1988; Nishikawa and Kitamura, 2008). Over the years, the Godunov-type methods has been considered as having the strongest possible physical basis (Roe, unpublished). However, this method contains a significant weakness in that it is not entropy stable (Barth, 1999), the concept of which will be discussed shortly.

When applied numerically, conservation laws do not always convey faithfully all information throughout the process of getting to the solution. Some of these information might be lost due to truncation, approximation, or a host of other sources that are unintended effects of discretization. Consequently, additional constraints are required to shore up the inconsistencies of the numerical scheme. One such constraint is the second law of thermodynamics, in which the entropy of the system undergoing an irreversible process must always increase. When translated into the numerical sense, the entropy must be controlled so that the scheme would produce results that reflect a positive entropy generation. Entropy control can be established through the judicious application of the artificially introduced numerical viscosity, as was initially recognized by Neumann and Richtmayer (1950).

The nature of discrete equations, particularly those of the finite volume scheme, is such that they can give rise to multiple unique solutions, only one of which is physically representative of the flow. Using entropy control could enable one to pick out the physically relevant solution from amongst the non-physical ones, such as in differentiating between shocks and the un-physical rarefaction, as discussed in Lax (1954). When entropy control is tuned correctly, a shock will retain its discontinuous profile, whilst a rarefaction would be reduced to a continuous function. As an example, consider the Roe scheme (Roe, 1981), one of the most widely used approximate Riemann solvers available due to its ability to produce nearly identical result to the exact Riemann solver. As good as the solver is, it still flawed in that it captures shocks and rarefaction indiscriminately. To remedy this, the solver is usually coupled with an entropy fix, for example the one introduced by (Harten and Hyman, 1983).

While adding correction terms may be practical depending on the situation, numerical schemes could be made more fundamentally sound by directly incorporating entropy conservation into the fundamental conservation equations of mass, momentum, and energy. Tadmor (1984) sought to achieve this via the addition of numerical viscosity. The work shows how an increased level of numerical viscosity would make a difference scheme converge towards the one weak solution of the approximated conservation equation that is unique and physically relevant. Schemes such as Godunov's, Lax-Freidrichs (Lax, 1954; Friedrich, 1954), and Eschemes (Osher, 1984) were studied for comparison, the results of which support this very conclusion.

The work is continued in Tadmor (1987), where entropy is conserved at the local level, and entropy generation is enforced whenever discontinuities occur. The characteristic of producing entropy across shocks qualifies a scheme for the designation of being an entropy-stable or entropy-admissible scheme. Specifically, the entropy stability requirement is prescribed in the form of an inequality of the entropy pair U and F:

$$\frac{\partial U}{\partial t} + \frac{\partial F}{\partial x} \le 0 \tag{2.2}$$

The scheme developed in Tadmor (1987) exactly conserves entropy in smooth regions, but is computationally expensive and would result in huge oscillations when discontinuities are encountered. The result shows that the scheme might suffer from insufficient numerical viscosity, meaning that there is still a lack of entropy generation in the flux function. However, adding more numerical viscosity is not a simple matter, as excessive amounts would invariably lead to a shock profile that is too diffused. Thus, the question remains regarding the exact amount of entropy generation needed.

As an attempt to answer this, Tadmor and Zhong (2006) used physical viscosity and heat conduction to dissipate entropy, eliminating the need for any additional numerical diffusion. The scheme uses an entropy conservative flux from the Euler equations and centered difference source terms, the combination of which approximate the Navier-Stokes equations in an entropy stable manner. Results demonstrate that this concept works well in terms of reduced oscillations around shock and contact discontinuities, but the scheme requires a very fine grid to achieve it. Alternatively, Ismail (2006) used both vorticity capturing and entropy control as means to eliminate shockwave anomalies, especially carbuncles. The thesis contends that the latter plays a more important part to combat the anomalies compared to the former. To achieve entropy control, the entropy conservation law was directly incorporated into the flux function. This method involves combining Roe's entropy conserving flux with Roe's entropy stable dissipative flux that uses a modified averaged formulation. The flux is then augmented with an entropy fix

that generate enough entropy production to ensure monotonicity.

Furthering this concept are works of Roe (unpublished) and Ismail and Roe (2009), where captured discontinuities were regulated using artificial terms of stability and production as introduced in Ismail (2006). For Burger's equation, the flux is:

$$f^* = f_c - f_s - f_p (2.3a)$$

$$f_c = \frac{1}{6}(u_L^2 + u_R u_L + u_R^2) \tag{2.3b}$$

$$f_s = \frac{1}{4}|u_L + u_R|[u] \tag{2.3c}$$

$$f_p = \frac{|[u]|[u]}{12} \tag{2.3d}$$

where the square brackets [] is the difference function, which in this instance  $[u] = u_R - u_L$ . Eq. (2.3) denotes the flux interface \* which is shared by two adjacent cell values denoted by the subscripts L and R representing the left and right cells respectively. The term  $f_c$  represents the entropy-conserved flux (Tadmor (1987), Roe (unpublished)). Coupling  $f_c$  with  $f_s$  represents an entropy stable flux as in Tadmor (2003) and the references therein. The third term  $f_p$  represents the production term. Recall that Eq. (2.3a) is also known as the original Roe-flux from Roe (1981) with an entropy fix by Harten and Hyman (1983).

The aim of this entropy-consistent flux, tested in a one dimensional setting, is to efficiently provide a completely stable solution that would hopefully remain that way in multi-dimensions to combat unwanted occurrences, particularly the carbuncle phenomenon. The key to achieving stability is to provide just enough dissipation to the flux to damp the oscillations around the shock, without making it too diffusive. Alternatives of generating dissipation, such as using central difference schemes, could produce relatively similar results, but they would require finer grid resolution or higher orders of accuracy to make them work. Therefore,

entropy consistency remains the most viable path in terms of producing relatively accurate low-cost schemes.

#### 2.2 First Order Systems

Many physical occurrences of scientific interest are mathematically describable through hyperbolic partial differential equations. Among the typical examples include the wave equation, the hyperbolic heat conduction equation and the Maxwell-Cattaneo equation. This type of equation may contain source terms on the right hand side, such as body forces or external effects; this term is considered 'stiff' if its solution is numerically unstable, or operates at a faster time scale as compared to other terms in the equation, to the point that it requires an extremely small time step. The stiffness is characterized by its relaxation time which describes its decay or rate of return to equilibrium. Important applications of the stiff hyperbolic system is in the realm of gas dynamics, chemical-kinetics and other advection problems that include interaction between the flow constituents (LeVeque and Yee, 1988; Yu and Chang, 1997; Donat et al., 2009).

Even before the advent of such applications, there already exist numerical methods that directly resolve second or higher-order partial differential equations. An early example of this approach is found in the hyperbolic system of conservation laws by Lax (1957), followed by more conventional ones (Jin and Levermore, 1996; Lowrie and Morel, 2000). However, instead of using conventional methods, one could also choose to solve hyperbolic PDEs such as the wave equation by firstly representing it as a first order system, which are series of simultaneously related first order differential equations (Van Leer, 2001; Evans, 2010).

Whichever the method chosen, the difficult part is still in dealing with stiff source terms. This was demonstrated in Roe and Arora (1993), in which the method

of characteristics for dispersive waves was studied. This method is tested by modelling heat conduction using several schemes that employ the hyperbolic heat equations relaxation system. The scheme that performed the best was the point implicit method. It is speculated that the success of this scheme is predicated on the inclusion of information from the grid point that lies between the characteristics, which introduces a coupling between two families of waves. An important finding of this paper is how the solution of the hyperbolic system relates to its relaxation time. For small values of time as compared to the relaxation constant, the solution will be highly discontinuous and invariably hyperbolic, whilst for larger ratios, the jumps in the solution decay towards a parabolic feature.

Another important feature that must be considered in stiff hyperbolic systems is asymptotic preservation, which indicates the behavior of a scheme approaching limits such as discontinuities. A scheme is considered asymptotic preserving if its discretization fully conserve the asymptotic properties of the continuous system from which it is based on. In continuation of his previous work, Arora (1996) extends the method of characteristics for hyperbolic systems to the finite volume method. The method was found to successfully capture underresolved asymptotic solutions for first-order accurate source term discretization.

However, asymptotic behavior cannot be captured correctly by hyperbolic systems unless a fine spatial grid is used to resolve the small relaxation rate. In Jin and Levermore (1996), the correct asymptotic behavior is built into the scheme by the introduction of a modified high-order Godunov method. With this scheme, a balance between the relaxation term and the spatial derivative term is achieved, eliminating the problem of inaccurate long-time solutions produced by hyperbolic systems with stiff relaxation. This idea of balance would prove to be important in the concept of a new hyperbolic systems put forth by Nishikawa.

In his series of papers starting with (Nishikawa and Roe, 2004), a numerical scheme with a uniform order of accuracy is developed using a first-order system approach to solve for advection-diffusion problems. Existing schemes that combine different computational strategies for advection and diffusion suffer from incompatibilities which would reduce the order of accuracy for the solution to the lowest between its component. To combat this issue, the new scheme was proposed as an alternative featuring a new spatial discretization method that retains the accuracy for all components of the flux function.

Later, the same concept was then reintroduced to compute the diffusion equation:

$$u_t = \nu(u_{xx} + u_{yy}) \tag{2.4}$$

with  $\nu$  being the diffusion coefficient. A steady-state solution is obtained in (Nishikawa, 2007) by reformulating the equation in the setting of a first order hyperbolic system:

$$u_t = \nu(p_x + q_y),\tag{2.5a}$$

$$p_t = (u_x - p)/T_r,$$
 (2.5b)

$$q_t = (u_y - q)/T_r \tag{2.5c}$$

The main idea is to focus on the steady state solution of the system, which is equivalent to the diffusion equation at the same condition. Consequently, time-dependent behavior is deemphasized by treating the time relaxation,  $T_r$ , as a free parameter. In other words, the scheme maintains the accuracy of its solution by avoiding stiffness and giving up time accuracy.

To get to the diffusion scheme, the hyperbolic model is discretized by an advection scheme, and the secondary equations are replaced by a direct approximation of

the secondary variables p and q to the spatial derivative of the primary variable. This scheme is automatically equipped with a damping term which would help eliminate large errors, speeds up convergence, and improve consistency.

With the basic concepts established, the strategy is extended to construct a hyperbolic system that combines advection and diffusion (Nishikawa, 2010b). Consider the advection-diffusion equation:

$$u_t + au_x = \nu u_{xx} \tag{2.6}$$

with a as the advection speed. This equation is dichotomized into an equivalent system of:

$$u_t + au_x = \nu p_x \tag{2.7a}$$

$$p_t = (u_x - p)/T_r \tag{2.7b}$$

Improving from the previous work, the time relaxation,  $T_r$ , and the associated length scale,  $L_r$  are optimized to accelerate convergence towards steady state with  $\mathcal{O}(h)$  time step. Another advantage provided by the method is uniform accuracy for all Reynolds numbers, meaning that the solution gradients can be maintained to the same order of accuracy of the main variable.

The concept of resolving equations into their first order versions is consolidated with a generalized diffusion scheme based on the hyperbolic relaxation system for various discretization methods (Nishikawa, 2010a). Schemes based on methods including finite volume, discontinuous Galerkin, and residual distribution are developed. It was shown that the new strategy provides improved accuracy for diffusion problems that are time dependent as compared to conventional methods, when irregular triangular grid is used.

The work is expanded with an upwind finite volume scheme for a first-order hyperbolic Navier-Stokes system (Nishikawa, 2011a)

$$\rho_t + (\rho u)_x = 0 \tag{2.8a}$$

$$(\rho u)_t + (\rho u^2 + p + \tau)_x = 0 (2.8b)$$

$$(\rho E)_t + (\rho u H - \tau u + q)_x = 0 (2.8c)$$

with E and H representing energy and entalphy respectively. Conventional approach utilizes a two step strategy in which a hyperbolic discretization method is used for the inviscid terms and a parabolic one for the viscous counterparts. Instead of using this strategy, the proposed hyperbolic system is set up by adding two equations to the three already defined:

$$\tau_t - \frac{\mu_\nu}{T_\nu} \left( u_x - \frac{\tau}{\mu_\nu} \right) = 0 \tag{2.9a}$$

$$q_t - \frac{\mu_h}{T_h} \left( -\frac{1}{\gamma(\gamma - 1)} T_x - \frac{q}{\mu_h} \right) = 0$$
 (2.9b)

$$\mu_{\nu} = \frac{4}{3}\mu, \quad \mu_{h} = \frac{\gamma\mu}{Pr} \tag{2.9c}$$

where  $\tau$  is the viscous stress, T is the temperature,  $\gamma$  is the ratio of specific heats, and Pr is the Prandtl number. Consistent with the principal idea, the terms of equation 2.9 are first-order equivalents of the higher-order components in the momentum equation. The system is now entirely hyperbolic, allowing for a uniform discretization method and eliminating the need for a parabolic treatment for the viscous terms.

#### 2.3 Current Developments

One of the objectives of the thesis is to exploit the advantages of entropy conservation and the first order hyperbolic system in a finite volume scheme. The concept itself has already been touched upon in a hyperbolic Euler system at low Mach numbers (Gustaffson, 1987; Wong et al., 2001), but the goal is to extend it to include the full physical viscosity effect. This idea was alluded to in Chen et al. (1994), where the limits of hyperbolic conservation laws with stiff relaxation terms was studied for a 2 by 2 system. The system is readily equipped with a convex entropy pair, entropy dissipation is implied by a strict stability criterion. However, the system used is not resolved into the first order, and no simulations were computed.

Another examination of hyperbolic systems with relaxation was done in Hittinger (2000). Consequently, an accurate yet underresolved Gudonov type method was developed by the coupling of wave propagation and relaxation. This method is applied to both linear and nonlinear systems that model a hyperbolic system with relaxation. Even with very good results, it would seem that such methods require considerably more computational cost than the one proposed in Nishikawa (2011a). Bearing this in mind, a synthesis between the hyperbolic first order system and the concept of entropy consistency is an attractive avenue to venture upon, since both concepts could be constructed to have a relatively low cost compared to any other schemes available today. Furthermore, potential developments of both the first-order system approach and the entropy consistency condition are promising in that they have yet to reach saturation and are still active fields of research, as evidenced by the following new papers.

The latest work regarding entropy stable schemes is documented in the series of papers by Fjordholm, Mishra, and Tadmor. These researchers mainly concentrate on entropy stability for shallow water equations (Fjordholm et al., 2008), and for higher order accuracy schemes (Fjordholm et al., 2011, 2013). Even with all the developments in the field up to now, there are a number of fundamental issues still unsolved, the biggest of which is how much entropy production is needed to achieve consistency. Additionally, the question remains whether this concept of entropy consistency can translate favorably in higher dimensional domains. Attempts to answer these problems have been forthcoming with the work of Bressan (2009) and Fisher and Carpenter (2013). In the former, the multiple and varying conditions for entropy was thoroughly described, providing us with a working understanding of the limits of entropy construction. In the latter, entropy consistency was shown to be applicable to the high-order accurate Weighted Essentially Non-Oscillatory Scheme (WENO) scheme.

Concurrently, Nishikawa has also been continuing the research on hyperbolic systems with works in Nishikawa (2012, 2013a,b). The earlier one focuses on source term formulation in the form of divergence, enabling one to construct a uniform scheme for the conservation equation and the source term, thereby ensuring the same order of accuracy for both. On the other hand, the latter two papers provide detailed description on the method to construct advection and diffusion schemes based on the hyperbolic system approach for up to third-order accuracy. These documents provide the framework for us to synthesize this approach with the concept of entropy consistency using the finite volume method. The key to achieve this lies in the selection of entropy variables that would map the the secondary variables of the system to the entropy domain using guidelines as established in existing literature.

#### CHAPTER 3

#### SCALAR EQUATIONS

Scalar equations, for example the linear advection equation, and Burgers' equation, are usually considered a good starting point for constructing numerical schemes. Such equations are widely used in the study of transport phenomena, serving as models of conservation laws that govern the evolving characteristics of a variable of interest across time and space. These equations are usually simple to discretize, relatively easy to analyze, and equally importantly, have exact solutions available for comparison with the numerical schemes. Additionally, they form the baseline for more complex systems such as the Euler and Navier-Stokes equations. Before any level of complexity can be analyzed, a thorough understanding must be acquired in the fundamentals of transport phenomena, amongst the most basic of which are mechanisms for advection and diffusion.

#### 3.1 Advection and Diffusion

Both properties mentioned earlier can be modelled simultaneously based on the advection-diffusion equation, a combination of the linear advection equation, which is a hyperbolic PDE, and the diffusion equation, a parabolic PDE:

$$u_t + au_x = \nu u_{xx} \tag{3.1}$$

Here, a is the advection speed having a quantity of a > 0, and  $\nu$  is the viscosity coefficient; the equation reduces to linear advection as  $\nu$  approaches 0. An exact solution for this equation is available (LeVeque, 2002) in the form of:

$$u(x,t) = \operatorname{erfc}\left(\frac{x - at}{\sqrt{4\beta t}}\right), \quad \beta = \frac{1}{2}a\Delta x(1 - u), \quad \operatorname{erfc}(x) = \frac{2}{\sqrt{\pi}} \int_0^\infty e^{-z^2} dz \quad (3.2)$$

As a numerical model, the advection-diffusion equation can be discretized in a number of ways, for example using a Taylor series expansion to construct a finite difference scheme (Toro, 1999). A first-order expansion would produce approximated values for  $u_x$  and  $u_t$ :

$$u_x \approx \frac{u_i^n - u_{i-1}^n}{\Delta x}, \quad u_t \approx \frac{u_i^{n+1} - u_i^n}{\Delta x}$$
 (3.3)

These values can then be used as input for practical difference schemes, the simplest amongst which is the first order upwind method, also known as the Courant, Issacson, and Rees (CIR) scheme (Courant et al., 1952). Substitution of data from equation 3.3 into the inviscid version of equation 3.1 yields:

$$u_i^{n+1} = u_i^n - c(u_i^n - u_{i-1}^n), \quad c = \frac{a\Delta t}{\Delta x}$$
 (3.4)

The coefficient c is widely known as the Courant-Friedrichs-Lewy (CFL) number (Courant et al., 1967), the ratio between the wave propagation speed a and the speed of the discretization. The value is usually set to a value less than 1. Despite having the advantage of being very simple, the downside of the CIR scheme is that it is prone to having smeared or spread solutions when discontinuities are encountered (Toro, 1999). This first-order upwind method, as well as many other finite difference methods, can also be formulated in a manner called the finite volume scheme. Instead of assigning discrete values at each point of a grid as in finite difference, the finite volume method considers the averaged values over the area in between the grid points, as shown in Figure 3.1. In both figures (a) and (b), the horizontal axis represents space whilst the vertical axis shows the evolution of time.

To formulate the finite volume form, consider the generalized scalar conservation

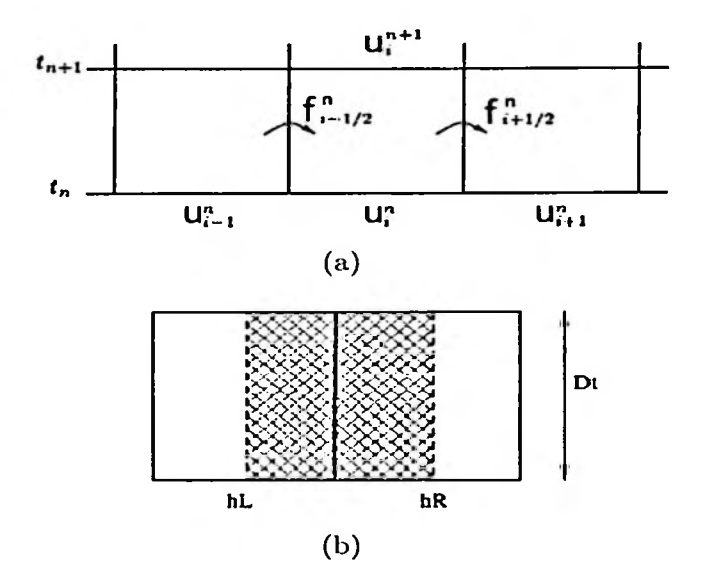


Figure 3.1: Grid representation of the finite volume method from (a) LeVeque (2002) and (b) Ismail and Roe (2009).

equation:

$$u_t + f(u)_x = 0 (3.5)$$

Integrating over space and time:

$$\int_{x_{i-\frac{1}{2}}}^{x_{i+\frac{1}{2}}} u(x, t_{n+1}) dx - \int_{x_{i-\frac{1}{2}}}^{x_{i+\frac{1}{2}}} u(x, t_n) dx$$

$$= \int_{t_n}^{t_{n+1}} f(u(x_{i-\frac{1}{2}}, t)) dt - \int_{t_n}^{t_{n+1}} f(u(x_{i+\frac{1}{2}}, t)) dt \tag{3.6}$$

Approximating the time integrals to the average flux along x, the equation 3.6 can be restated in the form of:

$$u_i^{n+1} = u_i^n - \frac{\Delta t}{\Delta x} \left( f_{i-\frac{1}{2}}^{n+\frac{1}{2}} - f_{i+\frac{1}{2}}^{n+\frac{1}{2}} \right)$$
 (3.7)

Numerical methods of this form are called conservative schemes, since it is derived from equations in conservation form with a 'telescopic' construction method. Con-

servation is important when working with problems that involve discontinuities because the absence of smoothness prevent non-conservative methods from converging to the correct solution (Hou and Lefloch, 1994). If constructed properly, the fluxes of  $f_{i\pm\frac{1}{2}}$  would numerically approximate the physical flux of equation 3.5. Different choices for these numerical fluxes lead to different conservative schemes, but when working with discontinuities, it would be advantageous to select those that satisfy the entropy condition:

$$\lambda(u_L) > \frac{1}{2}(u_L + u_R) > \lambda(u_R) \tag{3.8}$$

Here,  $\lambda(u)$  is the characteristic speed of the conservation equation (for example, the constant advection speed a in the linear advection equation), and the middle term is the speed of the discontinuity (Toro, 1999). The entropy condition is an additional governing law that determines the admissability of a solution, disallowing those that are physically incorrect or entropy violating, such as the rarefaction shock. This condition can be enforced either in an ad-hoc manner, or by incorporating it directly into the flux function as proposed by Tadmor (1984). In the following, a flux function with the entropy admissability feature built-in is derived.

### 3.1.1 Burgers' Equation

Consider again the governing equation for advection and diffusion, cast in vector form:

$$\mathbf{u}_t + \mathbf{f}_x = \nu \mathbf{u}_{xx} \tag{3.9}$$

A subset of this is the Burgers' equation, in which u and f are scalars:

$$u_t + f_x = \nu u_{xx}, \quad f_x = \left(\frac{u^2}{2}\right)_x$$
 (3.10)

To discretize an entropy consistent flux based on this equation, a mapping from the conserved variables to the corresponding entropy equation is sought. The following describes a fundamentally sound method to do so.

# 3.1.2 Roe's Entropy Conserving Flux

In this thesis, the chosen method is an entropy conserving flux formulation initially developed in Roe (unpublished), and further discussed in Ismail and Roe (2009). The inviscid part of the equation is discretized using a semi-discrete finite volume method, such that:

$$\left(\frac{\partial u}{\partial t}\right)_i \Delta x = -\left(f_{i+\frac{1}{2}} - f_{i-\frac{1}{2}}\right) \tag{3.11}$$

where  $\Delta x$  is the distance between two given finite volume interface, and  $f_{i\pm\frac{1}{2}}=f^*$  are the fluxes to be evaluated at each respective interface. In a dual cell system as shown in Figure 3.1(b), this equation can be viewed from a residual distribution approach thusly split into two parts:

$$h_L \frac{\partial u_L}{\partial t} = f_L - f^* \tag{3.12a}$$

$$h_R \frac{\partial u_R}{\partial t} = f^* - f_R \tag{3.12b}$$

The variable h is the length of each cell, whereas the subscripts L and R denotes the states on the left and right of the interface respectively. In this case,  $f^*$  is calculated at the border that separates the two cells. To establish conservation from the entropy point of view, a convex entropy function U(u) is introduced,

along with its associated entropy variable v, and an entropy flux F(U) satisfying the following:

$$v = \frac{dU}{du}, \quad \frac{dF}{dU} = \frac{df}{du(U)}$$
 (3.13)

An entropy stability inequality can be stated in terms of the entropy function as:

$$U_t + F_x \leqslant 0 \tag{3.14}$$

Entropy is conserved when equality is satisfied, but the entropy is more likely to increase (or decrease depending on the point of reference) within the system through physical or numerical means. Therefore, the entropy stability condition in equation 3.14 enforces entropy generation that is the crux of the second law of thermodynamics. Having said that, the exact amount by which it increases or decreases for any given situation remain unresolved, and is one topic that has yet to be explored fully. A definition is introduced in (Fisher and Carpenter, 2013), but the authors of the work concede that a global entropy consistency condition is difficult to enforce. There is, however, another entropy condition that can be implemented locally to get a global entropy consistency established by Tadmor (2003). As an alternative to these methods, a new entropy equation is proposed here:

$$U_t + F_x = k\nu U_{xx} \tag{3.15}$$

The term  $k\nu U_{xx}$  in equation 3.15 symbolizes the hypothesis that the increase of entropy in the system depends on the changes to U multiplied by a coefficient that represents its magnitude. This quantity represents the exact amount by which entropy is generated for the system when it undergoes an irreversible process. In any case, the entropy variable v from equation 3.13 replaces the variable v in

equation 3.12 yielding:

$$h_L \frac{\partial U_L}{\partial t} = v_L (f_L - f^*) \tag{3.16a}$$

$$h_R \frac{\partial U_R}{\partial t} = v_R (f^* - f_R)$$
 (3.16b)

Determining the change of entropy within each cell or element requires the sum of the two parts of equation 3.16:

$$\frac{\partial}{\partial t}(h_L U_L + h_R U_R) = (v_L f_L - v_R f_R) + (v_R - v_L) f^* 
= -[vf] + [v] f^*$$
(3.17)

where  $[v] = v_R - v_L$ . Similarly, the semi-discrete scheme representing the total entropy change predicted by the entropy conservation law of equation 3.14 is:

$$h_L \frac{\partial U_L}{\partial t} = F_L - F^* \tag{3.18a}$$

$$h_R \frac{\partial U_R}{\partial t} = F^* - F_R \tag{3.18b}$$

The total entropy of the system would then be:

$$\frac{\partial}{\partial t}(h_L U_L + h_R U_R) = F_L - F_R = -[F] \tag{3.19}$$

Based on the inequality of 3.14, it is given that the discrete fluxes in equation 3.17 would always be less than or equal to that of equation 3.19. Let's firstly assume that entropy is conserved exactly, implying that:

$$[F] = [vf] - [v]f^* (3.20)$$

Equation 3.20 is then solved as is for  $f^*$  which is the flux at the interface. Doing so requires a choice of entropy function that is preferably convex to allow for one-to-one mapping. For the advection-diffusion in equation 3.1, where f = au:

$$U = u^2, \quad v = \frac{dU}{du} = 2u, \quad F = au^2$$
 (3.21)

Substitute values from equation 3.21 into equation 3.20 and resolve for  $f^*$ :

$$[v]f^* = [vf] - [F] \tag{3.22a}$$

$$[2u](au^*) = [(2u)(au)] - [au^2]$$
(3.22b)

At this point, the identity property can be used where:

$$[ab] = \bar{a}[b] + \bar{b}[a] \tag{3.23}$$

Hence, the flux at the interface is essentially  $u^*$ :

$$[2u](au^*) = 2\bar{u}a[u] + 2a\bar{u}[u] - a\bar{u}[u] - a\bar{u}[u]$$
(3.24a)

$$u^* = \bar{u} \tag{3.24b}$$

The term  $\bar{u}$  can be any averaged quantity of u, for example, the simple arithmetic average where:

$$\bar{u} = \frac{1}{2}(u_L + u_R) \tag{3.25}$$

This essentially means that for the advection-diffusion equation model, the flux at the interface is simply the average of its left and right states. Let us repeat the same process using the Burgers' equation model instead, with  $f = \frac{1}{2}u^2$ :

$$U = u^2$$
,  $v = \frac{dU}{du} = 2u$ ,  $F = \frac{2}{3}u^3$  (3.26)

Substitute values from equation 3.26 into equation 3.20 and resolve for  $f^*$ :

$$[v]f^* = [vf] - [F] \tag{3.27a}$$

$$[2u](f^*) = [(2u)\frac{1}{2}u^2] - [\frac{2}{3}u^3]$$
 (3.27b)

Using the identity of equation 3.23, the entropy conserved flux for Burgers' equation,  $f_c^*$ , is found to be

$$f_c^* = \frac{1}{6}(u_L^2 + u_R u_L + u_R^2) \tag{3.28}$$

This flux formulation is applicable not only for scalars, but also for vectors. For the both the advection-diffusion and the Burgers' equation, their respective conservative fluxes would make up the advection part, whereas the diffusion is discretized separately. To be able to perform the discretization of both parts simultaneously, the equation itself would need to be cast in a different way, which will be discussed later. Before that, we consider the broader case of entropy inequality in which entropy is not necessarily conserved, but is required to always be generated.

# 3.1.3 Stability, Production, and Consistency

A drawback to the entropy conserving flux is its instability when used as a standalone function. The reason for this lies in the fact that the entropy of a system can only be generated, or stay at zero at the very least, when undergoing an irreversible process such as a shockwave. The entropy conservative flux cannot distinguish between positive and negative values, thus is unable to discriminately pick out only the 'entropy admissible' solutions. Moreover, it is not guaranteed that each local entropy flux would always add up to the global entropy change. For the physical law of entropy to remain true, the change of the discrete fluxes in equation 3.17 should at least be a match to the fluxes in equation 3.19, and the difference between the two quantities must be accounted for in the form of the entropy production  $\dot{U}$  as stated in Roe (unpublished):

$$\dot{U} = [F] - ([v]f^* - [vf]) \tag{3.29}$$

Production is built into the flux in part through upwinding, leading to the *entropy* consistent form recommended in Ismail and Roe (2009):

$$f^* = f_c^* - \frac{1}{2}(|\overline{a}| + \alpha|[a]|)[u]$$
 (3.30a)

$$= f_c^* - \frac{1}{2}(|\overline{a}| + \alpha|[a]|)\frac{du}{dv}[v]$$
(3.30b)

Using equation 3.29, the entropy generation thus becomes

$$\dot{U} = -\frac{1}{2}(|\overline{a}| + \alpha|[a]|)\frac{du}{dv}[v]^2 \leqslant 0 \tag{3.31}$$

In this equation,  $\bar{a}$  is the arithmetic averaging of velocity at the interface having left and right cell values, whilst  $\alpha$  is an analytically and empirically determined parameter by Ismail and Roe (2009). Notice how the production term is made up of components that are invariably positive. Considering its entropy conservative nature, the fact that the entropy production would always have the correct sign means the flux definitely satisfies the entropy inequality of equation 3.14. At a given cell interface having left and right states, upwinding is done by adding in

the entropy stability function  $f_s$ :

$$f^* = f_c - \frac{1}{2}|\overline{a}|[u] \tag{3.32a}$$

$$f_s = \frac{1}{2}|\overline{a}|[u] = \frac{1}{4}|u_L + u_R|(u_R - u_L)$$
 (3.32b)

To complete the flux as defined in 3.30, the production term is then added, expressed by  $f_p$ :

$$f_p = \frac{|u_R - u_L|(u_R - u_L)}{12} \tag{3.33a}$$

$$f^* = f_c - f_s - f_p (3.33b)$$

The flux function of  $f^*$  with this configuration (also presented in equation 2.3) represents the complete entropy consistent flux, the benchmark to which the other fluxes derived in this thesis are compared. Furthermore, the flux is deemed entropy consistent by virtue of producing enough entropy appropriate for the inviscid flux formulation.

For the viscous Burgers' equation with  $\nu u_{xx}$  on the right hand side, the same formulation can be used, with the additional step of incorporating the viscosity term into the entropy production portion of the flux. Thus, the physical and numerical viscosity is defined together as:

$$\dot{U} = -\frac{1}{2}(|\overline{a}| + \alpha[a])\frac{du}{dv}[v]^2 - \frac{\nu}{\Delta x}[u][v] 
= -\frac{1}{2}(|\overline{a}| + \alpha[a])\frac{du}{dv}[v]^2 - \frac{\nu}{(2\Delta x)}[v]^2$$
(3.34)

Again  $\dot{U} \leq 0$ , satisfying entropy inequality whilst realizing the equation of 3.15.

# 3.2 Hyperbolic First Order Systems

So far, the approach has focused on the discretization of the advection part of the scalar law, and adding to it diffusion in the form of production. Let us now consider an alternative to this and other conventional methods through the application of a first order, hyperbolic advection-diffusion system as developed by Nishikawa (2007, 2010b):

$$u_t + au_x = \nu d_x \tag{3.35a}$$

$$d_t = (u_x - d)/T_r \tag{3.35b}$$

In the system, u is the main variable that tracks velocity, whilst d can be viewed as the gradient variable or the secondary variable for diffusion.  $T_r$  is the relaxation time that can be set to any positive value. This system can also be written in vector form as:

$$\mathbf{u}_t + \mathbf{A}\mathbf{u}_x = \mathbf{q} \tag{3.36}$$

$$\mathbf{u} = \begin{bmatrix} u \\ d \end{bmatrix}, \quad \mathbf{A} = \begin{bmatrix} a & -\nu \\ -1/T_r & 0 \end{bmatrix}, \quad \mathbf{q} = \begin{bmatrix} 0 \\ -d/T_r \end{bmatrix}$$
 (3.37)

From here, the whole system can be discretized in a uniform manner to produce a pair of flux functions, as was demonstrated by Nishikawa using the residual distribution method. This is different from the common practice of representing advection, which is the hyperbolic part of the equation, as an upwind flux and resolving diffusion by central-differencing. In the following, we will utilize a equation systems approach based on the Burgers' equation, and incorporate within it the concept of entropy conservation using the finite volume method, to create new flux equations.

### 3.2.1 Burgers' First Order System

Similar to the advection-diffusion equation, the viscous Burgers' equation can be written in the form of a first-order system. Consider firstly the original form:

$$u_t + uu_x = u_t + f_x = q, \quad q = \nu u_{xx}, \quad f_x = \left(\frac{u^2}{2}\right)_x$$
 (3.38)

We set up the first order system for this equation:

$$u_t + f_x = \nu d_x \tag{3.39a}$$

$$d_t = (f_x - d)/T_r \tag{3.39b}$$

In vector form, the equation is expressly written as:

$$\mathbf{u}_t + \mathbf{f}_x = \mathbf{q} \tag{3.40}$$

The vectors are defined as:

$$\mathbf{u} = \begin{bmatrix} u \\ d \end{bmatrix}, \quad \mathbf{f} = \begin{bmatrix} u^2/2 - \nu d \\ -u/T_r \end{bmatrix}, \quad \mathbf{q} = \begin{bmatrix} 0 \\ -d/T_r \end{bmatrix}$$
 (3.41)

with  $d = \frac{\partial u}{\partial x}$ .

From this model, the aim is to obtain an entropy consistent flux function in the same vein as the inviscid Burgers equation. To achieve this, we need to define an entropy function that has some measure of "total energy" based on the primary variable u and its auxiliary term d. We seek to control this "total energy" through the concept of entropy conservation, entropy stability and entropy consistency. Based on the work of Hughes et al. (1986), we define an entropy pair (U, F)

satisfying

$$\frac{\partial U}{\partial \mathbf{u}} \frac{\partial \mathbf{f}}{\partial \mathbf{u}} = \frac{\partial F}{\partial \mathbf{u}} \tag{3.42}$$

with U and F split into inviscid and viscous components

$$U = U^{i} + U^{v} = u^{2} + \nu d^{2}, \quad F = F^{i} + F^{v} = (\frac{2}{3}u^{3}) - \frac{2}{T_{r}}\nu ud$$
 (3.43)

satisfying the entropy constraint given in equation 3.14. For inviscid flow( $\nu = 0$ ), this governing entropy equation will collapse into the original entropy equation for the inviscid Burgers' equation. The entropy variables are now defined as:

$$\mathbf{v} = \frac{\partial U}{\partial \mathbf{u}} = \begin{bmatrix} 2u \\ 2\nu d \end{bmatrix}$$
 (3.44)

The total flux at the interface combines both the inviscid flux  $\hat{\mathbf{f}}_i$  and the viscous flux  $\hat{\mathbf{f}}_v$  in a discrete form that is originally derived in Barth (1999) and modified to its current variation in Ismail and Roe (2009):

$$\mathbf{f}^* = \hat{\mathbf{f}}_{\mathbf{i}} + \hat{\mathbf{f}}_{\mathbf{v}} - \frac{1}{2}\hat{\mathbf{R}}\hat{\mathbf{\Lambda}}\hat{\mathbf{S}}\hat{\mathbf{R}}^{\mathrm{T}}[\mathbf{v}]$$
 (3.45)

Note that the quantities accented with the '^' symbol represent discrete averaged quantities. The first two terms,  $\hat{\mathbf{f}}_i$  and  $\hat{\mathbf{f}}_v$  are inviscid and viscous terms representing the symmetric part of the flux and the rest represents the asymmetric part. This asymmetric part can also be identified as the dissipation matrix, whose job is to maintain the stability via proper entropy generation for the flux. Its components, namely the eigenvalues  $\Lambda$  and eigenvectors  $\mathbf{R}$  will be defined later via equations 3.55 and 3.59, while the scaling parameter  $\mathbf{S}$  can be found in equation

3.79. The discrete inviscid and viscous fluxes are arranged as:

$$\hat{\mathbf{f}}_{i} = \begin{bmatrix} u_{1}^{2*} \\ 0 \end{bmatrix}, \quad \hat{\mathbf{f}}_{v} = \begin{bmatrix} -\nu d^{*} \\ -\frac{u_{2}^{*}}{Tr} \end{bmatrix}$$
 (3.46)

where the accent \* denote the averaged interface values to be determined. Here, two averaged quantities have been defined for the velocity  $(u_1^*, u_2^*)$ . One possible approach to determine these averaged quantities is based on finding an averaging such that the fluxes satisfy both the total entropy conservation and the inequality of equation 3.14. For these conditions to be met, we shall make an assumption that the relaxation time is finite and not problem dependent. Its value is set to  $T_r = 1.0$ for the time being so as to keep calculations simple. Observe that total entropy conservation does not mean that the physical viscosity does not produce entropy  $u^2$  (it should) but rather that there is no loss of total 'energy' as defined by  $U_{Total}$ during the the discrete averaging of the fluxes. The loss will be accounted for by the dissipation terms which includes both the physical and numerical diffusion. The dissipation terms generate the proper sign and magnitude of total entropy loss to obey the correct physics and at the same time ensure stability. To achieve entropy conservation, recall how the scalar cell flux in equation 3.17 is equated to the total flux of equation 3.19. The procedure is now applied to the system's approach, by replacing the scalar variables with vectors:

$$[\mathbf{v}]^T \mathbf{f}^* - [\mathbf{v} \cdot \mathbf{f}] = -[F] \tag{3.47}$$

Note that this is an under-determined equation hence there will be more than one set of solutions. However, only one set of solutions are needed to explicitly determine the averaged quantities. Equation 3.47, when expanded becomes

$$[2u]\frac{u_1^{2*}}{2} - 2\nu[u]d^* - 2\nu[d]u_2^* - [u^3] + 2\nu[ud] + 2\nu ud = -\frac{2}{3}[u^3] + 2\nu[ud]$$

$$([u]u_1^{2*} - [u^3]) + (2\nu[ud] - 2\nu[u]d^* - 2\nu[d]u_2^*) = -\frac{2}{3}[u^3]$$
(3.48)

Using the identity  $[ab] = \overline{a}[b] + \overline{b}[a]$ , the equation reduces to

$$[u]u_1^{2*} + 2\nu(\overline{u}[d] + \overline{d}[u]) - 2\nu[u]d^* - 2\nu[d]u_2^* = \frac{1}{3}[u](u_L^2 + u_L u_R + u_R^2)$$
 (3.49)

By equating the terms in the first on the left hand side to the right hand side of equation, the inviscid entropy conserved flux formulation is recovered,  $u_1^* = \frac{1}{3}(u_L^2 + u_L u_R + u_R^2)$ . And by choosing  $u_2^* = \overline{u}$  and  $d^* = \overline{d}$ , the whole equation cancels out thus obtaining entropy conserved fluxes for the inviscid and viscous parts:

$$\hat{\mathbf{f}}_{i} = \begin{bmatrix} \frac{1}{6}(u_L^2 + u_L u_R + u_R^2) \\ 0 \end{bmatrix}, \quad \hat{\mathbf{f}}_{v} = \begin{bmatrix} -\nu \overline{d} \\ -\frac{\overline{u}}{Tr} \end{bmatrix}$$
(3.50)

The total entropy production based on the flux discretization is:

$$\dot{U} = -\frac{[\mathbf{v}]}{2}^T \hat{\mathbf{R}} \hat{\mathbf{\Lambda}} \hat{\mathbf{S}} \hat{\mathbf{R}}^T [\mathbf{v}] \le 0$$
 (3.51)

This ensures the entropy defined in equation 3.43 is decreasing since the product is a positive definite matrix. Note that there will also be entropy production generated by the source term of the auxiliary equation (d) which may not always be of the correct sign. However, as a first step of controlling the entropy production in a first order systems approach, the focus herein is only on ensuring the the discrete flux is at least entropy stable. Stability can be achieved via entropy appropriate definition of the matrix constituents.

# 3.2.2 Eigenvalues and Eigenvectors

Herein the components of the dissipation matrix is defined, starting with the eigenvalues. Firstly, the Jacobian A is defined from the system flux f in equation 3.41:

$$\mathbf{A} = \frac{d\mathbf{f}}{d\mathbf{u}} = \begin{bmatrix} u & -\nu \\ -1/T_r & 0 \end{bmatrix}$$
 (3.52)

The eigenvalue  $\lambda$  is introduced, the definition of which can be obtained by calculating the determinant of the Jacobian in the form set to:

$$\det \begin{bmatrix} u - \lambda & -\nu \\ -1/T_r & -\lambda \end{bmatrix} = 0 \tag{3.53a}$$

$$(u - \lambda)(-\lambda) - \frac{\nu}{T_n} = 0 \tag{3.53b}$$

$$\lambda^2 - u\lambda - \frac{\nu}{T_r} = 0 \tag{3.53c}$$

 $\lambda$  is found to have two real, unique solutions in:

$$\lambda = \frac{-(-u) \pm \sqrt{u^2 - 4(1)(-\nu/T_r)}}{2(1)} \tag{3.54}$$

Hence the averaged eigenvalues for the system of equations 3.36 are:

$$\hat{\Lambda} = \begin{bmatrix} \hat{\lambda}_1 & 0 \\ 0 & \hat{\lambda}_2 \end{bmatrix}, \quad \hat{\lambda}_{1,2} = \frac{1}{2} (u \pm \sqrt{u^2 + \frac{4\nu}{T_r}})$$
 (3.55)

representing the characteristic waves speeds for u, d. In terms of discrete variables, these eigenvalues can be stated as:

$$\hat{\lambda}_1 = \frac{1}{2} (u_1^* + \sqrt{(u_1^*)^2 + \frac{4\nu}{T_r}}), \quad \hat{\lambda}_2 = \frac{1}{2} (u_2^* - \sqrt{(u_2^*)^2 + \frac{4\nu}{T_r}})$$
 (3.56)

Note that for  $\nu = 0$ , the eigenvalues reduces to just one nonzero quantity  $(\lambda_1 = u)$  which represents the pure transport of the inviscid Burgers equation.

We can then get the eigenvectors for the eigenvalues by setting  $Av = \lambda v$ :

$$[\mathbf{A}] \left[ \begin{array}{c} x \\ y \end{array} \right] = \lambda \left[ \begin{array}{c} x \\ y \end{array} \right] \tag{3.57}$$

Expanding both equations:

$$ux - \nu y = \lambda x \tag{3.58a}$$

$$-\frac{1}{T_r}x = \lambda y \tag{3.58b}$$

This will lead to the right eigenvectors:

$$R = \begin{bmatrix} -\lambda_1 T_r & -\lambda_2 T_r \\ 1 & 1 \end{bmatrix}$$
 (3.59)

The eigenvalues defined here is not strictly unique, as more dissipation can be introduced by augmenting them with additional terms.

## 3.2.3 ECS1, ECS2, and ECS3

We set the default eigenvalues for the dissipation matrix according to equation 3.55, and name the flux that utilizes these original terms as ECS1:

$$\Lambda_{ECS1} = \begin{bmatrix} \lambda_1 & 0 \\ 0 & \lambda_2 \end{bmatrix} \tag{3.60}$$

However, from the experience working with entropy consistent fluxes, we anticipate that there would be a need to add more dissipation to the system, leading

to the next definition. To increase the entropy and thus produce more diffusion, these eigenvalues can be enhanced with additional terms, similar to the method recommended by Ismail and Roe (2009):

$$\hat{\mathbf{\Lambda}}_{ECS2} = \begin{bmatrix} \hat{\lambda}_1 + \beta |\hat{\lambda}_1| & 0\\ 0 & \hat{\lambda}_2 + \beta |\hat{\lambda}_2| \end{bmatrix}$$
(3.61)

The coefficient is defined as  $\beta = 0.0001/\nu$ , while ECS2 denotes the flux that utilizes this set of eigenvalues. Another alternative is to add a different diffusion term based on  $\Delta u$ , designated as ECS3:

$$\hat{\Lambda}_{ECS3} = \begin{bmatrix} \hat{\lambda}_1 + \varsigma |\Delta \hat{u}| & 0\\ 0 & \hat{\lambda}_2 \end{bmatrix}$$
 (3.62)

However, the ECS3 is deemed to be outside of the entropy consistency theme and its results are not shown in the results section. All coefficients are empirically determined values that are chosen such that their combination will result in the minimization of oscillations in the system.

# 3.2.4 Length Scale and Time Relaxation

Using either  $\lambda_1$  or  $\lambda_2$ , the relaxation time  $T_r$  which appears in previous equations is defined as:

$$T_{r1} = \frac{L_r}{\lambda_1} = \frac{L_r}{\frac{1}{2} \left[ u - \sqrt{u^2 + \frac{4\nu}{T_r}} \right]}$$
 (3.63a)

$$T_{r2} = \frac{L_r}{\lambda_2} = \frac{L_r}{\frac{1}{2} \left[ u + \sqrt{u^2 + \frac{4\nu}{T_r}} \right]}$$
 (3.63b)

where  $L_r$  is a relaxation length scale that can be optimized based on the scheme. The value of  $T_r$  is proportional to  $\frac{L_r^2}{\nu}$ , and hence would have a low but finite value to reflect proximity to equilibrium conditions for diffusion, as opposed to frozen (high relaxation time). Here, the same definition as in Nishikawa (2010b) is used:

$$L_T = \frac{1}{2\pi} \left[ \frac{Re_{\pi}}{\sqrt{1 + Re_{\pi}^2 + 1}} + \sqrt{1 + \frac{2}{\sqrt{1 + Re_{\pi}^2 + 1}}} \right]$$
(3.64)

where

$$Re_{\pi} \equiv \frac{u(1/\pi)}{\nu} \tag{3.65}$$

To solve for  $T_{r2}$ ,  $\lambda_1$  is firstly simplified:

$$\lambda_1 = \frac{u}{2} \left[ 1 + \sqrt{1 - \frac{4\nu}{u^2 T_r}} \right] \tag{3.66}$$

This is so that it can be used as a conjugate for the denominator of  $T_r$ :

$$\frac{uT_r}{2} = \frac{L_r \left[ 1 - \sqrt{1 + \frac{4\nu}{u^2 T_r}} \right]}{\left[ 1 + \sqrt{1 + \frac{4\nu}{u^2 T_r}} \right] \left[ 1 - \sqrt{1 + \frac{4\nu}{u^2 T_r}} \right]}$$
(3.67)

multiplying out terms gets us:

$$\frac{uT_r}{2L_r} = \frac{1 - \sqrt{1 + \frac{4\nu}{u^2 T_r}}}{1 - (1 + \frac{4\nu}{u^2 T_r})}$$
(3.68)

rearranging of expressions on the left and right leads to:

$$\sqrt{1 + \frac{4\nu}{u^2 T_r}} = 1 + \frac{2\nu}{uL_r} \tag{3.69}$$

both sides are squared to eliminate the root:

$$1 + \frac{4\nu}{u^2 T_r} = 1 + \frac{4\nu}{u L_r} + \frac{4\nu^2}{u^2 L_r^2} \tag{3.70}$$

From here the equation can be simplified into:

$$\frac{1}{T_r} = \frac{u}{L_r} + \frac{\nu}{L_r^2} = \frac{uL_r + \nu}{L_r^2} \tag{3.71}$$

and finally  $T_r$  is defined as:

$$T_r = \frac{L_r}{u + \nu/L_r} \tag{3.72}$$

Thus, in addition to the length scale, the relaxation time is dependent on velocity and also viscosity. Since the  $L_r$  for a given problem is typically fixed and  $\nu$  commonly has a small value, the major determining factor for  $T_r$  is indeed u. However, to get to equation 3.50 from 3.46 in a manner that satisfies entropy conservation and inequality, the simplest way is to set the relaxation time as  $T_r = 1.0$ .

# 3.2.5 Ensuring Entropy Stability in the Dissipation Matrix

The dissipation matrix in the latter part of equation 3.45 is actually the diagonalized eigenstructure of the Jacobian A for the system flux f as stated in equation 3.40. In general, the diagonalization of A is commonly stated as:

$$A = R\Lambda R^{-1} \tag{3.73}$$

where

$$\Lambda = \begin{bmatrix} \lambda_1 & 0 \\ 0 & \lambda_2 \end{bmatrix} \tag{3.74}$$

However, a downside of having the A matrix set up in the manner as shown in equation 3.73 is that its sign cannot be guaranteed to always be correct. In order for the flux function to be entropy stable, the matrix need to be modified into this form:

$$\mathbf{A} = \mathbf{R} \mathbf{D} \mathbf{R}^T, \quad \mathbf{D} = \Lambda \mathbf{S} \tag{3.75}$$

and S must satisfy the differential relations as initially suggested by Barth (1999)

$$\mathbf{R}^{-1}\partial\mathbf{u} = \mathbf{S}\mathbf{R}^T\partial\mathbf{v} \tag{3.76}$$

Here, we define u as in equation 3.41, and v as in equation 3.44. The scaling matrix can then be obtained by finding the inverse and the transpose of the

eigenvectors in equation 3.59. After some manipulation:

$$\mathbf{R}^{-1}[\mathbf{u}] = \frac{1}{\lambda_1 - \lambda_2} \begin{bmatrix} -\frac{1}{T_r} & -\lambda_2 \\ \frac{1}{T_r} & \lambda_1 \end{bmatrix} \begin{bmatrix} du \\ dd \end{bmatrix}$$
(3.77a)

$$SR^{T}[\mathbf{v}] = \begin{bmatrix} S_{a} & S_{b} \\ S_{c} & S_{d} \end{bmatrix} \begin{bmatrix} -2\lambda_{1}T_{r} & 2\nu \\ -2\lambda_{2}T_{r} & 2\nu \end{bmatrix} \begin{bmatrix} du \\ dd \end{bmatrix}$$
(3.77b)

Comparing both sides of equation 3.76 and setting  $T_r = 1$ , the unknowns of  $S_a$  through  $S_d$  can be found by simultaneously solving these equations:

$$-\frac{1}{\lambda_1 - \lambda_2} = -2(S_a \lambda_1 + S_b \lambda_2) \tag{3.78a}$$

$$-\frac{\lambda_2}{\lambda_1 - \lambda_2} = 2\nu(S_a + S_b) \tag{3.78b}$$

$$\frac{1}{\lambda_1 - \lambda_2} = -2(S_c \lambda_1 + S_d \lambda_2) \tag{3.78c}$$

$$\frac{\lambda_1}{\lambda_1 - \lambda_2} = 2\nu (S_c + S_d) \tag{3.78d}$$

The scaling matrix can thus be resolved into:

$$\hat{\mathbf{S}} = \begin{bmatrix} \frac{\hat{\lambda}_{2}^{2} + \nu}{2\nu(\hat{\lambda}_{1} - \hat{\lambda}_{2})^{2} + \epsilon} & -\frac{\hat{\lambda}_{1}\hat{\lambda}_{2} + \nu}{2\nu(\hat{\lambda}_{1} - \hat{\lambda}_{2})^{2} + \epsilon} \\ -\frac{\hat{\lambda}_{1}\hat{\lambda}_{2} + \nu}{2\nu(\hat{\lambda}_{1} - \hat{\lambda}_{2})^{2} + \epsilon} & \frac{\hat{\lambda}_{1}^{2} + \nu}{2\nu(\hat{\lambda}_{1} - \hat{\lambda}_{2})^{2} + \epsilon} \end{bmatrix}$$
(3.79)

A very small coefficient  $\epsilon = 1.0 \times 10^{-10}$  has been added to the denominators to prevent the function from dividing by zero. Even though S is not a diagonal matrix, its components will satisfy 3.76 all the same.

#### 3.2.6 Source Term

The source term of the system flux as stated in equation 3.45,  $f_v$ , can be represented by:

$$[v_d]f_v^* = [v_d f_v] (3.80a)$$

$$[-2d](-\nu d^*) = \left[ (-2d)(-\nu d) \right]$$
 (3.80b)

$$d^* = (d_R - d_L) (3.80c)$$

$$\mathbf{f}_v = -\nu(d_R - d_L) \tag{3.80d}$$

The alternative is to use a central difference physical viscosity,  $f_{\nu}$ , based on the primary variable u instead of the secondary variable d:

$$f_{\nu} = \frac{\nu}{(\Delta x)^2} (u_R - 2u_C + u_L)$$
 (3.81)

uC is the velocity of the middle cell in a three cell sequence.

### 3.2.7 Flux Update

The finite volume scheme for the Burgers' system is completed with the flux update, defined as:

$$\mathbf{U}^{n+1} = \mathbf{U}^n - \frac{\Delta t}{\Delta h} (\mathbf{f}^{*,n} - \mathbf{f}^{*,n-1})$$
 (3.82)

The entropy variables on the next time step is obtained from the flux difference between the current and previous time steps. The schemes of ECS1 and ECS2 defined in this chapter is put through several tests to examine its effectiveness, the results of which will be discussed in later chapters.

#### CHAPTER 4

### FROM EULER TO NAVIER-STOKES

In describing the behavior of fluids in motion, foundations that are established with advection and diffusion are built up into something more and more complex, as additional parameters are added into the framework. Fundamental fluid parameters of density, velocity, and pressure are tracked and observed, and the dynamics of their interactions are summarized and generalized through rules of conservation. Such rules, for example Bernoulli's principle, Pascal's law, and the shallow water equations, are useful in a lot of ways, especially in that they provide predictive information on the unknowns given enough data from known quantities. As one strives to get a picture of what is actually happening in an ever-increasing level of clarity, more of these rules would be required, which will eventually lead to the Navier-Stokes equations. But before getting into the Navier-Stokes', studies often start with the simpler Euler equations. Consider the governing conservation equation, similar to equation 3.5 in the previous chapter:

$$\mathbf{u}_t + \mathbf{f}_x = 0 \tag{4.1}$$

As opposed to the scalar quantities in the advection-diffusion or the Burgers' equations, variables u and f in the Euler's equations are vectors consisting of:

$$\mathbf{u} = \begin{bmatrix} \rho \\ \rho u \\ \rho E \end{bmatrix}, \quad \mathbf{f} = \begin{bmatrix} \rho u \\ p + \rho u^2 \\ \rho u H \end{bmatrix}$$
(4.2)

Here, the density  $\rho$ , velocity u, and pressure p are primitive variables from which other variables are constructed. For example, momentum is defined as  $\rho u$ . Other

variables such as total energy E, and total enthalpy H are defined as:

$$e = \frac{p}{\rho(\gamma - 1)}, \quad E = e + \frac{u^2}{2}, \quad H = E + \frac{p}{\rho}$$
 (4.3)

with e being the specific energy and  $\gamma$  as the ratio of specific heats. Whilst this set of equations would be adequate to describe fluid flow analytically, most flow problems simply do not have analytical solutions; they are solved through the application of numerical techniques instead. However, computational methods almost automatically introduce errors into the solution, thus necessitating additional constraints that could limit these errors and bring numerical results closer to real-world solutions. An example of these constraints is the enforcement of the second law of thermodynamics, also known as entropy control. This 'control' of entropy is essentially a conceptual mechanism to ensure that for smooth flows, entropy is conserved, whilst in discontinuities, physical entropy is always generated (Lefloch et al., 2002). The manner in which these rules are governed is determined by the principles of entropy conservation.

# 4.1 Entropy Consistency for the Euler Equations

Entropy control can be achieved in many ways, but the most direct method is by embedding it explicitly in the numerical scheme. To this end, Harten (1983b) introduced the entropy function U and entropy variable  $\mathbf{v}$  for the Euler equations; these expressions are incorporated into the the governing laws to yield a conservation equation for entropy:

$$\frac{\partial U}{\partial t} + \frac{\partial F}{\partial x} = 0 \tag{4.4}$$

The entropy function in general is:

$$U = -\rho g(S), \quad S = \ln p - \gamma \ln \rho = \ln (\gamma - 1)(\rho E - \frac{\rho u^2}{2}) - \gamma \ln \rho$$
 (4.5)

with g(S) being some suitable function and S the definition of physical entropy. Consequently, the associated entropy variable can be obtained by calculating the gradient of U with respect to the vector  $\mathbf{u}$  as shown in Roe (unpublished):

$$\mathbf{v} = \frac{\partial U}{\partial \mathbf{u}} = \begin{bmatrix} v_1 \\ v_2 \\ v_3 \end{bmatrix} = \begin{bmatrix} -\frac{\partial(\rho g(S))}{\partial \rho} \\ -\frac{\partial(\rho g(S))}{\partial(\rho u)} \\ -\frac{\partial(\rho g(S))}{\partial(\rho E)} \end{bmatrix}$$
(4.6a)
$$= \begin{bmatrix} -g(S) - \rho g'(S) \frac{\partial(S(\rho))}{\partial \rho} \\ -\rho g'(S) \frac{\partial(S(\rho u))}{\partial(\rho u)} \\ -\rho g'(S) \frac{\partial(S(\rho E))}{\partial(\rho E)} \end{bmatrix}$$
(4.6b)

Solving for each element in v results in:

$$\mathbf{v} = g'(S)(-\rho) \begin{bmatrix} \frac{g(S)}{g'(S)(\rho)} + \frac{\partial}{\partial \rho} \\ \frac{\partial}{\partial (\rho u)} \\ \frac{\partial}{\partial (\rho E)} \end{bmatrix} (\ln(\gamma - 1)(\rho E - \frac{(\rho u)^2}{2\rho}) - \gamma \ln \rho) \quad (4.7a)$$

$$= g'(S)(-\rho) \begin{bmatrix} \frac{g(S)}{g'(S)(\rho)} + (\gamma - 1)\frac{E}{\rho p} - (\gamma - 1)\frac{E - u^2/2}{p} - \frac{\gamma}{\rho} \\ -\frac{(\gamma - 1)u}{p} \\ \frac{\gamma - 1}{p} \end{bmatrix}$$
(4.7b)  
$$= -(\gamma - 1)\frac{g'(S)}{p} \begin{bmatrix} E + \frac{p}{\gamma - 1}(\frac{g(S)}{g'(S)} - (\gamma + 1)) \\ -\rho u \\ \rho \end{bmatrix}$$
(4.7c)

$$= -(\gamma - 1)\frac{g'(S)}{p} \begin{bmatrix} E + \frac{p}{\gamma - 1}(\frac{g(S)}{g'(S)} - (\gamma + 1)) \\ -\rho u \\ \rho \end{bmatrix}$$
(4.7c)

It would make sense to construct g(S) in a manner that would simplify  $\mathbf{v}$  as much as possible, but Hughes et al. (1986) showed that there exist only one entropy function that is extendable to the Navier-Stokes equations:

$$U = -\frac{\rho S}{\gamma - 1} \tag{4.8}$$

By substitution into equation 4.6(b), this choice of U leads to  $\mathbf{v}$  becoming:

$$\mathbf{v} = \begin{bmatrix} \frac{\gamma - S}{\gamma - 1} - \frac{1}{2} \frac{\rho}{p} (u^2) \\ \frac{\rho u}{p} \\ -\frac{\rho}{p} \end{bmatrix}$$
(4.9)

With the entropy variables defined, they can now replace the original conservative variables in equation 4.1:

$$\mathbf{v}_u \ \mathbf{u}_t + \mathbf{v}_u \ \mathbf{A} \mathbf{u}_x = 0 \tag{4.10}$$

In equation 4.10, entropy is conserved along with the quantities of mass, momentum and energy. The matrix A is a Jacobian which will be addressed subsequently.

### 4.1.1 Discrete Entropy Conservative Fluxes

Entropy consistent flux derivation based on the finite volume formulation for Euler's equation is similar to that of the scalar equations established by Roe (unpublished) shown in 3.12:

$$h_L \frac{\partial u_L}{\partial t} = \mathbf{f}_L - \mathbf{f}^* \tag{4.11a}$$

$$h_R \frac{\partial u_R}{\partial t} = \mathbf{f}^* - \mathbf{f}_R \tag{4.11b}$$

The difference is that the fluxes of f consist of vectors as opposed to scalar quanti-

ties. With everything else being equal, the entropy conservative flux must adhere to a similar conversation equation as demonstrated in 3.20:

$$[\mathbf{v}^T]\mathbf{f}^* = [\mathbf{v}^T\mathbf{f}] - [F] \tag{4.12}$$

For the chosen form of physical entropy U, the term  $\mathbf{v}^T \mathbf{f}$  can be represented by (Ismail, 2006):

$$\mathbf{v}^T \mathbf{f} = \rho u + F \tag{4.13}$$

This results in the flux at the interface simplifying to:

$$[\mathbf{v}]\mathbf{f}^* = [\rho u] \tag{4.14}$$

There are a number of ways to interpret this relation, but a practical solution was found in Roe (unpublished). In the paper, the flux takes the form of:

$$[v_1]f_1^* + [v_2]f_2^* + [v_3]f_3^* - [\rho u] = 0 (4.15)$$

Define parameter vectors

$$z_1 = \sqrt{\frac{\rho}{p}}, \quad z_2 = \sqrt{\frac{\rho}{p}}u, \quad z_3 = \sqrt{\rho p}$$
 (4.16)

Construct f\* in the general form of equation 4.2, but with each of its constituents evaluated as functions of the parameter vectors, derivations of which is available in Ismail (2006):

$$\mathbf{f}^* = \begin{bmatrix} f_1^* \\ f_2^* \\ f_3^* \end{bmatrix} = \begin{bmatrix} \overline{z_2} z_3^{ln} \\ \frac{\overline{z_3} + \overline{z_2} f_1^*}{\overline{z_1}} \\ \frac{\frac{\gamma+1}{\gamma-1} \frac{f_1^*}{z_1^{ln}} + \overline{z_2} f_2^*}{\overline{z_2}} \end{bmatrix}$$
(4.17)

For a given quantity z, its arithmetic mean  $\overline{z}$  and logarithmic mean  $z^{ln}$  are obtained from their values at the left and right cells at each interface:

$$\overline{z} = \frac{z_L + z_R}{2}, \quad z^{ln} = \frac{z_L - z_R}{ln(z_L) - ln(z_R)}$$
 (4.18)

Quantities used to calculate the fluxes are thus approximated by the averaged states of the flow parameters, definitions of which are shown in Appendix A:

$$\hat{\rho} = \overline{z_1} z_3^{ln}, \quad \hat{u} = \frac{\overline{z_2}}{\overline{z_1}}, \quad \hat{p_1} = \frac{\overline{z_3}}{\overline{z_1}}$$
 (4.19a)

$$\hat{p}_{2} = \frac{\gamma + 1}{2\gamma} \frac{z_{3}^{ln}}{z_{1}^{ln}} + \frac{\gamma - 1}{2\gamma} \frac{\overline{z_{3}}}{\overline{z_{1}}}, \quad \hat{a} = \left(\frac{\gamma \hat{p}_{2}}{\hat{\rho}}\right)^{\frac{1}{2}}, \quad \hat{H} = \frac{\hat{a}^{2}}{\gamma - 1} + \frac{\hat{u}^{2}}{2}$$
(4.19b)

Therefore f\* can be described by the averaged variables as

$$\mathbf{f}^* = \begin{bmatrix} \hat{\rho}\hat{u} \\ \hat{p_1} + \hat{\rho}\hat{u}^2 \\ \hat{\rho}\hat{u}\hat{H} \end{bmatrix} = \mathbf{f}_c \tag{4.20}$$

## 4.1.2 Entropy Production and the Dissipative Flux

Having a conservative flux  $f^*$  constructed in the manner shown by equation 4.20 is sound theoretically. However, the symmetric functions of the input states from the left and right of the interface make  $f_c$  similar to central difference schemes, which are numerically unstable in nature. Another issue as seen from the Burgers' equation in the previous chapter, is the incompatibility of this type of conservative flux to the second law of thermodynamics, which states that entropy is always generated whenever an irreversible process is encountered. The actual relationship

of the entropy function and its flux should follow that of equation 3.14:

$$\frac{\partial U}{\partial t} + \frac{\partial F}{\partial x} \le 0 \tag{4.21}$$

The implication of this inequality is that equation 4.12, the basis of the conservative flux, does not always hold true, since it does not account for any entropy generation. One way to tackle these two problems is to add an upwinding term that provides stability to the flux, and a production term to account for extra entropy. For a system of equations, however, both issues can be countered by introducing a diffusion term that can provide a dissipative influence to the flux. Consider  $\dot{U}$  (Ismail and Roe, 2009), which is the difference between the total entropy change of the system and the entropy change borne out by the conservative flux:

$$\dot{U} = [\mathbf{v}]^T \mathbf{f}^* - [\mathbf{v}^T \mathbf{f}] + [F] \tag{4.22}$$

This term can be incorporated into the flux through the upwinding term, thus enforcing both entropy stability and production simultaneously by using a flux in the general form of:

$$\mathbf{f}^* = \mathbf{f}_c - \frac{1}{2}\mathbf{Q}[\mathbf{u}], \quad \mathbf{Q} = \mathbf{R}\Lambda\mathbf{L}$$
 (4.23)

 $f_c$  is the conservative flux and L is defined as the inverse of the right-eigenvector,  $L = R^{-1}$ . Meanwhile, R can be defined by using averaged quantities as

$$\hat{\mathbf{R}} = \begin{bmatrix} 1 & 1 & 1 \\ \hat{u} - \hat{a} & \hat{u} & \hat{u} + \hat{a} \\ \hat{H} - \hat{u}\hat{a} & \frac{1}{2}\hat{u}^2 & \hat{H} + \hat{u}\hat{a} \end{bmatrix}$$
(4.24)

whilst the eigenvalues for the inviscid Jacobian,  $\Lambda$ , is:

$$\hat{\mathbf{\Lambda}} = \begin{bmatrix} |\hat{u} - \hat{a}| & 0 & 0 \\ 0 & |\hat{u}| & 0 \\ 0 & 0 & |\hat{u} + \hat{a}| \end{bmatrix}$$
 (4.25)

The use of entropy variables instead of conventional conservative variables necessitate the application of the Merriam-Barth identity (Barth, 1999) with a slight adjustment, similar to that in equation 3.76:

$$\mathbf{R}^{-1}\partial\mathbf{u} = \mathbf{S}\mathbf{R}^T\partial\mathbf{v} \tag{4.26}$$

The brackets around [v] should be interpreted as [v] =  $\mathbf{v}_R - \mathbf{v}_L$ , a convention that applies similarly for [u] as well.  $\mathbf{R}^T$  is the transpose of  $\mathbf{R}$ , while the matrix  $\mathbf{S}$  is a form of proper scaling that enables conversion to the former from the latter, and can be resolved as:

$$\hat{\mathbf{S}} = \begin{bmatrix} \frac{\hat{\rho}}{2\gamma} & 0 & 0\\ 0 & \frac{(\gamma - 1)\hat{\rho}}{\gamma} & 0\\ 0 & 0 & \frac{\hat{\rho}}{2\gamma} \end{bmatrix}$$
(4.27)

Equation 4.26 highlights the main difference between the standard conservative flux, which uses the standard conservative variables **u**, and the entropy conservative flux using the mapped entropy variables **v**. The use of entropy variables ensure stability in the sense that the entropy of the system will always be generated, or at least remain zero. Thus the entropy stable version of equation 4.23 is

similar to equation 3.75:

$$\mathbf{f}^* = \mathbf{f}_c - \frac{1}{2}\mathbf{Q}[\mathbf{u}] = \mathbf{f}_c - \frac{1}{2}\mathbf{A}[\mathbf{v}] = \mathbf{f}_c - \frac{1}{2}\hat{\mathbf{R}}\hat{\mathbf{\Lambda}}\hat{\mathbf{S}}\hat{\mathbf{R}}^T \partial \mathbf{v}$$
 (4.28)

Equation 4.28 implies that the Jacobian A is approximated by the eigen-structure which has been inserted within it the proper scaling. From the right-eigenvectors and the finite volume discretization, a flux function can be defined to obtain a numerical scheme. However, as shown in equation 4.28 the function is merely an approximation for which the accuracy can be further improved upon by adding supplementary flow information. To get a more complete description of flow, other physical characteristics would need to be included to the equation model, such as body forces and energy losses. This has been achieved through direct discretization of the Navier-Stokes equations, as in the various numerical schemes currently available. As opposed to most schemes, the work in this thesis is an attempt to employ an alternative method by recasting the Navier-Stokes in the form of a first-order hyperbolic system.

### 4.2 Conservation Laws for the Navier-Stokes Equations

The Navier-Stokes equation describes the conservation of mass, momentum, and energy similarly to the Euler equations, and additionally the losses attributed to each of these parameters due to stresses from fluid viscosity and heat transfer. In one dimension:

$$\frac{\partial \rho}{\partial t} + \frac{\partial (\rho u)}{\partial x} = 0 \tag{4.29a}$$

$$\frac{\partial(\rho u)}{\partial t} + \frac{\partial(\rho u^2 + p + \tau)}{\partial x} = 0 \tag{4.29b}$$

$$\frac{\partial(\rho E)}{\partial t} + \frac{\partial(\rho u H - \tau u + q)}{\partial x} = 0 \tag{4.29c}$$

The variable  $\tau$  represents the viscous stress and q symbolizes the heat flux. The definition for each variable is as follows:

$$E = e + \frac{u^2}{2}, \quad H = E + \frac{p}{\rho}, \quad e = \frac{p(\gamma - 1)}{\rho}$$

$$\tau = \frac{4}{3}\mu \frac{\partial u}{\partial x}, \quad q = -\frac{\mu}{Pr(\gamma - 1)} \frac{\partial T}{\partial x}, \quad \mu = \frac{M_{\infty}}{Re_{\infty}} \frac{1 + C/T_{\infty}}{T + C/T_{\infty}} T^{\frac{3}{2}}$$
(4.30a)

The newly introduced  $\mu$  is the viscosity as defined by Sutherland's law, involving values of the free stream Mach number  $M_{\infty}$ , the free stream Reynolds number  $Re_{\infty}$ , the free stream and ambient temperatures respectively  $T_{\infty}$  and T, and the Sutherland constant C = 110.5[K]. The three conservation equations in 4.29 can be written in many ways, depending on the method of derivation or their intended application. Consider the alternative of an equivalent first order system proposed by Nishikawa (2011a), in which the higher order terms from the Navier-Stokes equations are separated into an auxiliary equation, with the heat flux omitted:

$$\frac{\partial \rho}{\partial t} + \frac{\partial (\rho u)}{\partial x} = 0 \tag{4.31a}$$

$$\frac{\partial(\rho u)}{\partial t} + \frac{\partial(\rho u^2 + p - \tau)}{\partial x} = 0 \tag{4.31b}$$

$$\frac{\partial(\rho E)}{\partial t} + \frac{\partial(\rho uH - \tau u + q)}{\partial x} = 0 \tag{4.31c}$$

$$\frac{\partial \tau}{\partial t} - \frac{\mu_v}{T_v} \left( \frac{\partial u}{\partial x} - \frac{\tau}{\mu_v} \right) = 0 \tag{4.31d}$$

The scaled viscosity  $\mu_v$  and the relaxation time  $T_v$  are defined in the following with subscript v denoting the viscous stress:

$$\mu_v = \frac{4}{3}\mu \quad T_v = \frac{L^2}{\nu_v} \quad \nu_v = \frac{\mu_v}{\rho}$$
 (4.32)

L is a length scale as defined in 3.64, whilst  $\nu_v$  is the kinematic viscosity. In the

form similar to equation 4.1, the system is represented by:

$$\mathbf{P}^{-1}\frac{\partial \mathbf{u}}{\partial t} + \frac{\partial \mathbf{f}}{\partial x} = \mathbf{B} \tag{4.33}$$

The matrix **P** is a local preconditioning for the viscous stress and heat flux, whilst matrix **B** contains the balance for those two secondary variables. Since both matrices affect only the auxiliary equations in the system, equation 4.33 can still be considered as conservative. Individually, the vectors are defined as:

$$\mathbf{u} = \begin{bmatrix} \rho \\ \rho u \\ \rho E \\ \tau \end{bmatrix}, \quad \mathbf{f} = \mathbf{f}_i + \mathbf{f}_v = \begin{bmatrix} \rho u \\ \rho u^2 + p \\ \rho u H \\ 0 \end{bmatrix} + \begin{bmatrix} 0 \\ -\tau \\ -\tau u \\ -u \end{bmatrix},$$

$$\mathbf{B} = \begin{bmatrix} 0 \\ 0 \\ 0 \\ \frac{\tau}{\mu_{\nu}} \end{bmatrix}, \quad \mathbf{P}^{-1} = \begin{bmatrix} 1 & 0 & 0 & 0 \\ 0 & 1 & 0 & 0 \\ 0 & 0 & 1 & 0 \\ 0 & 0 & 0 & \frac{T_{\nu}}{\mu_{\nu}} \end{bmatrix}$$
(4.34)

For the purpose of constructing a numerical flux, the Jacobian matrix A is introduced, where

$$PA = P\frac{\partial f}{\partial u} = PA_i + PA_v \tag{4.35}$$

As a matter of convenience, the Jacobian is split into the inviscid  $A_i$  and its viscous counterpart  $A_v$ . These Jacobians contains eigenvalues and eigenvectors configured as so:

$$\mathbf{A}_i = \mathbf{\Lambda}_i \mathbf{R}_i \mathbf{L}_i, \quad \mathbf{A}_v = \mathbf{\Lambda}_v \mathbf{R}_v \mathbf{L}_v \tag{4.36}$$

The eigenvalue  $\Lambda_i$  can be defined using averaged quantities as:

$$\hat{\Lambda}_{i} = \begin{bmatrix} \lambda_{1,i} & \lambda_{2,i} & \lambda_{3,i} & \lambda_{4,i} \end{bmatrix} = \begin{bmatrix} |\hat{u} - \hat{a}| & 0 & 0 & 0 \\ 0 & |\hat{u}| & 0 & 0 \\ 0 & 0 & |\hat{u} + \hat{a}| & 0 \\ 0 & 0 & 0 & 0 \end{bmatrix}$$
(4.37)

The components of this set of eigenvalues consist of averaged quantities identical to equation 4.25. It follows that the right eigenvectors  $\mathbf{R}_i$  corresponding to the inviscid Jacobian are defined as

$$\hat{\mathbf{R}}_{i} = \begin{bmatrix} \mathbf{r}_{1,i} & \mathbf{r}_{2,i} & \mathbf{r}_{3,i} & \mathbf{r}_{4,i} \end{bmatrix} = \begin{bmatrix} 1 & 1 & 1 & 0 \\ \hat{u} - \hat{a} & \hat{u} & \hat{u} + \hat{a} & 0 \\ \hat{H} - \hat{u}\hat{a} & \frac{1}{2}\hat{u}^{2} & \hat{H} + \hat{u}\hat{a} & 0 \\ 0 & 0 & 0 & 0 \end{bmatrix}$$
(4.38)

Conversely, eigenvalues of the viscous Jacobian  $\Lambda_v$  are:

whilst the associated viscous right eigenvectors are:

$$\hat{\mathbf{R}}_{v} = \begin{bmatrix} \mathbf{r}_{1,v} & \mathbf{r}_{2,v} & \mathbf{r}_{3,v} & \mathbf{r}_{4,v} \end{bmatrix} = \begin{bmatrix} 0 & \frac{1}{\hat{u}} & 0 & 0 \\ 0 & 1 & 1 & 1 \\ 1 & 0 & \hat{u} + \frac{\tau}{(Pr_{n}^{2}-1)\hat{\rho}} & \hat{u} - \frac{\tau}{(Pr_{n}^{2}-1)\hat{\rho}} \\ 0 & 0 & a_{v} & -a_{v} \end{bmatrix}$$

$$(4.40)$$

The Prandtl number  $Pr_n$  is defined by the wave speeds  $a_v$  and  $a_h$ :

$$Pr_n \equiv \frac{a_v}{a_h}, \quad a_v = \sqrt{\frac{\nu_v}{T_v}} \tag{4.41}$$

The left eigenvectors  $\mathbf{L}_i$  and  $\mathbf{L}_v$  can be found by taking the inverse of the right eigenvectors  $\mathbf{R}_i$  and  $\mathbf{R}_v$  respectively. With all the components defined, the full Jacobian in Nishikawa (2011a) is:

$$PA = \sum_{k=1}^{3} \Lambda_{i,k} R_{i,k} L_{i,k} + \sum_{k=1}^{4} \Lambda_{v,k} R_{v,k} L_{v,k}$$
(4.42)

Thus, the flux at the interface is described as:

$$f^* = \frac{1}{2}[f_R + f_L] - \frac{1}{2}P^{-1}|PA|\Delta u$$
 (4.43)

However, the entropy consistent version of this system will use a slightly different set-up for the Jacobian, based on equation 4.28 as proposed in Ismail (2006).

# 4.3 Entropy Consistent Fluxes for the First-Order System of Navier-Stokes Equations

For the purpose of creating a new flux function, the concept of entropy consistency is combined with the Navier-Stokes first order system. This can be achieved by modifying equation 4.43 into an entropy consistent expression for the interface flux in the form of equation 4.28. Modifications include:

- The elimination of the term for heat flux and all its associated variables.

  This is so that the effects of the viscous stress can be observed in isolation.
- The conservative variables [u] are mapped to their associated set of entropy variables [v] via the introduction of the entropy function U.
- An extended version for  $f_c$  is constructed to replace  $\frac{1}{2}[f_R + f_L]$ ,
- The original Jacobian of PA in equation 4.42 is converted into its entropy stable equivalent.

The first step is to construct an entropy function which depends on both the inviscid and viscous fluxes similar to the strategy used for the Burgers equation. Since  $U = -\rho S/(\gamma - 1)$  is the only entropy function from Euler equations that can be extended to the Navier-Stokes equations Hughes et al. (1986), it is chosen to represent the inviscid fluxes. On the other side, the viscous entropy functions must be of the form of the viscous stresses  $(\tau)$  and the temperature gradients (q). For this paper, we concentrate on the effects of viscosity by eliminating the influence of heat transfer from the system, meaning that q = 0. Overall, these entropy functions are defined as:

$$U_i = -\frac{\rho S}{\gamma - 1}, \quad U_v = \tau^2 + \rho u^2 \tag{4.44}$$

with its fluxes defined as

$$F_i = -\frac{\rho u S}{\gamma - 1}, \quad F_v = -2u\tau \tag{4.45}$$

Unlike the Burgers equation in which entropy is viewed as one parameter consisting the summation of inviscid and viscous parts, the Navier-Stokes entropies are two different entities that are practically untied from each other. This is due to the philosophy espoused by Nishikawa (2011a) and adopted in this paper specifically for the Navier-Stokes model, which is to treat the inviscid and viscous portions of the equations as two individual, yet interconnected hyperbolic systems. Thus, defining the function and the fluxes in this way means that each type would only need to adhere to the entropy conditions of their own respective systems, one for the inviscid (physical) and the other for the viscous part. Both  $U^i$  and  $U^v$  independently satisfy the entropy inequality of equation 3.13, and the constraint of the entropy pair theorem given in equation 3.8 from Hughes et al. (1986). Following that, the entropy variables and its discrete fluxes are split into two separate parts:

$$\mathbf{v}_i = \frac{\partial U_i}{\partial \mathbf{u}}, \quad \mathbf{v}_v = \frac{\partial U_v}{\partial \mathbf{u}}, \quad \hat{\mathbf{f}} = \hat{\mathbf{f}}_i + \hat{\mathbf{f}}_v$$
 (4.46)

The inviscid variables are defined as:

$$\mathbf{v}_{i} = \begin{bmatrix} \frac{\gamma - S}{\gamma - 1} - \frac{1}{2} \frac{\rho u^{2}}{p} \\ \frac{\rho u}{p} \\ -\frac{\rho}{p} \\ 0 \end{bmatrix}, \quad \hat{\mathbf{f}}_{i} = \begin{bmatrix} \hat{\rho} \hat{u}_{1} \\ \hat{p}_{1} + \hat{\rho}(\hat{u}_{1})^{2} \\ \hat{\rho} \hat{u}_{1} \hat{H} \\ 0 \end{bmatrix}$$
(4.47)

The flux  $\hat{\mathbf{f}}$  consists of averaged quantities that are to be determined by ensuring entropy is conserved. Similar to equation 4.12, entropy conservation requires

$$[\mathbf{v}_i]^T \mathbf{f}_i^* - [\mathbf{v}_i \cdot \mathbf{f}_i] = -[F_i] \tag{4.48}$$

Using the identity  $[\mathbf{v}_i \cdot \mathbf{f}_i] - [F_i] = [\rho u]$ , this equation becomes

$$[\mathbf{v}_i]^T \hat{\mathbf{f}}_i = [\rho u] \tag{4.49}$$

By choosing the averaged quantities as given in Appendix A, the discrete inviscid fluxes conserve the inviscid part of entropy  $U_i$  as shown in Ismail and Roe (2009). The remaining averaged quantity for the flux of  $\tau$  is now determined, starting with the viscous entropy variables and discrete fluxes:

$$\mathbf{v}_{v} = \begin{bmatrix} -u^{2} \\ 2u \\ 0 \\ 2\tau \end{bmatrix}, \quad \hat{\mathbf{f}}_{v} = \begin{bmatrix} 0 \\ -\tau^{*} \\ -\tau^{*}u_{2}^{*} \\ -\frac{\mu_{v}}{T_{v}}u_{2}^{*} \end{bmatrix}$$
(4.50)

As before, the entropy balance is enforced through the expression:

$$[\mathbf{v}_v]^T \mathbf{f}_v^* - [\mathbf{v}_v \cdot \mathbf{f}_v] = -[F_v]$$
 (4.51a)

$$-[2u]\tau^* - [2\tau]\frac{\mu_v}{T_v}u_2^* + [2u\tau^*] + [2\tau\frac{\mu_v}{T_v}u_2^*] = [2u\tau]$$
 (4.51b)

$$-[u]\tau^* - \frac{\mu_v}{T_v}[\tau]u_2^* + [\frac{\mu_v}{T_v}\tau u_2^*] = 0$$
 (4.51c)

Using the identity  $[ab] = \overline{a}[b] + \overline{b}[a]$ , the equation expands to

$$-[u]\tau^* - \frac{\mu_v}{T_v}[\tau]u_2^* + \frac{\mu_v}{T_v}([\tau]\overline{u} + \overline{\tau}[u]) = 0$$
 (4.52)

The intent here is to control the viscous numerical fluxes to conserve 'entropy' and not to generate more of it, hence:

$$\tau^* = \frac{\mu_v}{T_v} \overline{\tau}, \quad u_2^* = \overline{u} \tag{4.53}$$

Conservation of the entropy flux would allow us to have better control over the diffusion, since all of it would be confined to the dissipation expressions. To this end, the Jacobian matrix A is introduced for both parts of the system, in a form similar to the Burgers' equation model:

$$PA = P\frac{\partial f}{\partial u} = PA_i + PA_v = R_i |\Lambda_i S_i| (R_i)^T + R_v |\Lambda_v S_v| (R_v)^T$$
(4.54)

The dissipation expression for PA presented here has been shown in Roe (unpublished) to be more suitable for entropy consistency. Following equation 4.28:

$$\mathbf{f}^* = \hat{\mathbf{f}}_i - \frac{1}{2}\hat{\mathbf{R}}_i|\hat{\mathbf{\Lambda}}_i\hat{\mathbf{S}}_i|(\hat{\mathbf{R}}_i)^T[\mathbf{v}_i] + \hat{\mathbf{f}}_v - \frac{1}{2}\hat{\mathbf{R}}_v|\hat{\mathbf{\Lambda}}_v\hat{\mathbf{S}}_v|(\hat{\mathbf{R}}_v)^T[\mathbf{v}_v]$$
(4.55)

With the system flux fully defined, the entropy generation of the system can be determined by analysis on each of its components. For the inviscid part:

$$\dot{U}_i = [\mathbf{v}_i]^T \hat{\mathbf{f}}_i - [\hat{\rho}\hat{u}] - \frac{1}{2} [\mathbf{v}_i]^T (\hat{\mathbf{R}}_i | \hat{\mathbf{\Lambda}}_i \hat{\mathbf{S}}_i | \hat{\mathbf{R}}_i^T [\mathbf{v}_i])$$
(4.56a)

$$= -\frac{1}{2} (\hat{\mathbf{R}}_i | \hat{\mathbf{\Lambda}}_i \hat{\mathbf{S}}_i | \hat{\mathbf{R}}_i^T [\mathbf{v}_i]^2)$$
(4.56b)

$$\leq 0 \tag{4.56c}$$

Meanwhile, for the viscous part:

$$\dot{U}_v = [\mathbf{v}_v]^T \mathbf{f}_v^* - [\mathbf{v}_v \cdot \hat{\mathbf{f}}_v] - [F_v] - \frac{1}{2} [\mathbf{v}_v]^T (\hat{\mathbf{R}}_v | \hat{\mathbf{\Lambda}}_v \hat{\mathbf{S}}_v | \hat{\mathbf{R}}_v^T [\mathbf{v}_v])$$
(4.57a)

$$= -\frac{1}{2} (\hat{\mathbf{R}}_v | \hat{\mathbf{\Lambda}}_v \hat{\mathbf{S}}_v | \hat{\mathbf{R}}_v^T [\mathbf{v}_v]^2)$$

$$(4.57b)$$

$$\leq 0 \tag{4.57c}$$

Since entropy is conserved for both the inviscid and viscous variables, entropy production is generated exclusively from their respective dissipation matrices. The fact that the matrices are the negative of positive definite terms therefore guarantees that the entropy for the whole system would be a decreasing function. These dissipation matrices  $(\hat{\mathbf{R}}_i|\hat{\boldsymbol{\Lambda}}_i|\hat{\mathbf{R}}_i^T[\mathbf{v}_i])$  and  $(\hat{\mathbf{R}}_v|\hat{\boldsymbol{\Lambda}}_v|\hat{\mathbf{R}}_v^T[\mathbf{v}_v])$  are diagonalized from their respective flux Jacobians, which is obtained by setting  $A = \frac{\partial \mathbf{f}}{\partial \mathbf{u}}$ . For the viscous fluxes:

$$\mathbf{A}_{v} = \begin{bmatrix} 0 & 0 & 0 & 0 \\ 0 & 0 & 0 & -1 \\ \frac{\tau u}{\rho} & -\frac{\tau}{\rho} & 0 & -u \\ \frac{u}{\rho} & -\frac{1}{\rho} & 0 & 0 \end{bmatrix}$$
 (4.58)

From  $A_i$  and  $A_v$ , The eigenvalues  $\Lambda_i$  and  $\Lambda_v$  are calculated to be:

The components of this set of eigenvalues consist of averaged quantities identical to those defined in Ismail and Roe (2009). It follows that the associated right eigenvectors  $\mathbf{R}^{i}$  corresponding to the inviscid eigenvalues are:

$$\hat{\mathbf{R}}_{i} = \begin{bmatrix} 1 & 1 & 1 & 0 \\ \hat{u} - \hat{a} & \hat{u} & \hat{u} + \hat{a} & 0 \\ \hat{H} - \hat{u}\hat{a} & \frac{1}{2}\hat{u}^{2} & \hat{H} + \hat{u}\hat{a} & 0 \\ 0 & 0 & 0 & 0 \end{bmatrix}$$
(4.60)

The inviscid eigenvectors are also identical to the one determined by Ismail and Roe (2009), excluding the extra row and column of zero-vectors due to the presence of the viscous transport equation. On the other hand, the right eigenvectors  $\mathbf{R}^{v}$  corresponding to the viscous eigenvalues are:

$$\hat{\mathbf{R}}_{v} = \begin{bmatrix} 0 & \frac{1}{\bar{u}} & 0 & 0 \\ 0 & 1 & \sqrt{\bar{\rho}} & -\sqrt{\bar{\rho}} \\ 1 & 0 & \bar{\tau} + \sqrt{\bar{\rho}}\bar{u} & \bar{\tau} - \sqrt{\bar{\rho}}\bar{u} \\ 0 & 0 & 1 & 1 \end{bmatrix}$$
(4.61)

In the viscous set of eigenvectors, the averaged variables  $\bar{\tau}$  and  $\bar{u}$  are "entropy-conserving" quantities derived from equation 4.53. Next, the scaling matrices  $S_i$ 

and  $S_v$  can then be found based on equation 4.26 by setting:

$$\mathbf{R}_{i}^{-1}\partial\mathbf{u} = \mathbf{S}_{i}\mathbf{R}_{i}^{T}\partial\mathbf{v}_{i}, \quad \mathbf{R}_{v}^{-1}\partial\mathbf{u} = \mathbf{S}_{v}\mathbf{R}_{v}^{T}\partial\mathbf{v}_{v}$$
 (4.62)

These matrices are obtained by solving their respective expressions, with  $S_i$  having a familiar form:

$$\hat{\mathbf{S}}_{i} = \begin{bmatrix} \frac{\hat{\rho}}{2\gamma} & 0 & 0 & 0 \\ 0 & \frac{(\gamma - 1)\hat{\rho}}{\gamma} & 0 & 0 \\ 0 & 0 & \frac{\hat{\rho}}{2\gamma} & 0 \\ 0 & 0 & 0 & 0 \end{bmatrix}$$
(4.63)

For  $S_v$  however, the first two rows of the viscous dissipation matrix will not affect the overall dissipation since the first two eigenvalues are zero. Thus the viscous scaling matrix is computed such that only the last two rows are determined (the rest are set to zeros) to satisfy the differential relations of equation 4.62 for the viscous part of the system. This equation is expanded into:

$$\hat{\mathbf{R}}_{v}^{-1} = \begin{bmatrix} \bar{u}^{2} & -\bar{u} & 1 & -\bar{\tau} \\ \bar{u} & 0 & 0 & 0 \\ -\frac{\bar{u}}{2\sqrt{\bar{\rho}}} & \frac{1}{2\sqrt{\bar{\rho}}} & 0 & \frac{1}{2} \\ \frac{\bar{u}}{2\sqrt{\bar{\rho}}} & -\frac{1}{2\sqrt{\bar{\rho}}} & 0 & \frac{1}{2} \end{bmatrix}, \quad \partial \mathbf{u} = \begin{bmatrix} d\rho \\ d\rho u \\ d\rho E \\ d\tau \end{bmatrix} = \begin{bmatrix} du_{1} \\ du_{2} \\ du_{3} \\ du_{4} \end{bmatrix}$$
(4.64a)
$$\hat{\mathbf{R}}_{v}^{T} = \begin{bmatrix} 0 & 0 & 1 & 0 \\ \frac{1}{\bar{u}} & 1 & 0 & 0 \\ 0 & \sqrt{\bar{\rho}} & \bar{\tau} + \sqrt{\bar{\rho}\bar{u}} & 1 \\ 0 & -\sqrt{\bar{\rho}} & \bar{\tau} - \sqrt{\bar{\rho}\bar{u}} & 1 \end{bmatrix}, \quad \partial \mathbf{v}_{v} = \begin{bmatrix} -du^{2} \\ 2du \\ 0 \\ 2d\tau \end{bmatrix} = \begin{bmatrix} -d(\frac{u_{2}^{2}}{u_{1}^{2}}) \\ 2d(\frac{u_{2}}{u_{1}}) \\ 0 \\ 2du_{4} \end{bmatrix}$$

$$(4.64b)$$

The entropy variable partial differential is thus:

$$\partial \mathbf{v}_{v} = \begin{bmatrix} -u_{2}^{2}d(\frac{1}{u_{1}^{2}}) - \frac{1}{u_{1}^{2}}du_{2}^{2} \\ 2u_{2}d(\frac{1}{u_{1}}) + 2\frac{1}{u_{1}}du_{2} \\ 0 \\ 2du_{4} \end{bmatrix} = \begin{bmatrix} -2\frac{u_{1}^{2}u_{2}du_{2} - u_{2}^{2}u_{1}du_{1}}{u_{1}^{4}} \\ 2\frac{u_{1}du_{2} - u_{2}du_{1}}{u_{1}^{2}} \\ 0 \\ 2du_{4} \end{bmatrix}$$
(4.65)

Using this  $\partial \mathbf{v}_v$  result, equation 4.62 can be further elaborated as:

$$\begin{bmatrix} \bar{u}^{2}du_{1} - \bar{u}du_{2} + du_{3} - \tau du_{4} \\ \bar{u}du_{1} \\ \frac{-\bar{u}du_{1} + du_{2}}{2\sqrt{\bar{\rho}}} + \frac{du_{4}}{2} \\ \frac{\bar{u}du_{1} - du_{2}}{2\sqrt{\bar{\rho}}} + \frac{du_{4}}{2} \end{bmatrix} = \mathbf{S}_{v} \begin{bmatrix} 0 \\ 2(\frac{u_{1}du_{2} - u_{2}du_{1}}{u_{1}^{2}} - \frac{u_{1}^{2}u_{2}du_{2} - u_{2}^{2}u_{1}du_{1}}{\bar{u}u_{1}^{4}}) \\ 2\sqrt{\bar{\rho}}\frac{u_{1}du_{2} - u_{2}du_{1}}{u_{1}^{2}} + 2du_{4} \\ -2\sqrt{\bar{\rho}}\frac{u_{1}du_{2} - u_{2}du_{1}}{u_{1}^{2}} + 2du_{4} \end{bmatrix}$$

$$(4.66)$$

Consider the  $S_v$  matrix having the form of:

$$\hat{\mathbf{S}}_{v} = \begin{bmatrix} 0 & 0 & 0 & 0 \\ 0 & 0 & 0 & 0 \\ K_{1} & K_{2} & K_{3} & K_{4} \\ K_{2} & K_{1} & K_{4} & K_{3} \end{bmatrix}$$
(4.67a)

To obtain the components of  $S_v$ , we can start with the third row of the matrix and find its dot product with the term  $R_v^T \partial \mathbf{v}_v$ :

$$\mathbf{S}_{v}\mathbf{R}_{v}^{T}\partial\mathbf{v}_{v} =$$

$$\begin{bmatrix}
0 \\
2[(K_2 + \sqrt{\bar{\rho}}(K_3 - K_4))\frac{u_1du_2 - u_2du_1}{u_1^2} - K_2\frac{u_1^2u_2du_2 - u_2^2u_1du_1}{\bar{u}u_1^4} + (K_3 + K_4)du_4] \\
2[(K_1 + \sqrt{\bar{\rho}}(K_4 - K_3))\frac{u_1du_2 - u_2du_1}{u_1^2} - K_1\frac{u_1^2u_2du_2 - u_2^2u_1du_1}{\bar{u}u_1^4} + (K_3 + K_4)du_4]
\end{bmatrix}$$
(4.68)

The terms of  $du_1$ ,  $du_2$ , and  $du_4$  are grouped into three equations:

$$\frac{\bar{u}}{2\sqrt{\bar{\rho}}} = 2[(K_2 + \sqrt{\bar{\rho}}(K_3 - K_4))\frac{u_2}{u_1^2} - K_2\frac{u_2^2u_1}{\bar{u}u_1^4}]$$
(4.69a)

$$\frac{1}{2\sqrt{\bar{\rho}}} = 2[(K_2 + \sqrt{\bar{\rho}}(K_3 - K_4))\frac{u_1}{u_1^2} - K_2\frac{u_1^2 u_2}{\bar{u}u_1^4}]$$
(4.69b)

$$\frac{1}{2} = 2(K_3 + K_4) \tag{4.69c}$$

These equations can be solved simultaneously to get the three unknowns of  $K_2$ ,  $K_3$ , and  $K_4$ :

$$K_2 = \frac{\bar{\rho}^{3/2}(\bar{u}+1)}{4} \tag{4.70}$$

$$K_{\bar{3}} = \frac{(1 + \frac{\bar{u}}{2} - \frac{\bar{\rho}\bar{u}}{2})}{4} \tag{4.71}$$

$$K_4 = \frac{\bar{u}(\bar{\rho} - 1)}{8} \tag{4.72}$$

Repeating the same process for the fourth row of  $\mathbf{S}_{v}\mathbf{R}_{v}^{T}\partial\mathbf{v}_{v}$  to get the final component for  $\mathbf{S}_{v}$ :

$$K_1 = \frac{-\bar{\rho}^{3/2}(\bar{u}+1)}{4} \tag{4.73}$$

These set of equations can be checked to satisfy the relations of 4.64. Variables in the terms of  $K_1 - K_4$  are simple arithmetic averaging of the left and right states at each interface. Finally, with all its components defined, the flux at the interface can be represented by the expression in equation 4.55.

# 4.4 Second Order Accuracy

The semi discrete nature of the entropy-consistent fluxes discussed earlier allows for a little flexibility in terms of options for extension to higher order accuracy. The second order accurate EC1 and EC2 fluxes by Ismail and Roe (2009) (the basis for the ECS fluxes in this thesis) utilizes the Hancock scheme, in which the updates for space and time are done simultaneously. However, the downside of using such a scheme is that the accuracy is set to second order and cannot be improved upon further. To get around this restriction, the higher order fluxes here are updated separately for time and space. For time integration, the method of choice is the Runge-Kutta (RK) method, which divides each time step into smaller increments or intervals and approximates the unknowns by weighted averaging of slope estimates at each interval. Its second-order version (RK2) is also known as the midpoint method described in a predictor-corrector algorithm:

$$u^{n+1} = u^n + \Delta t f(t^n + \frac{1}{2}\Delta t, u^n + \frac{1}{2}\Delta t f(t^n, u^n))$$
 (4.74)

The term  $f(t_n, u_n)$  and its variations represent the flux function at its respective point  $t_n$  in time. The Runge-Kutta method is actually more commonly known as a fourth-order (RK4) scheme, and is extendable to even higher orders by increasing the interval count, thus increasing the number of slope estimates between each time step.

For spatial discretization, higher order accuracy is achieved by reconstructing the left and right states of the interface fluxes. In the case of second-order accuracy, this is simply done by means of linear interpolation. A bigger concern is to avoid spurious oscillations due to the reconstruction, which is prevented through the application of flux limiters. Here, two types of limiters are chosen, one of which

is the 'minmod' limiter  $(\phi_{mm}(r))$  available in Sweby (1984) defined as:

$$\phi_{mm}(r) = max[0, min(1, r)]; \quad \lim_{r \to \infty} \phi_{mm}(r) = 1$$
 (4.75)

and the superbee limited  $(\phi_{sb}(r))$ , also available from Sweby (1984) defined as:

$$\phi_{sb}(r) = max[0, min(2r, 1), min(r, 2)]; \quad \lim_{r \to \infty} \phi_{sb}(r) = 2$$
 (4.76)

Other available limiters could also be considered, but the two limiters chosen above have already been proven to work well with entropy-consistent fluxes (Ismail, 2006).

#### 4.5 Extension to Two Dimensions

Nishikawa (2011a) also derived a first order system based on two-dimensional compressible Navier-Stokes equations. Consider the version in which the heat flux is neglected:

$$\frac{\partial \rho}{\partial t} + \frac{\partial (\rho u)}{\partial x} + \frac{\partial (\rho v)}{\partial y} = 0$$

$$(4.77a)$$

$$\frac{\partial (\rho u)}{\partial t} + \frac{\partial (\rho u^2 + p - \tau_{xx})}{\partial x} + \frac{\partial (\rho uv - \tau_{yx})}{\partial y} = 0$$

$$(4.77b)$$

$$\frac{\partial (\rho v)}{\partial t} + \frac{\partial (\rho uv - \tau_{xy})}{\partial x} + \frac{\partial (\rho v^2 + p - \tau_{yy})}{\partial y} = 0$$

$$(4.77c)$$

$$\frac{\partial (\rho E)}{\partial t} + \frac{\partial (\rho uH - \tau_{xx}u - \tau_{xy}v)}{\partial x} + \frac{\partial (\rho vH - \tau_{yx}u - \tau_{yy}v)}{\partial y} = 0$$

$$(4.77d)$$

$$\tau_{xx} = \frac{2}{3}\mu \left(2\frac{\partial u}{\partial x} - \frac{\partial v}{\partial y}\right), \quad \tau_{xy} = \tau_{yx} = \mu \left(\frac{\partial u}{\partial y} - \frac{\partial v}{\partial x}\right), \quad \tau_{yy} = \frac{2}{3}\mu \left(2\frac{\partial v}{\partial y} - \frac{\partial u}{\partial x}\right)$$

$$(4.77e)$$

The newly introduced v is the velocity in the y-direction, and is different from the previously defined  $\mathbf{v}$ , which is the set of entropy variables. In the first-order system, the terms of equation 4.77(e) are replaced by their equivalent evolution equations:

$$\frac{\partial \tau_{xx}}{\partial t} = \frac{\mu_{\nu}}{T_{\nu}} \left( \frac{\partial u}{\partial x} - \frac{1}{2} \frac{\partial v}{\partial y} - \frac{\tau_{xx}}{\mu_{\nu}} \right) \tag{4.78a}$$

$$\frac{\partial \tau_{yy}}{\partial t} = \frac{\mu_{\nu}}{T_{\nu}} \left( \frac{\partial v}{\partial y} - \frac{1}{2} \frac{\partial u}{\partial x} - \frac{\tau_{yy}}{\mu_{\nu}} \right) \tag{4.78b}$$

$$\frac{\partial \tau_{xy}}{\partial t} = \frac{\mu_{\nu}}{T_{\nu}} \left( \frac{3}{4} \frac{\partial u}{\partial y} + \frac{3}{4} \frac{\partial v}{\partial x} - \frac{\tau_{xy}}{\mu_{\nu}} \right) \tag{4.78c}$$

In conservative form, the system is represented by:

$$\mathbf{P}^{-1}\frac{\partial \mathbf{u}}{\partial t} + \frac{\partial \mathbf{f}}{\partial x} + \frac{\partial \mathbf{g}}{\partial y} = \mathbf{B}$$
 (4.79)

Similar to the one-dimensional system, P is a pre-conditioning matrix that is included to balance the forces from the source term B. These vectors are defined as:

$$\mathbf{u} = \begin{bmatrix} \rho \\ \rho u \\ \rho v \\ \rho E \\ \tau_{xx} \\ \tau_{xy} \\ \tau_{yy} \end{bmatrix}, \quad \mathbf{f} = \mathbf{f}_i + \mathbf{f}_v = \begin{bmatrix} \rho u \\ \rho u^2 + p \\ \rho uv \\ \rho uH \\ 0 \\ 0 \end{bmatrix} + \begin{bmatrix} 0 \\ -\tau_{xx} \\ -\tau_{xy} \\ -\tau_{xx} u - \tau_{xy}v \\ -u \\ -3v/4 \\ u/2 \end{bmatrix},$$

$$\mathbf{g} = \mathbf{g}_{i} + \mathbf{g}_{v} = \begin{bmatrix} \rho v \\ \rho u v \\ \rho v^{2} + p \\ \rho v H \\ 0 \\ 0 \\ 0 \end{bmatrix} + \begin{bmatrix} 0 \\ -\tau_{xy} \\ -\tau_{yy} \\ -\tau_{xy} u - \tau_{yy} v \\ v / 2 \\ -3u / 4 \\ -v \end{bmatrix},$$

$$\mathbf{B} = \begin{bmatrix} 0 \\ 0 \\ 0 \\ 0 \\ 0 \\ \frac{\tau_{xx}}{\mu_{v}} \end{bmatrix}, \quad \mathbf{P}^{-1} = \begin{bmatrix} 1 & 0 & 0 & 0 & 0 & 0 & 0 \\ 0 & 1 & 0 & 0 & 0 & 0 & 0 \\ 0 & 0 & 1 & 0 & 0 & 0 & 0 \\ 0 & 0 & 0 & 1 & 0 & 0 & 0 & 0 \\ 0 & 0 & 0 & 0 & \frac{T_{v}}{\mu_{v}} & 0 & 0 \\ 0 & 0 & 0 & 0 & 0 & \frac{T_{v}}{\mu_{v}} & 0 \\ 0 & 0 & 0 & 0 & 0 & 0 & \frac{T_{v}}{\mu_{v}} \end{bmatrix}$$

$$(4.80)$$

We introduce the Jacobian matrices, consisting of the inviscid  $A_i$  and its viscous counterpart  $A_v$  as they relate to P:

$$\mathbf{P}\mathbf{A} = \mathbf{P}\frac{\partial \mathbf{f}}{\partial \mathbf{u}}n_x + \frac{\partial \mathbf{g}}{\partial \mathbf{u}}n_y = \mathbf{P}\mathbf{A}_i + \mathbf{P}\mathbf{A}_v \tag{4.81}$$

The Jacobian matrices  $A_i$  and  $A_v$  are found by differentiating the inviscid and viscous parts of f and g with respect to g individually. For the inviscid part of g, its Jacobian g is the familiar looking set of Eulerian quantities in a 7 by 7 matrix:

Naturally, the last three rows and columns consist of zeroes. On the other hand,

the Jacobian for the viscous  $A_{f,v}$  is defined as:

Similar to that of f, the Jacobian for the inviscid part of g,  $A_{g,i}$ , is calculated by differentiating with respect to u:

Conversely, the Jacobian for the viscous  $A_{g,v}$  is:

Similar to the one-dimensional first order system, the two-dimensional counterpart will have a flux function in the form of equation 4.28 and 4.55:

$$\mathbf{f}^* = \mathbf{f}_c - \frac{1}{2} \mathbf{R}_i \Lambda_i \mathbf{S}_i (\mathbf{R}_i)^T [\mathbf{v}_i] + \mathbf{f}_v - \frac{1}{2} \mathbf{R}_v \Lambda_v \mathbf{S}_v (\mathbf{R}_v)^T [\mathbf{v}_v]$$
 (4.86)

To discretize the system, consider an arbitrarily shaped two-dimensional grid element as shown in Figure 4.1. Define:

$$\Delta l_f = \sqrt{(\Delta x)_f^2 + (\Delta y)_f^2}, \quad q_f = \frac{u\Delta y + v\Delta x}{\Delta l_f}, \quad r_f = \frac{u\Delta x + v\Delta y}{\Delta l_f}$$
(4.87)

The conservative flux  $\mathbf{f}_c$  and the accompanying viscous flux  $\mathbf{f}_{\nu}$  in 4.86 can be

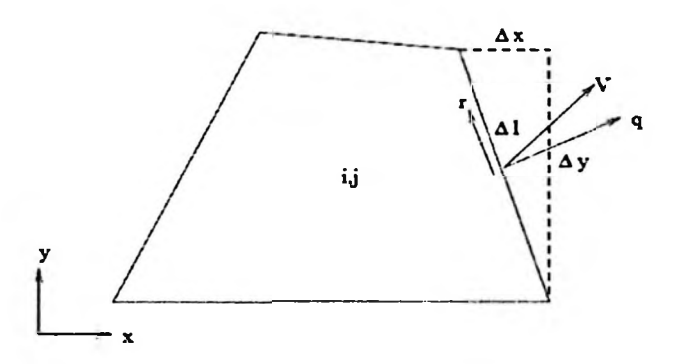


Figure 4.1: Grid representation of the finite volume method from Ismail (2006).

formulated as the sum of the respective components of f and g:

$$\hat{\mathbf{f}}_{c} = \mathbf{f}_{i} + \mathbf{g}_{i} = \begin{bmatrix} \hat{\rho}\hat{q}_{f} \\ \hat{p}_{1} + \hat{\rho}\hat{u}\hat{q}_{f} \\ -\hat{p}_{1} + \hat{\rho}\hat{v}\hat{q}_{f} \\ \hat{\rho}\hat{q}_{f}\hat{H} \\ 0 \\ 0 \\ 0 \end{bmatrix}$$

$$(4.88a)$$

$$\hat{\mathbf{f}}_{\nu} = \mathbf{f}_{v} + \mathbf{g}_{v} = \begin{bmatrix}
0 \\
-\bar{\tau}_{xx} - \bar{\tau}_{xy} \\
-\bar{\tau}_{xy} - \bar{\tau}_{yy} \\
(-\bar{\tau}_{xx} - \bar{\tau}_{xy})\bar{u} + (-\bar{\tau}_{xy} - \bar{\tau}_{yy})\bar{v} + \bar{q}_{x} + \bar{q}_{y} \\
-\bar{u} + \bar{v}/2 \\
-3\bar{v}/4 - 3\bar{u}/4 \\
\bar{u}/2 - \bar{v}
\end{bmatrix} (4.88b)$$

Mean variables were used for  $\hat{\mathbf{f}}_{\nu}$  based on the formulation in equation 4.53.

# 4.5.1 Upwind flux via entropy conservation approach

To formulate an upwind flux for the Navier-Stokes equations, the eigenstructure of the Jacobian is again separated into inviscid and viscous parts. The inviscid Jacobian contains inviscid eigenvalues and eigenvectors, with the eigenvalues  $\Lambda_i$  defined as:

The variable  $u_n$  is defined as  $u_n = u_x n_x + u_y n_y$ . The right eigenvectors  $\mathbf{R}_i$  corresponding to the inviscid Jacobian are defined as

$$\hat{\mathbf{R}}_{i} = \begin{bmatrix} \mathbf{r}_{1,i} & \mathbf{r}_{2,i} & \mathbf{r}_{3,i} & \mathbf{r}_{4,i} & \mathbf{r}_{5,i} & \mathbf{r}_{6,i} & \mathbf{r}_{7,i} \end{bmatrix}$$

$$= \begin{bmatrix} 1 & 1 & 0 & 1 & 0 & 0 & 0 \\ \hat{u} - \hat{a} & \hat{u} & 0 & \hat{u} + \hat{a} & 0 & 0 & 0 \\ \hat{v} - \hat{a} & \hat{v} & 0 & \hat{v} + \hat{a} & 0 & 0 & 0 \\ \hat{H} - \hat{q}_{f} \hat{a} & \frac{\hat{u}^{2} + \hat{v}^{2}}{2} & \hat{r}_{f} & \hat{H} + \hat{q}_{f} \hat{a} & 0 & 0 & 0 \\ 0 & 0 & 0 & 0 & 1 & 0 & 0 \\ 0 & 0 & 0 & 0 & 0 & 1 & 0 \\ 0 & 0 & 0 & 0 & 0 & 0 & 1 \end{bmatrix}$$

$$(4.90a)$$

Conversely, eigenvalues of the viscous Jacobian  $\Lambda_v$  are:

whilst the viscous right eigenvectors associated with  $\mathbf{A}_{f,v}$  and  $\mathbf{A}_{g,v}$  are:

$$\hat{\mathbf{R}}_{f,v} = \begin{bmatrix} 0 & 0 & 1 & 0 & 0 & 0 & 0 \\ 0 & 0 & \bar{u} & 1 & 1 & 0 & 0 \\ 0 & 0 & \bar{v} & 0 & 0 & 1 & 1 \\ 1 & 0 & 0 & \bar{u} + \frac{\bar{\tau}_{xx}}{\sqrt{\bar{\rho}}} & \bar{u} - \frac{\bar{\tau}_{xx}}{\sqrt{\bar{\rho}}} & \bar{v} + \frac{2\bar{\tau}_{xy}}{\sqrt{3\bar{\rho}}} & \bar{v} - \frac{2\bar{\tau}_{xy}}{\sqrt{3\bar{\rho}}} \\ 0 & 0 & 0 & \frac{1}{\sqrt{\bar{\rho}}} & -\frac{1}{\sqrt{\bar{\rho}}} & 0 & 0 \\ 0 & 0 & 0 & 0 & \frac{\sqrt{3}}{2\sqrt{\bar{\rho}}} & -\frac{\sqrt{3}}{2\sqrt{\bar{\rho}}} \\ 0 & 1 & 0 & -\frac{1}{2\sqrt{\bar{\rho}}} & \frac{1}{2\sqrt{\bar{\rho}}} & 0 & 0 \end{bmatrix}$$

$$(4.92)$$

$$\hat{\mathbf{R}}_{g,v} = \begin{bmatrix} 0 & 0 & 1 & 0 & 0 & 0 & 0 \\ 0 & 0 & \bar{u} & 0 & 0 & 1 & 1 \\ 0 & 0 & \bar{v} & 1 & 1 & 0 & 0 \\ 1 & 0 & 0 & \bar{v} + \frac{\bar{\tau}_{yy}}{\sqrt{\bar{\rho}}} & \bar{v} - \frac{\bar{\tau}_{yy}}{\sqrt{\bar{\rho}}} & \bar{u} + \frac{2\bar{\tau}_{xy}}{\sqrt{3\bar{\rho}}} & \bar{u} - \frac{2\bar{\tau}_{xy}}{\sqrt{3\bar{\rho}}} \\ 0 & 1 & 0 & \frac{1}{2\sqrt{\bar{\rho}}} & -\frac{1}{2\sqrt{\bar{\rho}}} & 0 & 0 \\ 0 & 0 & 0 & 0 & 0 & \frac{\sqrt{3}}{2\sqrt{\bar{\rho}}} & -\frac{\sqrt{3}}{2\sqrt{\bar{\rho}}} \\ 0 & 0 & 0 & -\frac{1}{\sqrt{\bar{\rho}}} & \frac{1}{\sqrt{\bar{\rho}}} & 0 & 0 \end{bmatrix}$$

$$(4.93)$$

For the purpose of obtaining an entropy consistent flux similar to the one developed for one-dimensional Navier-Stokes, the Jacobian PA is replaced with the formulation as shown previously in equations 4.26 and 4.62. The scaling matrix  $S_i$  with averaged components is thus calculated to be:

For  $S_v$  however, the first three rows of the viscous dissipation matrix will not affect the overall dissipation since the first three eigenvalues are zero. Thus the viscous scaling matrix is computed such that only the last four rows are determined (the rest are set to zeros) to satisfy the differential relations of equation 4.62 for the viscous part of the system. This equation is expanded into:

$$\partial \mathbf{u} = \begin{bmatrix} d\rho \\ d\rho u \\ d\rho v \\ d\rho E \\ d\tau_{xx} \\ d\tau_{xy} \\ d\tau_{yy} \end{bmatrix} = \begin{bmatrix} du_1 \\ du_2 \\ du_3 \\ du_4 \\ du_5 \\ du_6 \\ du_7 \end{bmatrix}, \quad \partial \mathbf{v}_v = \begin{bmatrix} -du^2 - dv^2 \\ 2du \\ 2dv \\ 2dv \\ 0 \end{bmatrix} = \begin{bmatrix} -d(\frac{u_2^2}{u_1^2}) - d(\frac{u_3^2}{u_1^2}) \\ 2d(\frac{u_2}{u_1}) \\ 2d(\frac{u_3}{u_1}) \\ 0 \\ 2d\tau_{xx} \\ 2d\tau_{xy} \\ 2d\tau_{yy} \end{bmatrix} = \begin{bmatrix} -d(\frac{u_2^2}{u_1^2}) - d(\frac{u_3^2}{u_1^2}) \\ 2d(\frac{u_3}{u_1}) \\ 0 \\ 2d\tau_{xx} \\ 2d\tau_{xy} \\ 2d\tau_{yy} \end{bmatrix}$$

$$(4.96)$$

Similar to the one-dimensional formulation of the viscous eigen-structure starting

in equation 4.64, averaged values are used based on the definition from equation 4.53. The entropy variable partial differential is thus:

Using this  $\partial \mathbf{v}_v$  result, equation 4.62 can be further elaborated as:

$$\hat{\mathbf{R}}_{f,v}^{-1} \partial \mathbf{u} = \begin{bmatrix} (\bar{u}^2 + \bar{v}^2)du_1 - \bar{u}du_2 - \bar{v}du_3 + du_4 - \bar{\tau}_{xx}du_5 - \frac{4}{3}\bar{\tau}_{xy}du_6 \\ \frac{1}{2}du_5 + du_7 \\ du_1 \\ -\frac{\bar{u}}{2}du_1 + \frac{1}{2}du_2 + \frac{\sqrt{\bar{\rho}}}{2}du_5 \\ -\frac{\bar{u}}{2}du_1 + \frac{1}{2}du_2 - \frac{\sqrt{\bar{\rho}}}{2}du_5 \\ \frac{\bar{v}}{2}du_1 + \frac{1}{2}du_3 + \sqrt{\frac{\bar{\rho}}{3}}du_6 \\ \frac{\bar{v}}{2}du_1 + \frac{1}{2}du_3 - \sqrt{\frac{\bar{\rho}}{3}}du_6 \end{bmatrix}$$

$$(4.98a)$$

$$= \mathbf{S}_{v} \begin{bmatrix} 2du_{7} \\ -d(\frac{u_{2}^{2}}{u_{1}^{2}}) - d(\frac{u_{3}^{2}}{u_{1}^{2}}) + 2\bar{u}d(\frac{u_{2}}{u_{1}}) + 2\bar{v}d(\frac{u_{3}}{u_{1}}) \\ 2d(\frac{u_{2}}{u_{1}}) + \frac{2}{\sqrt{\bar{\rho}}}du_{5} - \frac{1}{\sqrt{\bar{\rho}}}du_{7} \\ 2d(\frac{u_{2}}{u_{1}}) - \frac{2}{\sqrt{\bar{\rho}}}du_{5} + \frac{1}{\sqrt{\bar{\rho}}}du_{7} \\ 2d(\frac{u_{3}}{u_{1}}) + \sqrt{\frac{3}{\bar{\rho}}}du_{6} \\ 2d(\frac{u_{3}}{u_{1}}) - \sqrt{\frac{3}{\bar{\rho}}}du_{6} \end{bmatrix}$$

$$(4.98b)$$

Consider the  $S_v$  matrix having the form of:

To obtain the components of  $\hat{\mathbf{S}}_v$ , we can start with the fourth row of the matrix and find its dot product with the term  $\mathbf{R}_v^T \partial \mathbf{v}_v$ :

$$\hat{S}_{v}R_{v}^{T}\partial v_{v} = 2K_{2}du_{7} + 2K_{3}\left[-\frac{u_{1}^{2}u_{2}du_{2} - u_{2}^{2}u_{1}du_{1}}{u_{1}^{4}} - \frac{u_{1}^{2}u_{3}du_{3} - u_{3}^{2}u_{1}du_{1}}{u_{1}^{4}} + \bar{u}\frac{u_{1}du_{2} - u_{2}du_{1}}{u_{1}^{2}} + \bar{v}\frac{u_{1}du_{3} - u_{3}du_{1}}{u_{1}^{2}}\right] + K_{4}\left[2\frac{u_{1}du_{2} - u_{2}du_{1}}{u_{1}^{2}} + \frac{2}{\sqrt{\bar{\rho}}}du_{5} - \frac{1}{\sqrt{\bar{\rho}}}du_{7}\right] + K_{5}\left[2\frac{u_{1}du_{2} - u_{2}du_{1}}{u_{1}^{2}} - \frac{2}{\sqrt{\bar{\rho}}}du_{5} + \frac{1}{\sqrt{\bar{\rho}}}du_{7}\right] + K_{6}\left[2\frac{u_{1}du_{3} - u_{3}du_{1}}{u_{1}^{2}} + \sqrt{\frac{3}{\bar{\rho}}}du_{6}\right] + K_{7}\left[2\frac{u_{1}du_{3} - u_{3}du_{1}}{u_{1}^{2}} - \sqrt{\frac{3}{\bar{\rho}}}du_{6}\right]$$
(4.100a)

The terms of  $du_1$  through  $du_7$  from the fourth row are grouped into their own

equations:

$$du_1: -\frac{\bar{u}}{4} = K_3 \frac{u_2^2 + u_3^2}{u_1^3} - \frac{u_2}{u_1^2} (K_3 \bar{u} + K_4 + K_5) - \frac{u_3}{u_1^2} (K_3 \bar{v} + K_6 + K_7)$$

$$= -\frac{u_2}{u_1^2} (K_4 + K_5) - \frac{u_3}{u_1^2} (K_6 + K_7)$$
(4.101a)

$$du_2: \frac{1}{4} = -K_3 \frac{u_2}{u_1^2} + \frac{u_1}{u_1^2} (K_3 \bar{u} + K_4 + K_5) = \frac{1}{\bar{\rho}} (K_4 + K_5)$$
 (4.101b)

$$du_3: 0 = -K_3 \frac{u_3}{u_1^2} + \frac{u_1}{u_1^2} (K_3 \bar{v} + K_6 + K_7) = \frac{1}{\bar{\rho}} (K_6 + K_7)$$
 (4.101c)

$$du_4:0=0 (4.101d)$$

$$du_5: \frac{\bar{\rho}}{4} = (K_4 - K_5) \tag{4.101e}$$

$$du_6: 0 = \sqrt{\frac{3}{\bar{\rho}}}(K_6 - K_7) \tag{4.101f}$$

$$du_7: 0 = 2K_2 + \frac{1}{\sqrt{\bar{\rho}}}(K_5 - K_4) \tag{4.101g}$$

From this set of equations, the variables can be solved thusly:

$$K_1 = K_3 = 0 (4.102a)$$

$$\frac{\bar{\rho}}{4} = (K_4 + K_5), \quad \frac{\bar{\rho}}{4} = (K_4 - K_5)$$
 (4.102b)

$$K_4 = \frac{\bar{\rho}}{4}, \quad K_5 = 0$$
 (4.102c)

$$0 = -\frac{1}{\bar{\rho}}(K_6 + K_7), \quad 0 = \sqrt{\frac{3}{\bar{\rho}}}(K_6 - K_7)$$
 (4.102d)

$$K_6 = K_7 = 0, \quad K_2 = \frac{\sqrt{\bar{\rho}}}{8}$$
 (4.102e)

For the fifth row of the matrix, the computation would yield the same result for all coefficients, with  $K_2$  and  $K_4$  being the only non-zero terms; however,  $K_4$  is in the fifth column instead of the fourth. Moving on to the sixth row, their terms

can stated as:

$$S_{v}R_{v}^{T}\partial \mathbf{v}_{v} = 2K_{2}du_{7} + 2K_{3}\left[-\frac{u_{1}^{2}u_{2}du_{2} - u_{2}^{2}u_{1}du_{1}}{u_{1}^{4}}\right]$$

$$-\frac{u_{1}^{2}u_{3}du_{3} - u_{3}^{2}u_{1}du_{1}}{u_{1}^{4}} + \bar{u}\frac{u_{1}du_{2} - u_{2}du_{1}}{u_{1}^{2}} + \bar{v}\frac{u_{1}du_{3} - u_{3}du_{1}}{u_{1}^{2}}\right]$$

$$+K_{4}\left[2\frac{u_{1}du_{2} - u_{2}du_{1}}{u_{1}^{2}} + \frac{2}{\sqrt{\bar{\rho}}}du_{5} - \frac{1}{\sqrt{\bar{\rho}}}du_{7}\right]$$

$$+K_{5}\left[2\frac{u_{1}du_{2} - u_{2}du_{1}}{u_{1}^{2}} - \frac{2}{\sqrt{\bar{\rho}}}du_{5} + \frac{1}{\sqrt{\bar{\rho}}}du_{7}\right]$$

$$+K_{6}\left[2\frac{u_{1}du_{3} - u_{3}du_{1}}{u_{1}^{2}} + \sqrt{\frac{3}{\bar{\rho}}}du_{6}\right] + K_{7}\left[2\frac{u_{1}du_{3} - u_{3}du_{1}}{u_{1}^{2}} - \sqrt{\frac{3}{\bar{\rho}}}du_{6}\right]$$

$$(4.103a)$$

The terms of  $du_1$  through  $du_7$  from the sixth row are grouped into their own equations:

$$du_1: -\frac{\bar{u}}{4} = K_3 \frac{u_2^2 + u_3^2}{u_1^3} - \frac{u_2}{u_1^2} (K_3 \bar{u} + K_4 + K_5) - \frac{u_3}{u_1^2} (K_3 \bar{v} + K_6 + K_7)$$

$$= -\frac{u_2}{u_1^2} (K_4 + K_5) - \frac{u_3}{u_1^2} (K_6 + K_7)$$

$$(4.104a)$$

$$du_2: 0 = -K_3 \frac{u_2}{u_1^2} + \frac{u_1}{u_1^2} (K_3 \bar{u} + K_4 + K_5) = \frac{1}{\bar{\rho}} (K_4 + K_5)$$
 (4.104b)

$$du_3: \frac{1}{4} = -K_3 \frac{u_3}{u_1^2} + \frac{u_1}{u_1^2} (K_3 \bar{v} + K_6 + K_7) = \frac{1}{\bar{\rho}} (K_6 + K_7)$$
 (4.104c)

$$du_4:0=0 (4.104d)$$

$$du_5: 0 = \frac{2}{\sqrt{\bar{\rho}}}(K_4 - K_5) \tag{4.104e}$$

$$du_6: \sqrt{\frac{\bar{\rho}}{3}} = \sqrt{\frac{3}{\bar{\rho}}}(K_6 - K_7) \tag{4.104f}$$

$$du_7: 0 = 2K_2 + \frac{1}{\sqrt{\bar{\rho}}}(K_5 - K_4) \tag{4.104g}$$

From these equations, the variables can be solved thusly:

$$K_1 = K_3 = K_4 = K_5 = 0 (4.105a)$$

$$\frac{1}{4} = \frac{1}{\bar{\rho}}(K_6 + K_7), \quad \sqrt{\frac{\bar{\rho}}{3}} = \sqrt{\frac{3}{\bar{\rho}}}(K_6 - K_7)$$
 (4.105b)

$$K_6 = \frac{7\bar{\rho}}{24}, \quad K_7 = -\frac{\bar{\rho}}{24}, \quad K_2 = 0$$
 (4.105c)

Calculations for the seventh row would yield the same values for  $K_6$  and  $K_7$ , but with their places interchanged. Therefore:

Finally, with all its components defined, the flux at the interface can be represented by the expression as shown in equation 4.86.

# 4.5.2 Upwind flux via abbreviated system approach

A couple of alternative approaches of constructing the flux were shown in Nishikawa (2011b). Both methods segregate the inviscid and viscous portions of the flux into separate systems just like in the previous subsection, with the inviscid part utilizing the well-established Roe method to obtain the solution updates. The major difference, however, lies in the formulation of the viscous flux. The first alternative uses the a new gradient formula applied to the traditional concept of central

differencing to compute the viscous stresses and heat fluxes that form the numerical viscous flux. This method is bound to be stable since central differencing is already a well-understood concept, and only the prescribed gradient formula is the new addition. The drawback is that the method requires a relatively larger stencil, involving data from multiple neighboring cells which make variable calculations a little more complicated.

The second proposition, from which a comparable result to the first method is obtainable, is the entropy conservative flux approach as shown in the above. The viscous flux has a similar form to the inviscid one and requires only data from the immediate interface, which makes it highly attractive. Additionally, the flux formulation is decidedly less cumbersome than the entropy conservative approach, due to the fact that the secondary variable of the viscous stresses is calculated directly from the real-time values of the main variables, and not through their own time-updates. To get an idea of how the algorithm works, a flowchart has been included in Appendix B.

#### CHAPTER 5

# RESULTS AND DISCUSSION

#### 5.1 Introduction

This chapter documents the combined results obtained from the methods developed in Chapter 3 and Chapter 4. These results include:

- One dimensional flux functions solving for Burgers' equation. The system flux is compared with the established entropy-consistent (EC) flux for the simple test cases of steady shock and the square wave initial condition.
- One dimensional flux functions solving for the Navier-Stokes equations. The system flux is again bench-marked against the ES, EC1, and EC2 fluxes.
   Stationary shock and Sod's shock tube problem are investigated.
- Two dimensional flux functions for the Navier-Stokes equations. Case studies are flow over a flat plate, flow over a forward facing step, flow over a cylinder, and flow over and airfoil. Comparisons are made with other fluxes and selected experimental results.

### 5.2 Burgers' Equation

Results of one dimensional flux functions solving for Burgers' equation as shown in Chapter 3 is presented herein. Results for stationary shock simulation is presented first, followed by the those for the square wave initial condition.

## 5.2.1 Stationary shock

The entropy consistent flux with added viscosity was tested in a steady state stationary shock situation with the following initial conditions:

$$u(x,0) = \begin{cases} 1, & \text{if } x < 0 \\ -1, & \text{if } x \geqslant 0 \end{cases}$$
 (5.1)

The fluxes are then compared to the exact solution for Burgers' equation at the corresponding particular value of viscosity being used, as found in Xu (2000) for a single value of viscosity, as well as Masatsuka (2009) for variable viscosities:

$$u = \left(1 - \tanh\frac{x}{2\nu}\right) \tag{5.2}$$

For these tests, 40 computational cells were used with non-reflecting boundary conditions on the left and right sides of the domain. The CFL number was set to 0.1. The result for ECS1 and ECS2 fluxes, with a viscosity coefficient of 0.001, is found in Figure 5.1. The result of the entropy-consistent (EC) flux from Ismail and Roe (2009) is also included for comparison. Tests were also done at lower viscosity ranges, but those runs yield almost exactly similar results to that of  $\nu = 0.001$ . Therefore, other results are omitted for brevity, with the result shown here classified as low viscosity. In Figure 5.1(a), ECS1 exhibits big oscillations, whilst ECS2 produces smaller oscillations for u both before the shock and afterwards. This result is reflected Figure 5.1(b), where big changes in d across the shock occurs for ECS2, while small perturbations is seen from ECS1. A probable reason for this phenomenon lies in how both the entropy production term and the viscosity term affects the workings of the respective fluxes. For ECS1, the minimal of additional production term that produces numerical en-

tropy, coupled with a low coefficient value for viscosity, leads to a result that is severely lacking in entropy production. The plot of velocity difference confirms this observation, since its magnitude of change is small compared to ECS2 and the exact solution. In contrast, the production term in the ECS2 flux is providing somewhat more entropy to the solution compared to ECS1, even with the viscosity being as low as it is. However, the amount of entropy produced is still not enough to eliminate all oscillations, as seen in the magnitude of d for ECS2 compared to the exact solution. As a consequence, the ECS1 flux manifests its entropy inadequacy as oscillations, which is expected for an entropy conservative flux with minimal effect from its dissipation matrix, while the ECS2 provides a slightly less oscillatory solution for velocity with the physical viscosity source term proving to be inconsequential for this particular case.

The test is then repeated, but now the physical viscosity term is increased in each flux function. The viscosity coefficient is set at  $\nu=0.01$ , which is classified for the purpose of conciseness as medium viscosity, with the results shown in Figure 5.2. The oscillations in both the ECS1 and ECS2 fluxes are now reduced, compared to the previous case. For this case, our conjecture is that the physical viscosity coefficient is large enough, enabling the viscosity term in the ECS1 flux to produce adequate entropy without much help from the production term. However, even when the production term is indeed present as is with the ECS2 flux, the oscillations does not seem to have been eliminated completely. This may be due to the fact that the secondary variable d, that stores the velocity difference which is to calculate production, is not a 'real-time' value. Instead, this variable is updated based on the time-step before the current one, which means the production added to the flux is limited to the requirement of the previous iteration. Hence, the production may seem out of sync with the main variable update, a limitation for

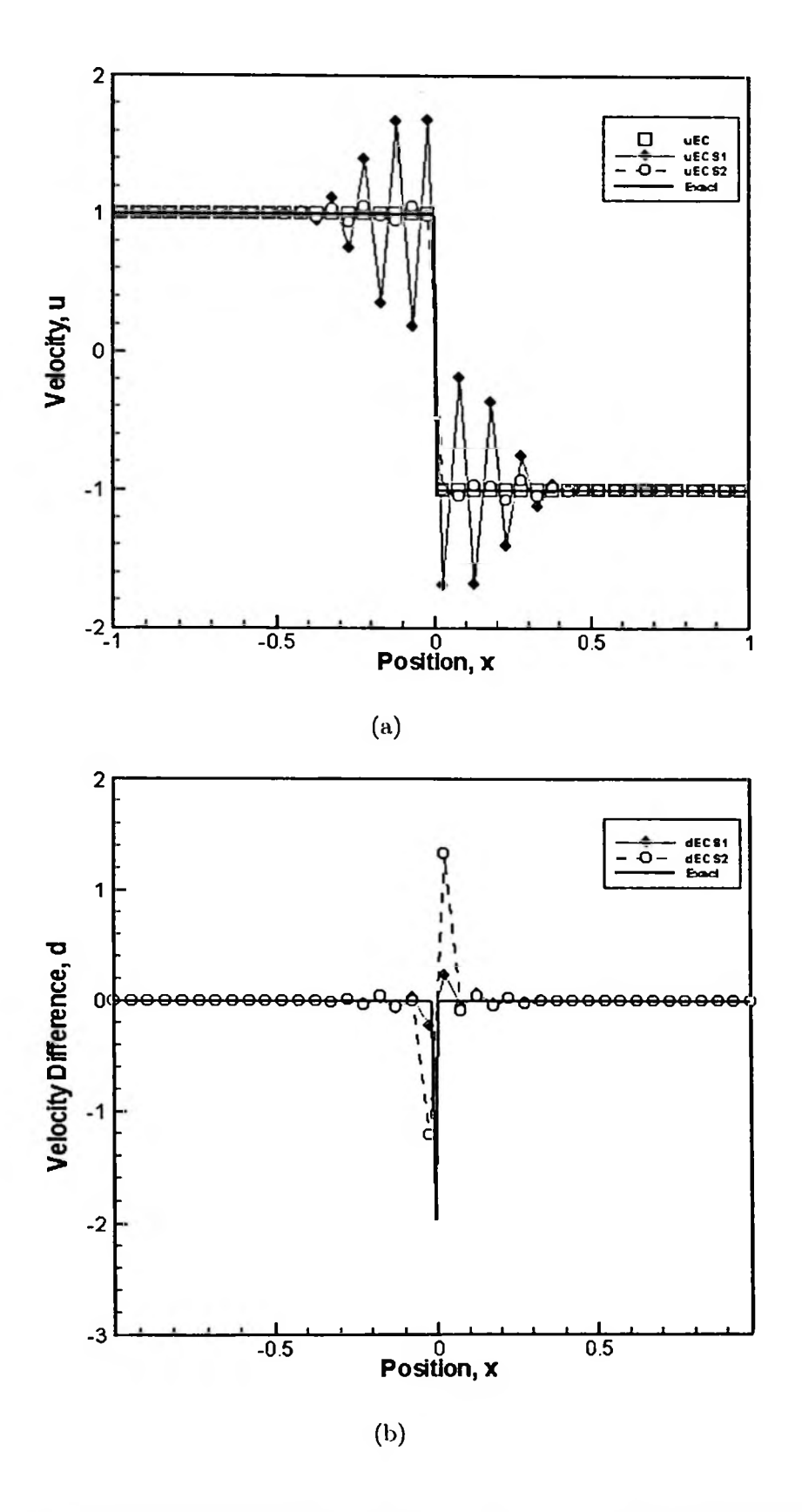


Figure 5.1: Steady state shock solution with low viscosity terms for the tested fluxes in terms of (a) velocity, and (b) velocity difference.

a two-equation system flux.

We then increase the viscosity level further to  $\nu = 0.1$ , with results shown in Figure 5.3. Observe that the oscillation have now disappeared, and both ECS1 and ECS2 fluxes match the exact solution fairly closely. Looking at the velocity difference in Figure 5.3(b), which represents the entropy generation of the flux, the entropy produced by the ECS fluxes far exceeds the amount as available from the exact solution. Thus it can be said that at this setting, the viscosity term has now dominated the flux function, to point where the solution ceases to be a discontinuity and turns into a smooth function.

## 5.2.2 The square wave initial condition

The entropy consistent flux with added viscosity was next tested with a square wave initial condition defined as:

$$u(x,0) = \begin{cases} -1, & \text{if } \frac{1}{3} \leqslant |x| \leqslant 1\\ 1, & \text{if } |x| < \frac{1}{3} \end{cases}$$
 (5.3)

The point of this test case is to see whether the fluxes can avoid capturing the non-physical rarefaction shock, unlike the Roe flux and most other schemes without entropy control. For these tests, 40 computational cells were used with non-reflecting boundary conditions on the left and right sides of the domain. The CFL number was set to 0.1. This low value was chosen due to the constraints that is dictated by both the stability limit of advection-diffusion problem and the nature of explicit semi discrete flux functions which works best using a low CFL number. The flux function based on Burgers' equation works well even when simulated at a CFL value of up to 0.8, but this may not be the case for the Navier-Stokes based scheme. Therefore, to maintain uniformity, the CFL value is kept

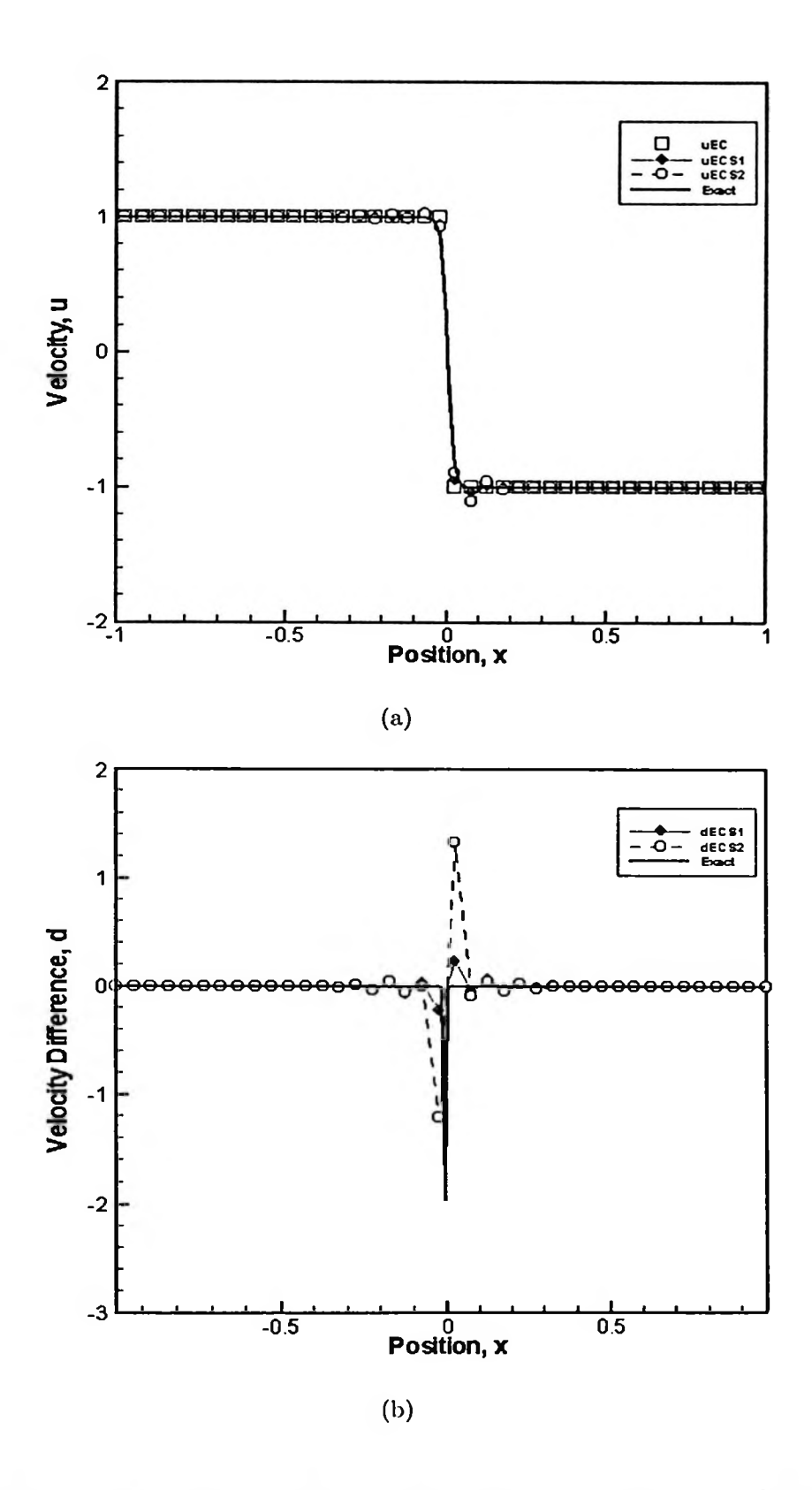


Figure 5.2: Steady state shock solution with medium viscosity terms for the tested fluxes in terms of (a) velocity, and (b) velocity difference.

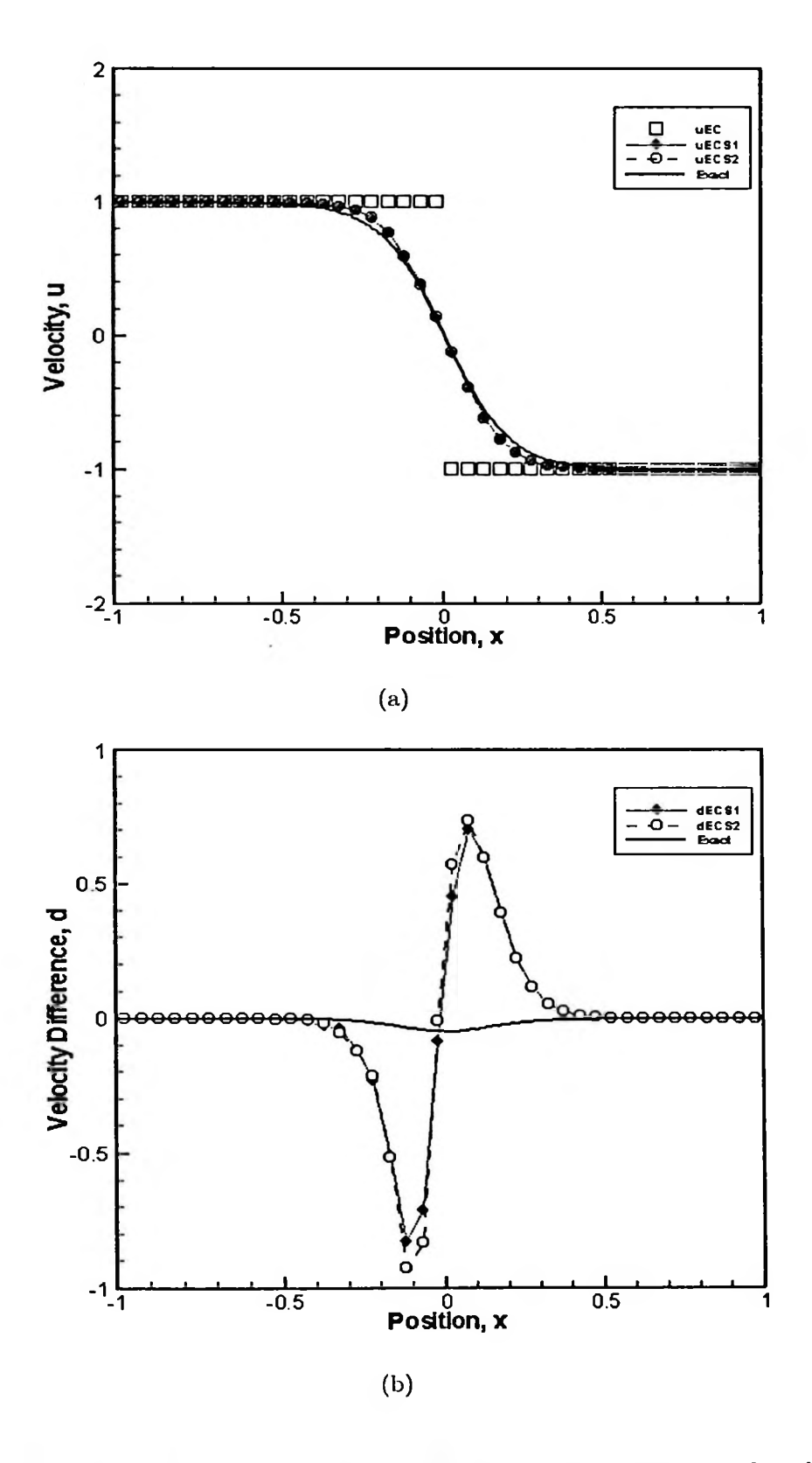


Figure 5.3: Steady state shock solution with high viscosity terms for the tested fluxes in terms of (a) velocity, and (b) velocity difference.

at 0.1 unless stated otherwise. The exact solution for this initial condition can be found in Laney (1998).

Figures 5.4 (a) and (b) show the ECS1 and ECS2 results for the velocity u, at low viscosity ( $\nu=1e-10$ ) and at high viscosity ( $\nu=0.1$ ). Results for two different viscosity conditions are shown since the  $f_d^*$  term in ECS2 is dependent on  $\nu$ . The variable u is again compared with the EC flux and the exact solution. As seen in the plots, the ECS1 and ECS2 fluxes behave similarly to the EC flux around the rarefaction area, which matches the characteristic that we are looking for. The rarefaction fan for all three fluxes are less steep compared to the solution given by the exact Riemann solver in the solid line mostly due to the low CFL number used in the simulation. As for the second shock occurrence in the domain, the ECS1 and ECS2 fluxes exhibit a similar pattern to the previous case, with the ECS1 flux being oscillatory around the shock and the ECS2 flux being the more diffusive of the two. The ECS2 plot is actually closely similar to the EC flux without the entropy production term. These results could be improved by adding a physical viscosity term to the fluxes.

### 5.3 Navier-Stokes Equations

Next is the results for the fluxes modelling the Navier-Stokes equations, as described in Chapter 4. The one-dimensional flux is presented first, followed by the two-dimensional solutions in the subsequent section. For the one-dimensional case, the best of the first-order system flux is compared with its predecessors, namely the Roe flux and the entropy consistent fluxes, in the cases of stationary shock and Sod's viscous shock tube problem.

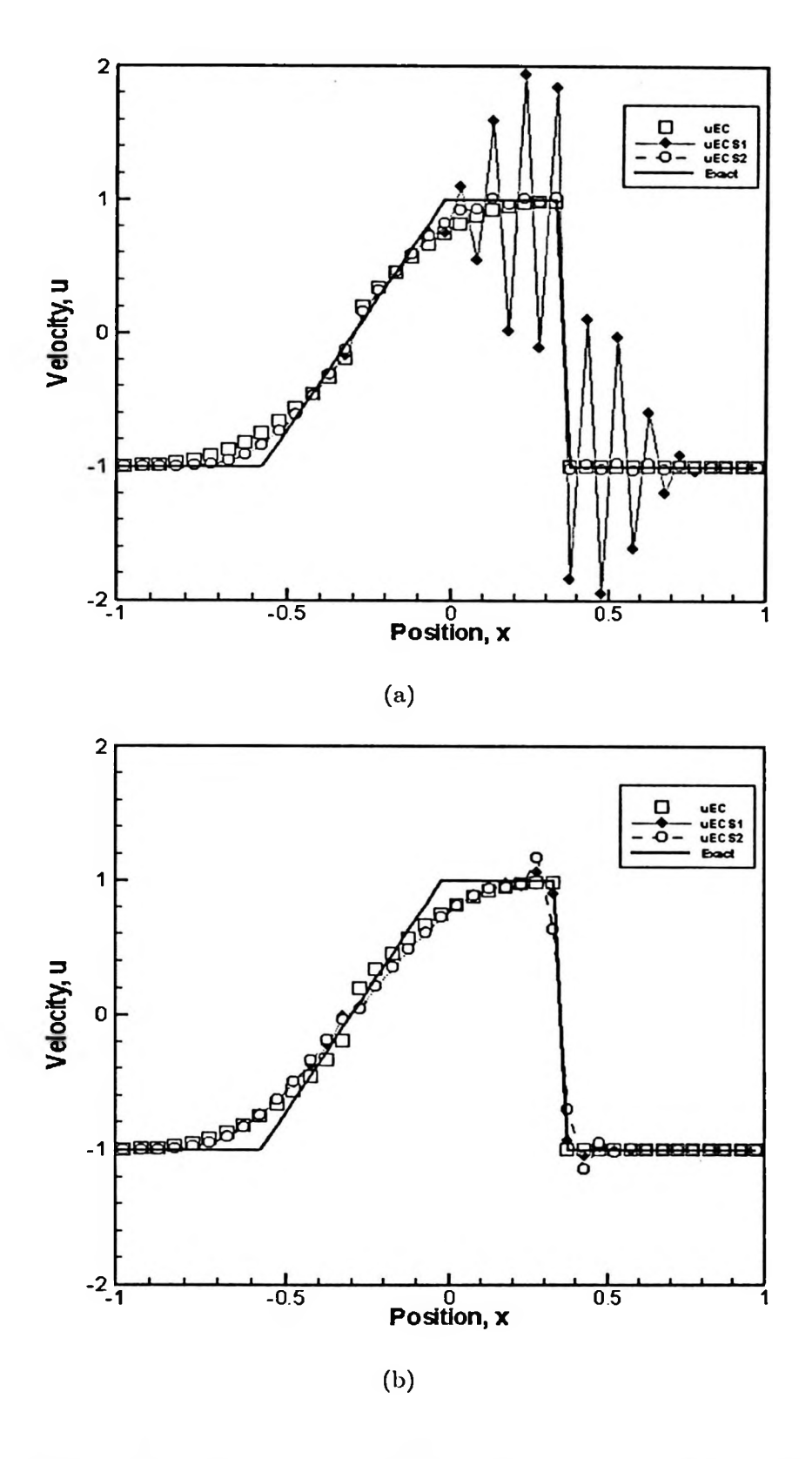


Figure 5.4: ECS2 flux compared to EC flux and exact solution, with (a) low viscosity, and (b) viscosity coefficient set at 0.1.

Table 5.1: Tests matrix for the steady shock problem

Variables	Ma = 1.5	Ma = 7.0	Ma = 20.0		
$\nu = 1.0 \times 10^{-7}$	1	<b>√</b>	1		
$\nu = 1.0 \times 10^{-4}$	<b>✓</b>	1	<b>√</b>		
$\nu = 1.0 \times 10^{-3}$	1	1	<b>✓</b>		
$\nu = 1.0 \times 10^{-2}$	1	1	1		

#### 5.3.1 Stationary shock

In the case of the stationary shock, the flow variables are initially set according to the Rankine-Hugoniot jump condition, with the left and right states of the shock labelled as (0) and (1) respectively:

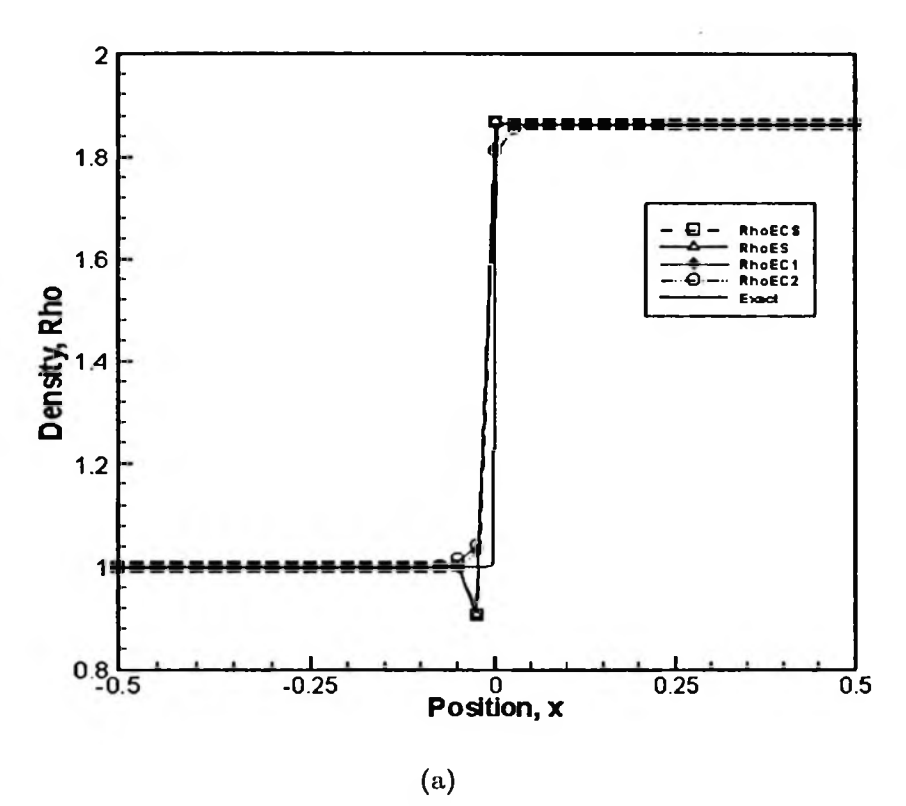
$$u_{0} = \begin{bmatrix} f(M_{0}) \\ 1 \\ \frac{g(M_{0})}{\gamma(\gamma-1)M_{0}^{2}} + \frac{1}{2f(M_{0})} \end{bmatrix} \quad u_{1} = \begin{bmatrix} 1 \\ 1 \\ \frac{1}{\gamma(\gamma-1)M_{0}^{2}} + \frac{1}{2} \end{bmatrix}$$
 (5.4a)  
$$f(M_{0}) = (\frac{2}{(\gamma+1)M_{0}^{2}} + \frac{\gamma-1}{\gamma+1})^{-1}$$
 (5.4b)

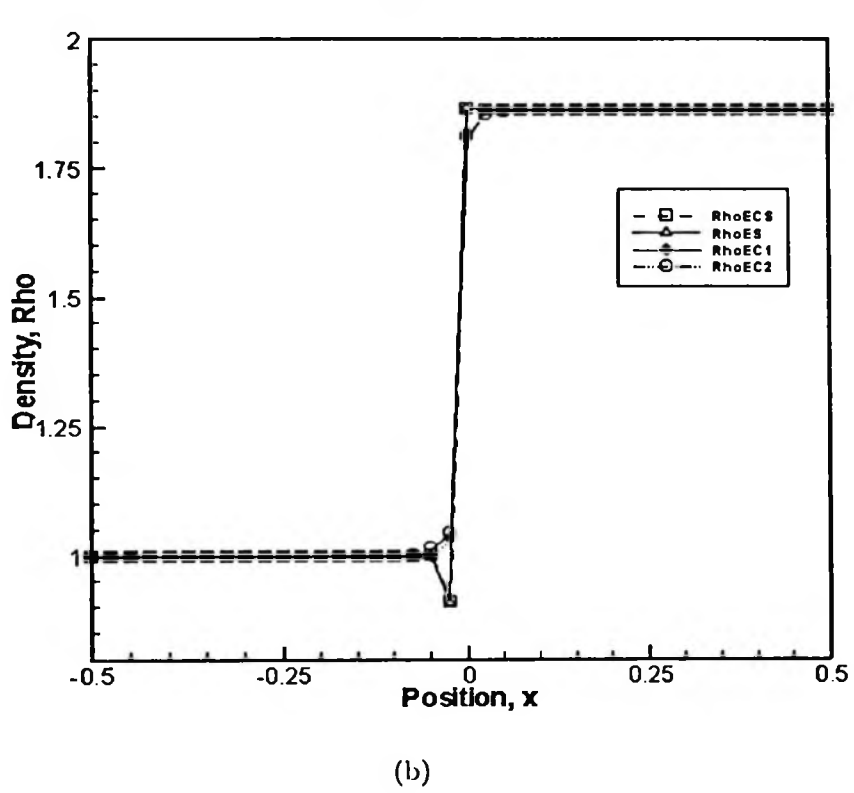
$$f(M_0) = \left(\frac{2}{(\gamma+1)M_0^2} + \frac{\gamma-1}{\gamma+1}\right)^{-1} \tag{5.4b}$$

$$g(M_0) = \frac{2\gamma M_0^2}{\gamma + 1} - \frac{\gamma - 1}{\gamma + 1} \tag{5.4c}$$

This initial condition is such that the shock is expected to occur somewhere at position x = 0; thus the domain of interest is positioned from x = -0.5, and extends to x = 0.5. As in the previous case, a 40 cell setup was used, with non-reflecting boundary conditions on the left and right. The test matrix is summarized in Table 5.1.

Results for this ECS scheme is shown, firstly for a Mach number of 1.5 in Figure 5.5. Here the ECS scheme is compared to the original Entropy Stable scheme (ES), Entropy Consistent Scheme 1 (EC1), and Entropy Consistent Scheme 2 (EC2), all from Ismail and Roe (2009). Four viscosity coefficient values of  $1.0 \times 10^{-7}$ ,





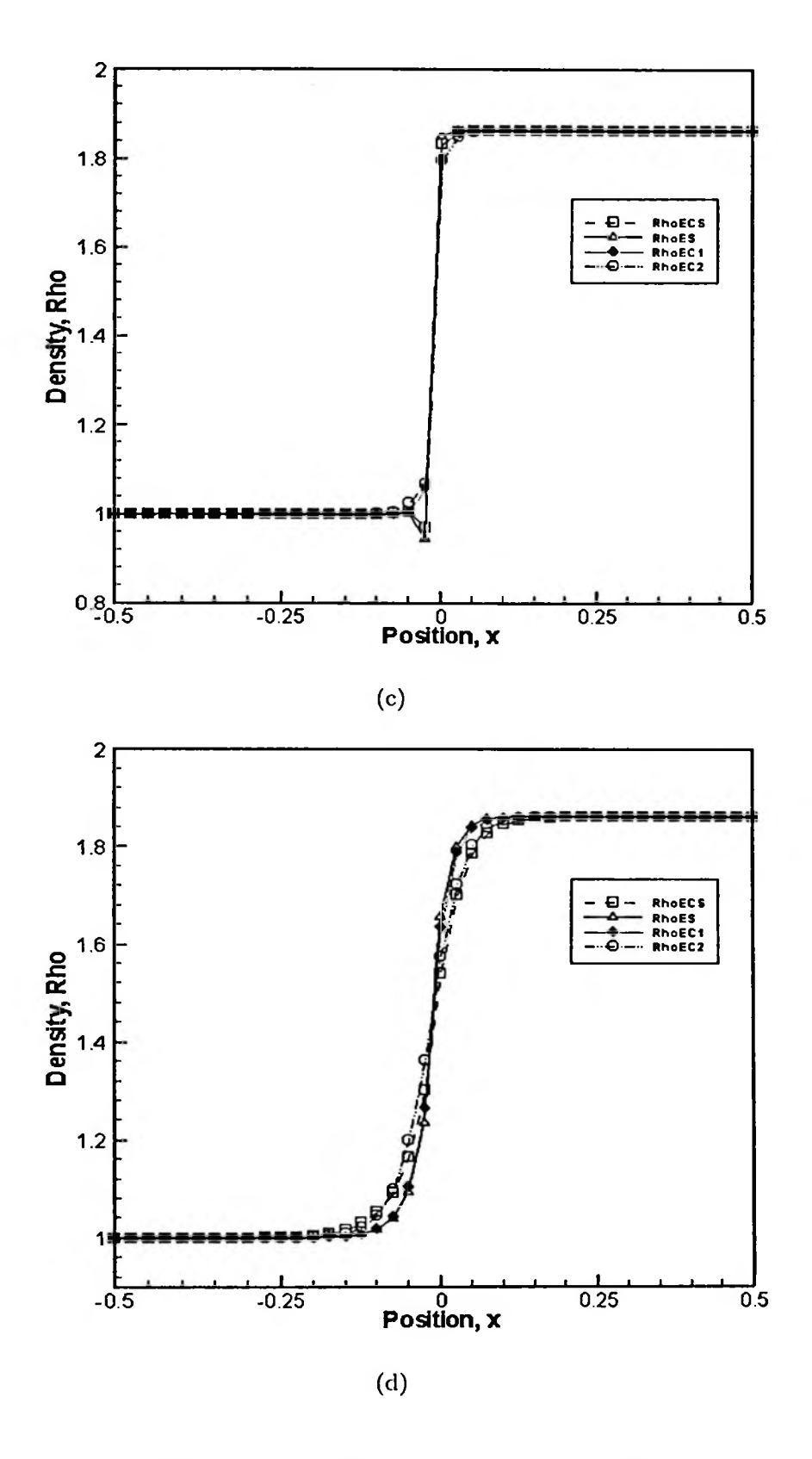


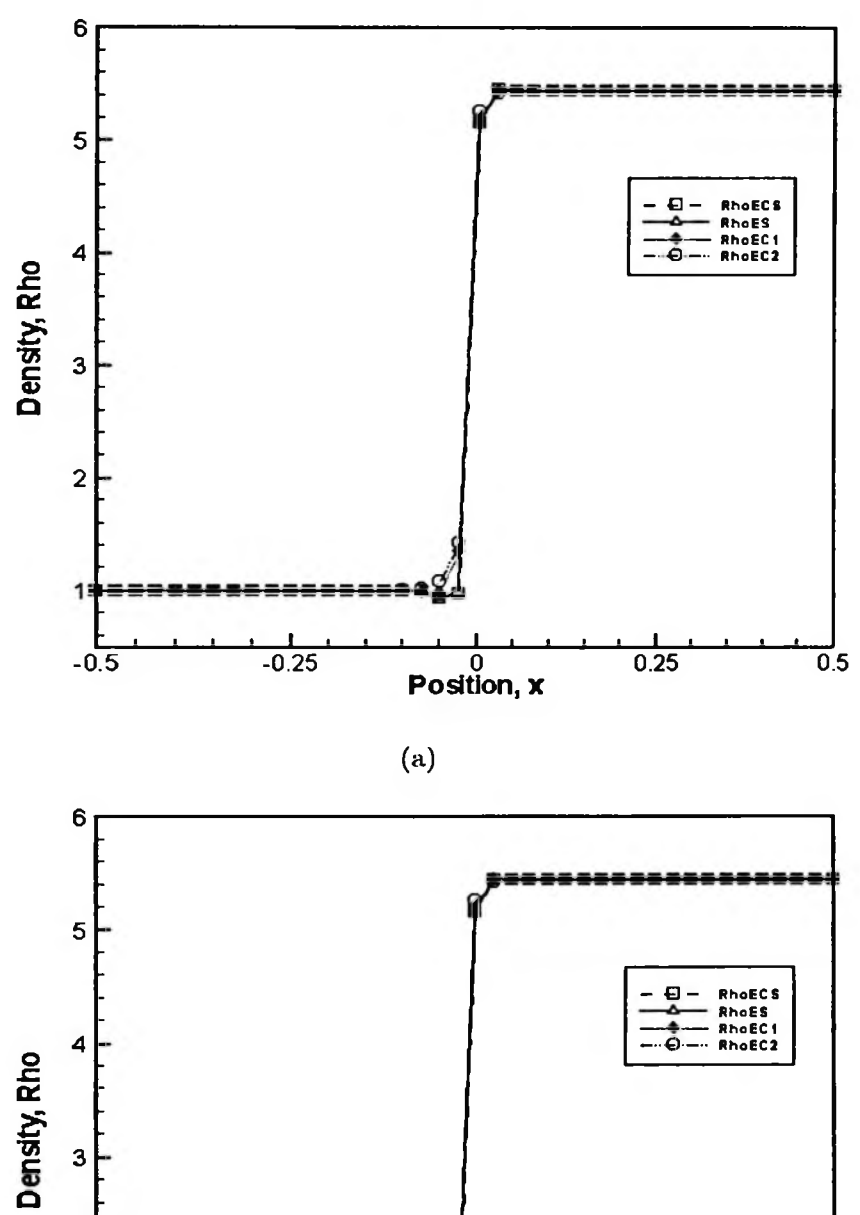
Figure 5.5: Steady state shock solution of density at Mach number 1.5 with viscosity coefficient of (a)  $1.0 \times 10^{-7}$ , (b)  $10^{-4}$ , (c)  $10^{-3}$ , and (d)  $10^{-2}$ .

 $1.0 \times 10^{-4}$ ,  $1.0 \times 10^{-3}$ , and  $1.0 \times 10^{-2}$ , were chosen to represent low to high viscosity levels.

At very low viscosity values of Figure 5.5(a), the result for ECS is identical to the ES scheme, particularly in the presence of an undershoot just before the shock. This is expected since at very low viscosities, the effect of the source terms in the system is almost non-existent and thus the scheme reduces to the entropy stable Navier-Stokes scheme. With that result in mind, the viscosity value is increased to  $\nu = 0.0001$  as shown in Figure 5.5(b). It is seen that the result for ECS is still closely similar to that of the ES flux for all Mach numbers shown, even with this higher viscosity.

However if the viscosity coefficient is increased further to  $\nu=0.001$ , a slight change in the pattern of the ECS flux can be observed, as shown in Figure 5.5(c). Here it can be seen that an undershoot is still present for the result of ECS, but its magnitude is now slightly less than the ES flux. This shows the source term of  $\tau$  in the system is starting to take effect. The viscosity is then increased again to the high value of  $\nu=0.01$ , results of which is shown in Figure 5.5(d). It appears that the source term in the ECS scheme has a considerably larger diffusive effect to the density profile at this viscosity as compared to the other three schemes considered.

The same pattern can also be seen at Mach 7.0 in Figure 5.6, even though the ECS scheme tends to produce a slightly non-monotone solution before the shock at this Mach number. In the high Mach number case of Figure 5.7, the undershoot is again reduced for ECS compared to ES, but now the undershoot is smeared over four or five cells. Additionally, the scheme becomes somewhat unstable in high viscosity and high Mach number situations, as seen in Figures 5.6(d) and 5.7(d). From the plots shown previously, it can be said that even with the hyperbolic



0 0.25 0.5 Position, x

(b)

-0.25

2

-0.5

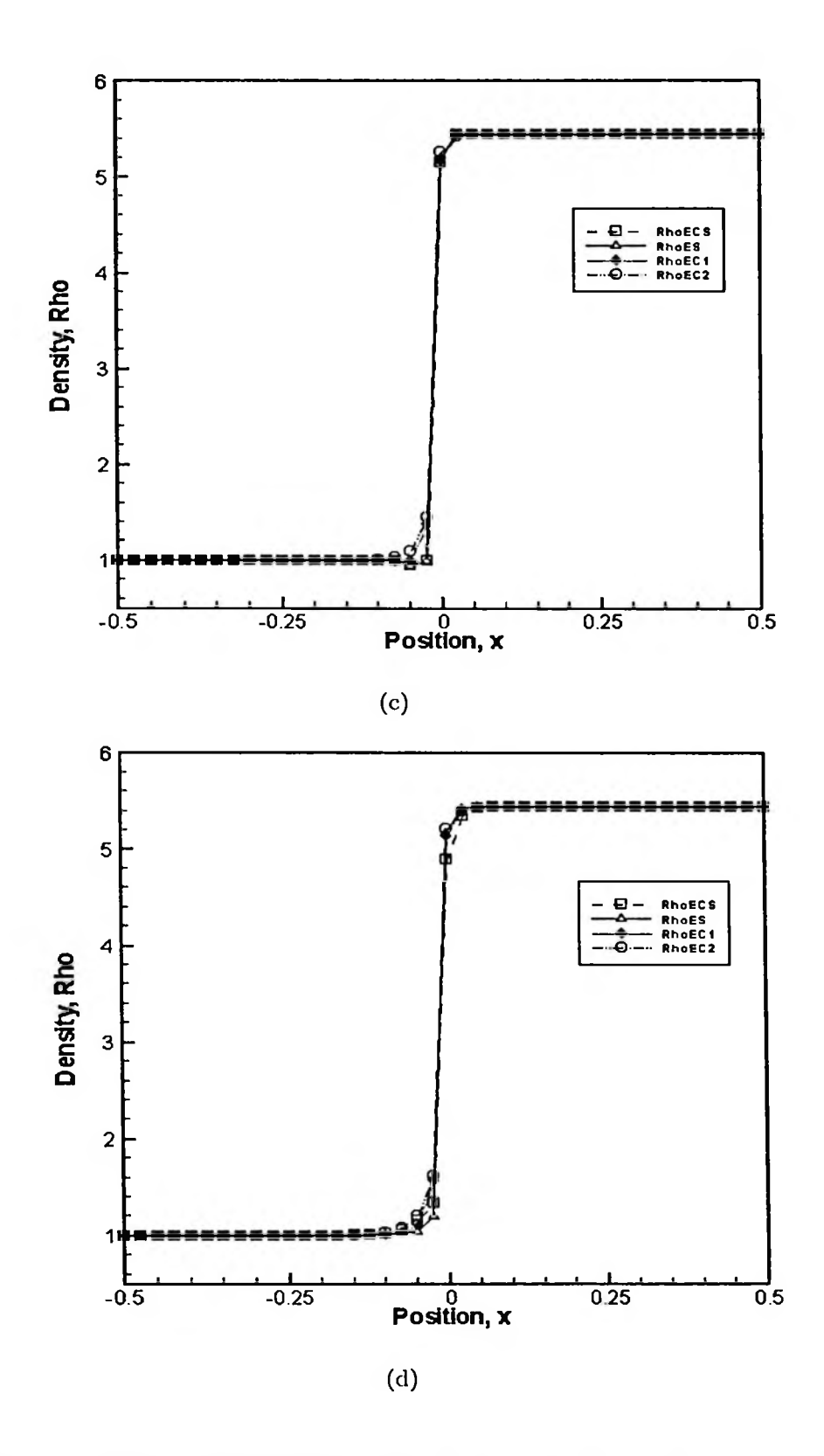
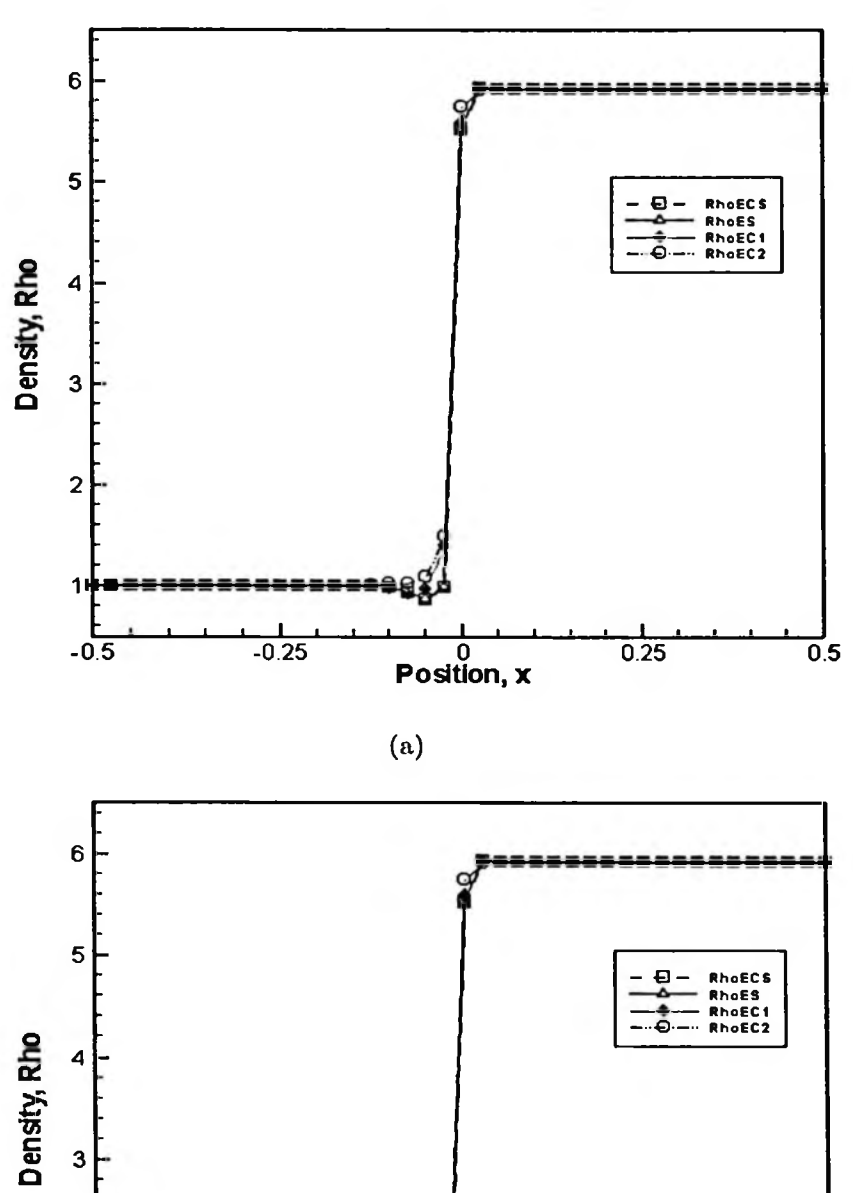


Figure 5.6: Steady state shock solution of density at Mach number 7.0 with viscosity coefficient of (a)  $1.0 \times 10^{-7}$ , (b)  $10^{-4}$ , (c)  $10^{-3}$ , and (d)  $10^{-2}$ .



2

-0.5

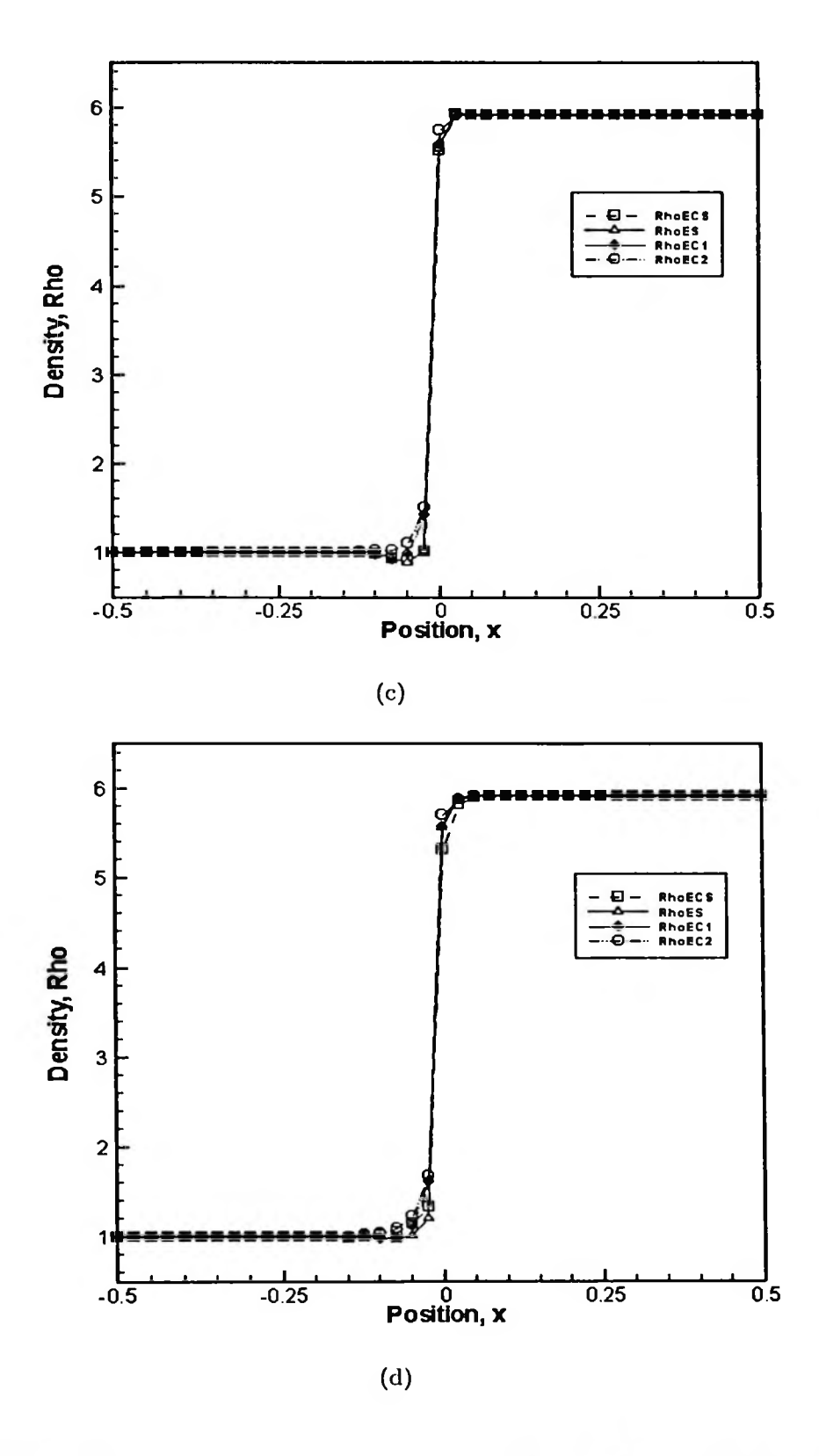


Figure 5.7: Steady state shock solution of density at Mach number 20.0 with viscosity coefficient of (a)  $1.0 \times 10^{-7}$ , (b)  $10^{-4}$ , (c)  $10^{-3}$ , and (d)  $10^{-2}$ .

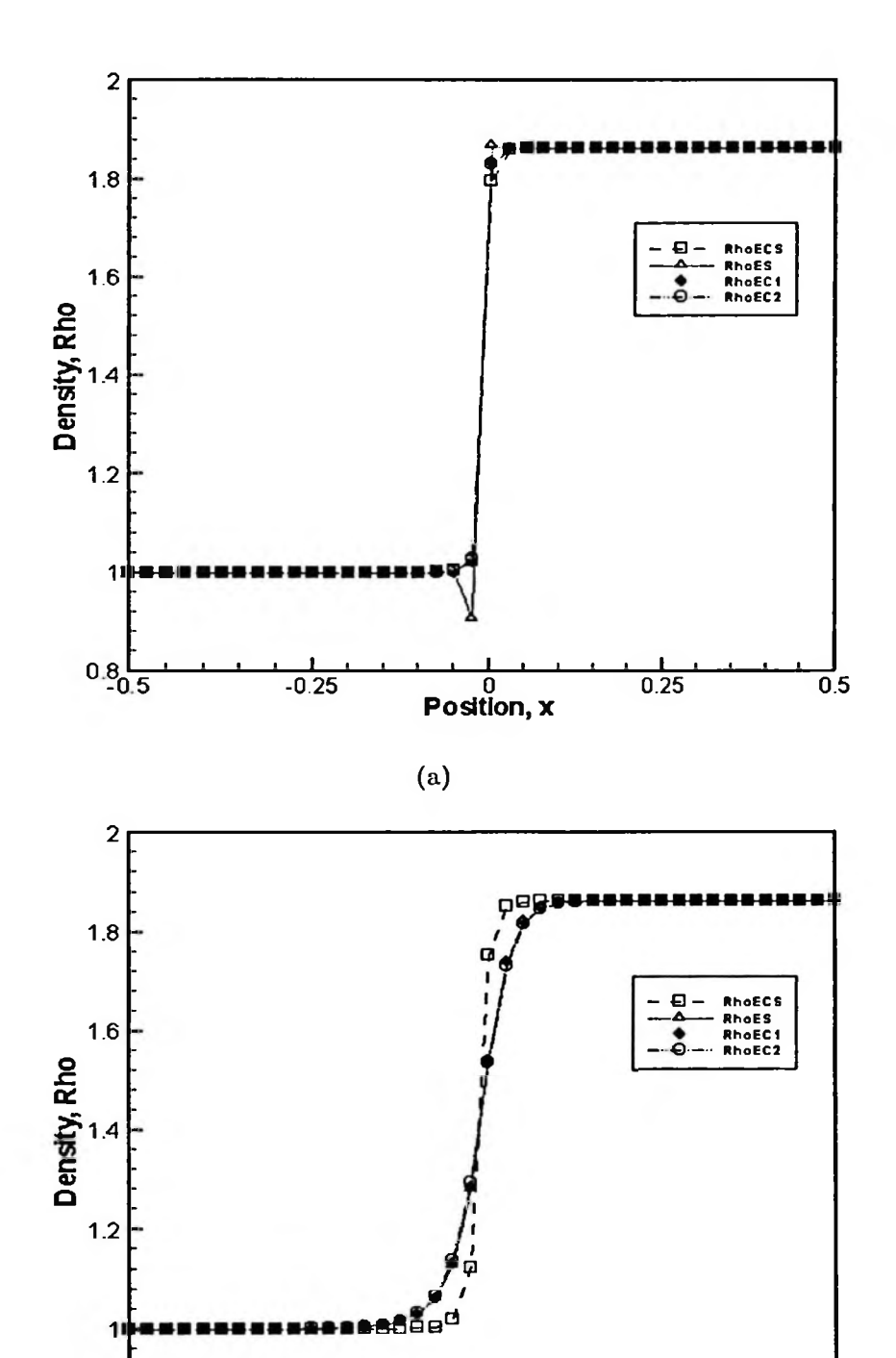
source terms used in the first-order system, the density profile still requires an entropy fix in the same vein as those used in the EC1 and EC2 schemes. To produce monotone solutions, extra dissipation is needed specifically to the acoustic waves, and this cannot be achieved using hyperbolic source terms exclusively, since these terms affect all waves indiscriminately.

Figure 5.8 shows the second-order accurate results for the tested fluxes at selected settings of either Ma = 1.5 or Ma = 20.0, and either  $\nu = 1e - 7$  or  $\nu = 1e - 2$ . These results corroborate the observations made in the first-order cases, having similar trends to that of their counterparts. In support of the density profiles, Figure 5.9 show the viscous stress plots for the same cases as the previous figure. The levels of  $\tau$  in these figures are found to vary according to the viscosity coefficient and the free stream Mach number at the inlet.

# 5.3.2 Sod's shock tube problem

Next, the fluxes are compared in the case of Sod's problem (Sod, 1978), a common test of competency for shock capturing Riemann solvers. This scenario simulates a shock tube having two compartments separated by a diaphragm, with the initial condition for left and right states described in Table 5.2. At the start of the test, the diaphragm is removed to allow for the interaction between the gases from the left and right half of the tube. After a time interval of 0.0061 seconds, the results for the test is recorded in terms of density, velocity, and pressure, shown in Figure 5.10 (a), (b), and (c) respectively.

From the moment the diaphragm is burst, three types of discontinuities will develop. The first type is the rarefaction wave, which forms and propagates from the right half of the tube toward the left. This wave can be characterized by the downward slope between positions x = 2 to x = 6 in all three plots of the figure.



(b)

Position, x

0.25

0.5

-0.25

0.8

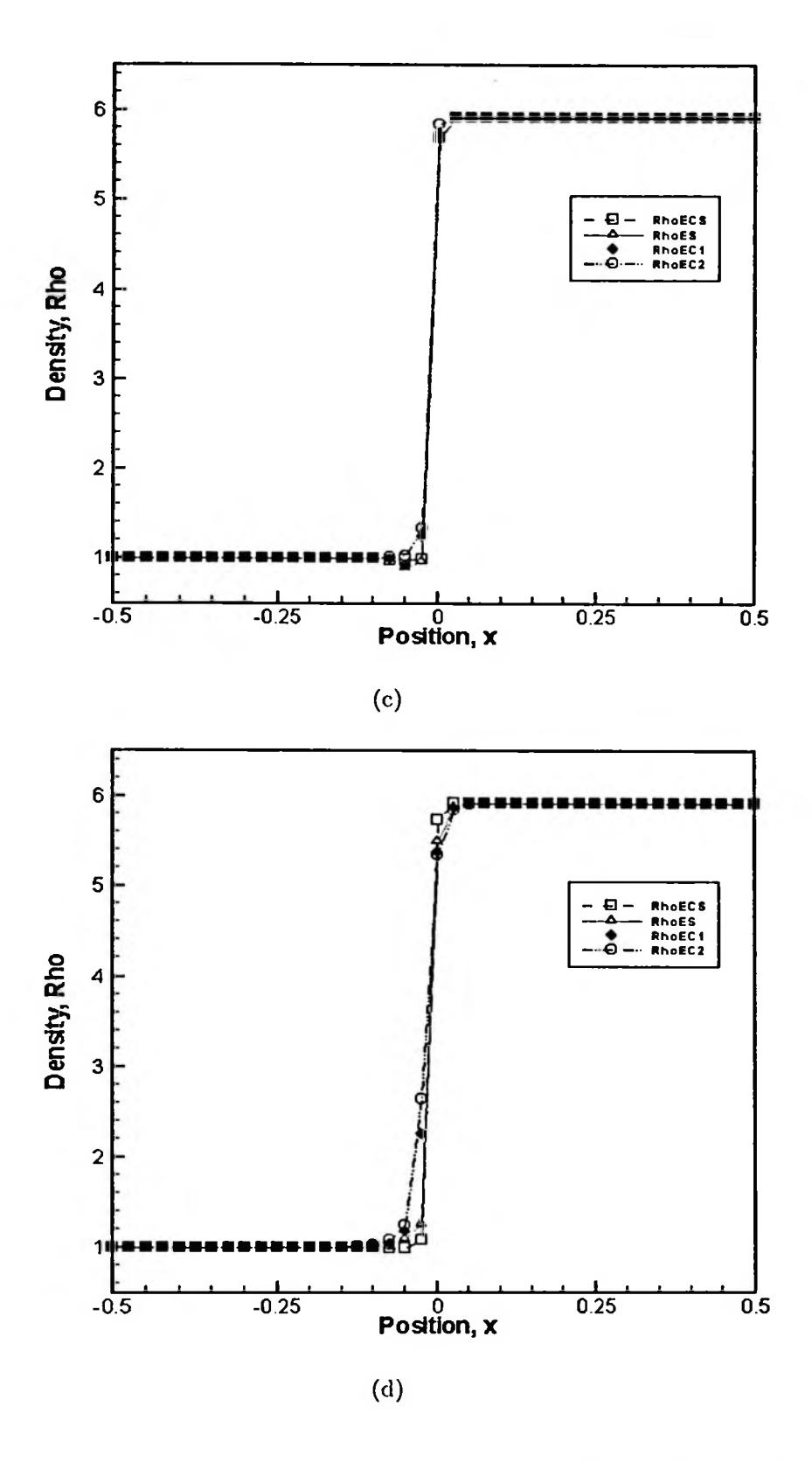
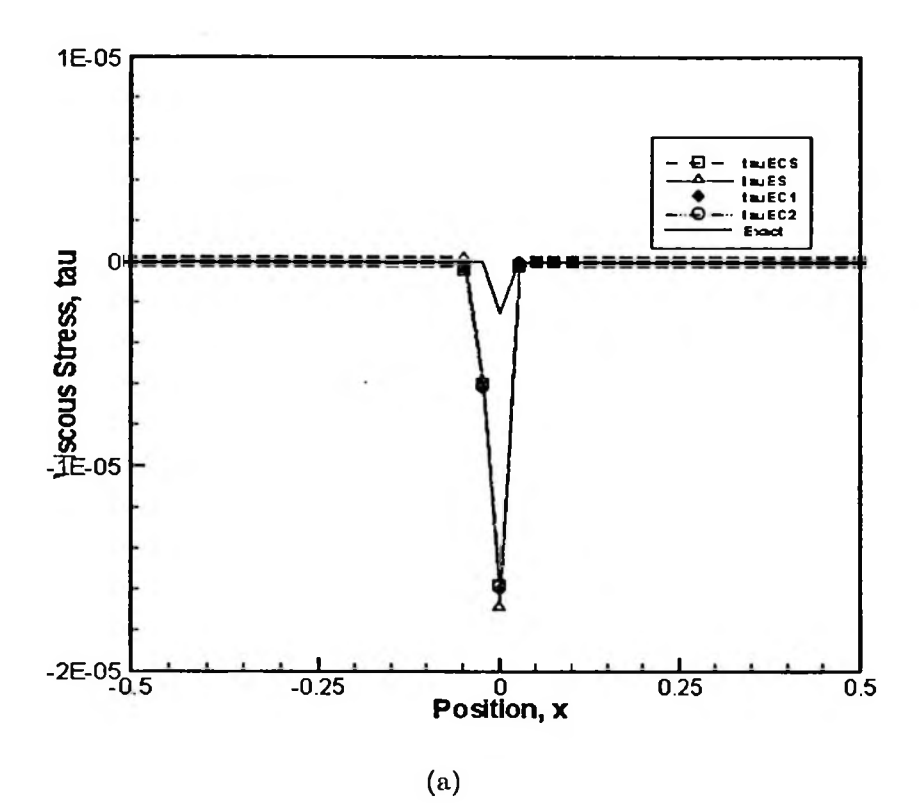
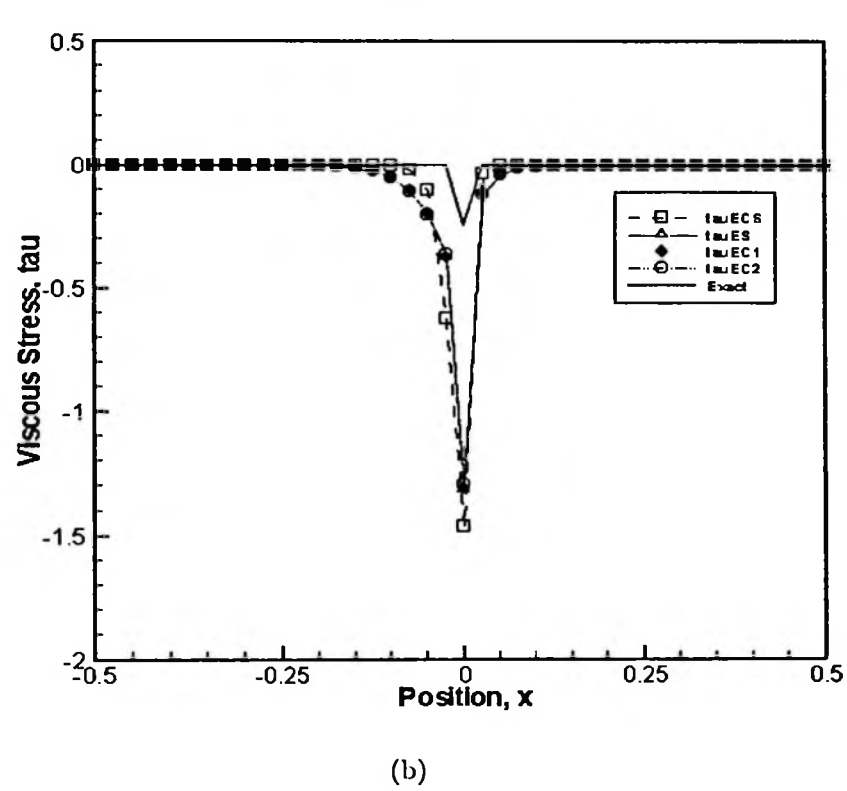


Figure 5.8: Second order density plot of steady shock for the EC fluxes in the case of (a)  $Ma=1.5, \nu=1e-7$ , (b)  $Ma=1.5, \nu=1e-2$ , (c)  $Ma=20.0, \nu=1e-7$ , and (d)  $Ma=20.0, \nu=1e-2$ .





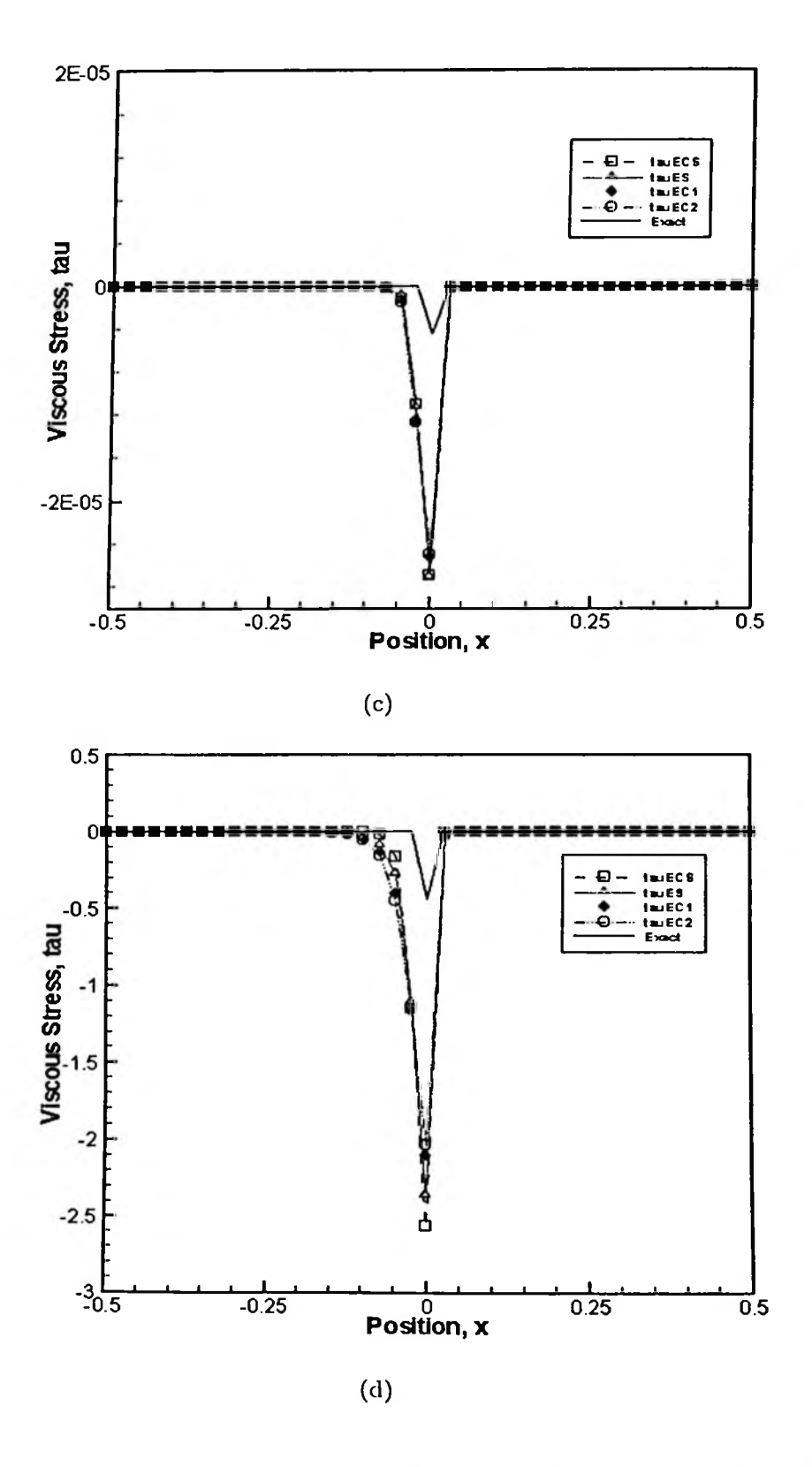
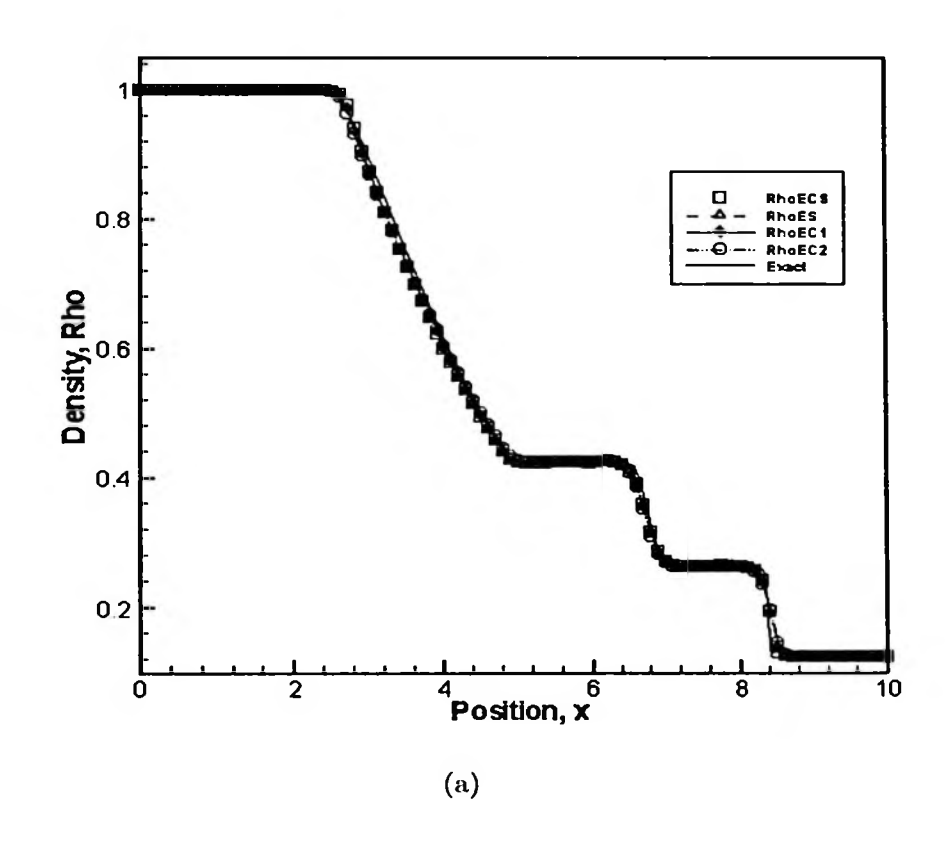


Figure 5.9: Second order viscous stress plot of steady shock for the EC fluxes in the case of (a)  $Ma=1.5, \nu=1e-7$ , (b)  $Ma=1.5, \nu=1e-2$ , (c)  $Ma=20.0, \nu=1e-7$ , and (d)  $Ma=20.0, \nu_{10}$ 8le-2.

Table 5.2: Initial conditions for Sod's problem

Parameter	Left State	Right State
Density	1.0	0.125
Velocity	0.0	0.0
Pressure	$1.0 \times 10^{5}$	$1.0\times10^4$



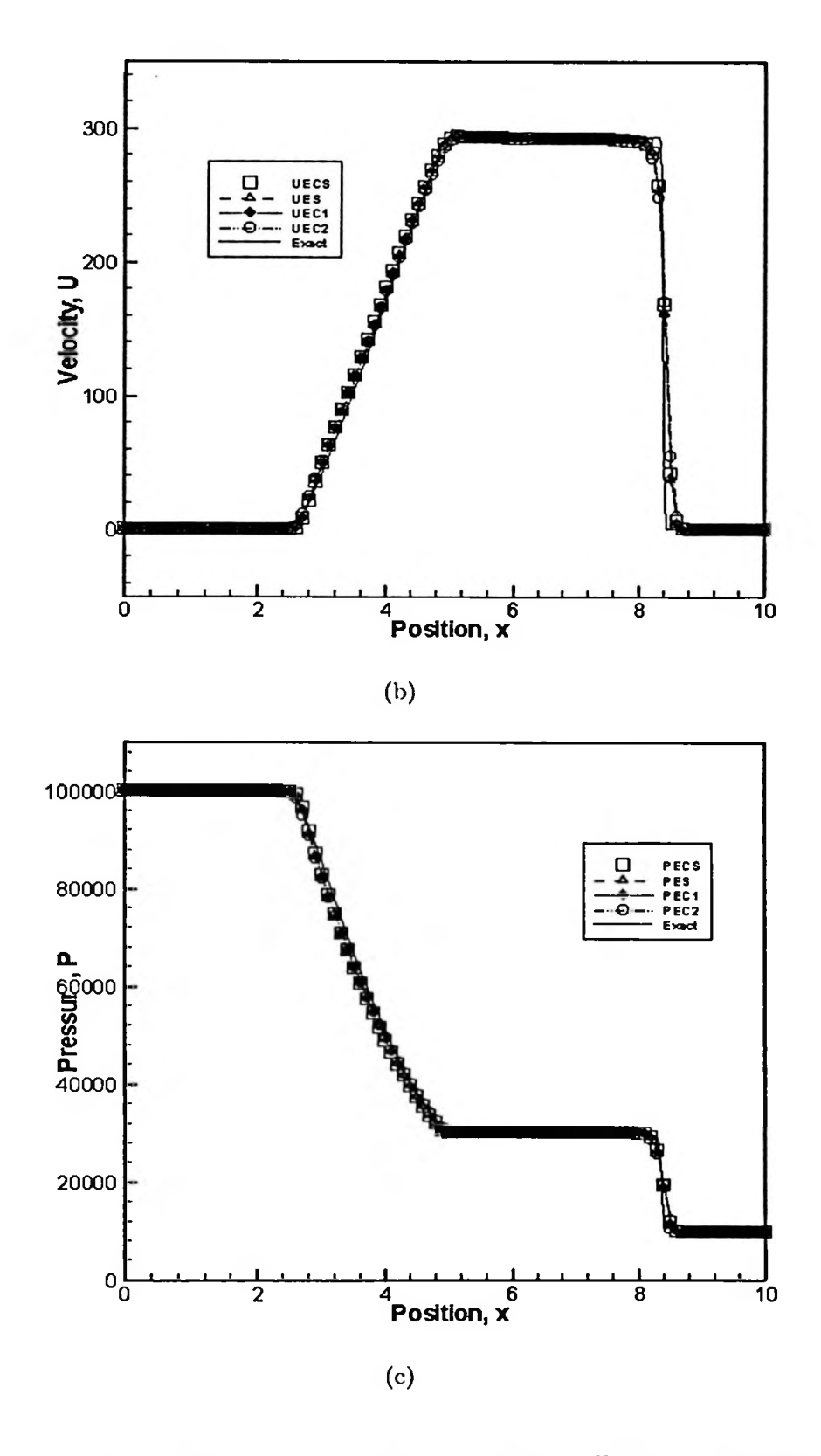


Figure 5.10: Results of Sod's problem with viscosity coefficient of 0.01 for different system cases showing data of (a) density, (b) velocity, and (c) pressure.

The second discontinuity is the shockwave, which moves in the opposite direction from the rarefaction. At the point in time in which the data is captured, the shock position lies in between positions x = 8 to x = 10 in the tube. Lastly, the interaction between these two waves produces a third type called the contact discontinuity, apparent only in the plot for density.

The results in all three plots of the figure show that the new ECS flux is in close agreement with all of the schemes it is compared to, namely the ES, EC1, and EC2 fluxes. Just like its predecessors, the ECS flux is able to differentiate between rarefaction and shockwave, with the slope of the rarefaction having a more graduated characteristic as compared to the steep drop of the shock. Furthermore, the flux thus does not exhibit any significant overshoots or oscillations in the region of the shock. This test verifies that the Navier-Stokes version of the first-order system flux is at least entropy stable at second-order accuracy.

#### 5.4 The Two Dimensional Case

Finally, the Navier-Stokes fluxes are extended to two dimensions. Test cases for the two dimensional case include flow over a flat plate, flow over a forward facing step, flow over a cylinder, and flow over an airfoil. Each case represents an examination of each different characteristic of the ECS flux in terms of its solutions as compared to the other fluxes considered.

# 5.4.1 Flow over a flat plate

The two-dimensional, entropy consistent first-order Navier-Stokes flux (ECS) is firstly tested in the problem of flow over a semi-infinite flat plate, in which the standard boundary conditions were used. The grid showing the meshing for this problem is shown in Figure 5.11.

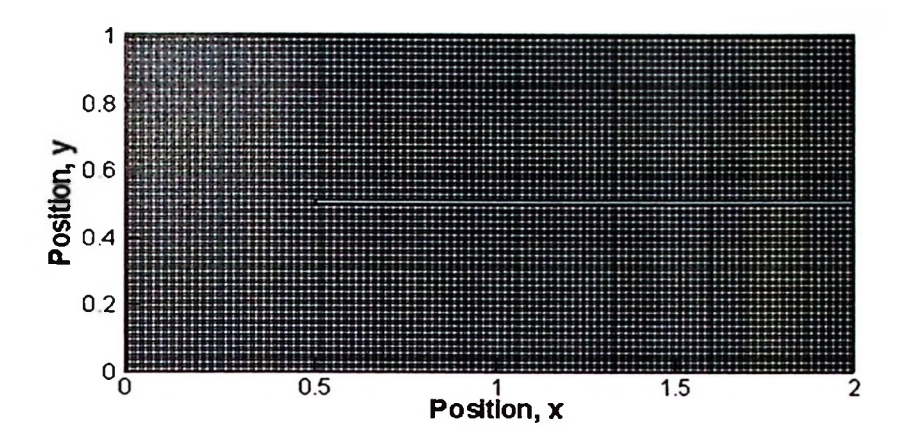


Figure 5.11: Sample grid of the flat plate.

Figure 5.12(a) shows the Mach number contour of the flow simulation for a free stream Mach number of Ma = 0.3 and Reynolds number Re = 3000, which corresponds to a viscosity coefficient of  $1.4 \times 10^{-4}$ . Velocity data are then nondimensionalized and compared to the Blasius exact solution in 5.12(b), and the solutions by the fluxes of EC1 and EC2 from Ismail and Roe (2009). For the ECS flux, there appears to be a slight bump up in terms of velocity growth at the region of 0 < n < 2, resulting in the non-linearity of the ECS plot profile in that area. Meanwhile, the EC1 and EC2 solutions simulate that the flow would reach free stream velocity value closer to the wall than the ECS flux and the Blasius solution; this essentially means that these fluxes predict a thinner boundary layer than the exact solution, which is expected for artificially diffused fluxes. On the other hand, the overall trend show that the ECS flux is able to capture the boundary layer profile reasonably well, at least in the laminar region. It is significant to note that this boundary layer result has been achieved without the use of any special treatment to the near-wall region. Otherwise, the result can be improved by implementing one of many methods of boundary layer approximation.

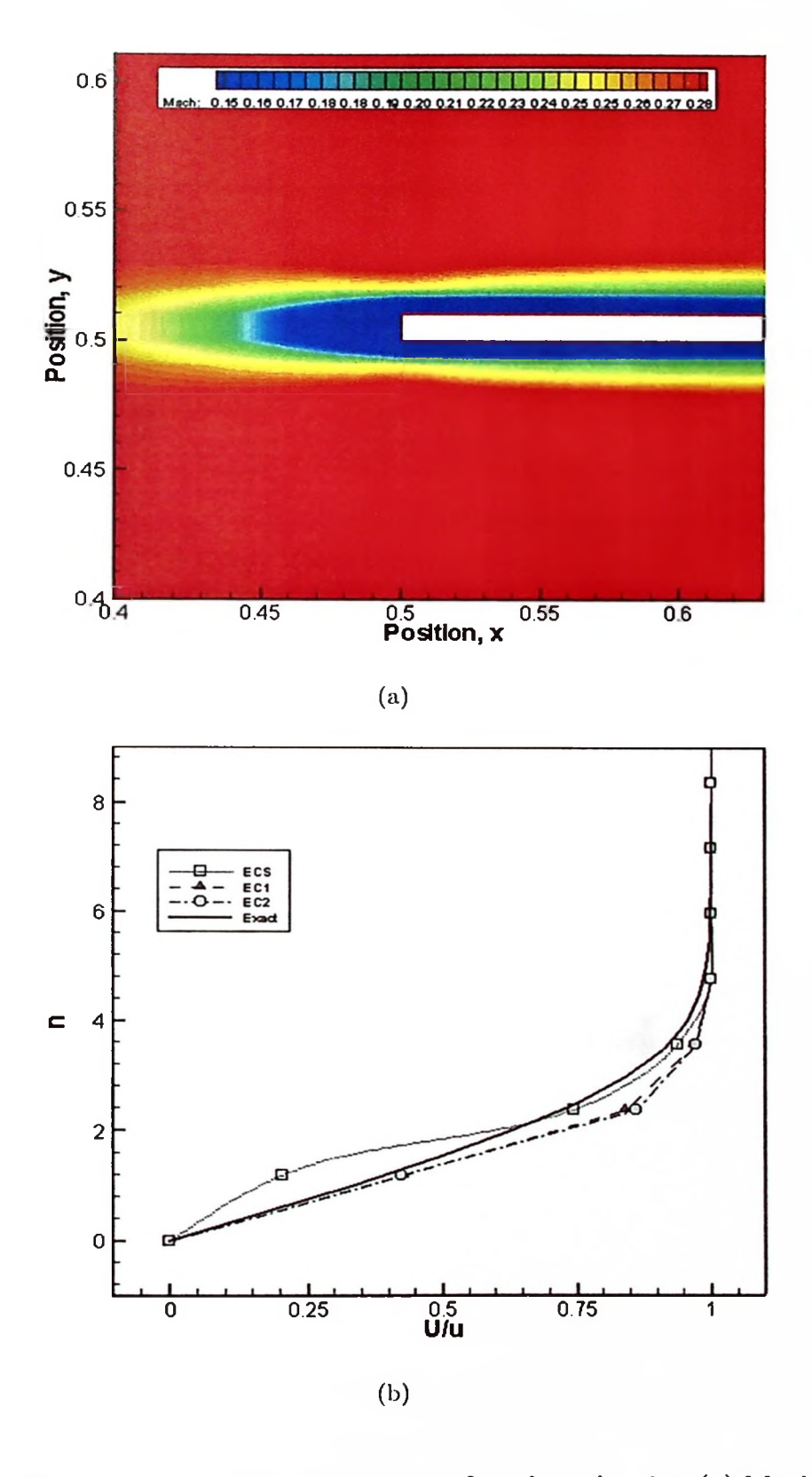


Figure 5.12: Simulation result for flow over a flat plate showing (a) Mach number contour, and (b) comparison of velocity magnitude with Blasius solution.

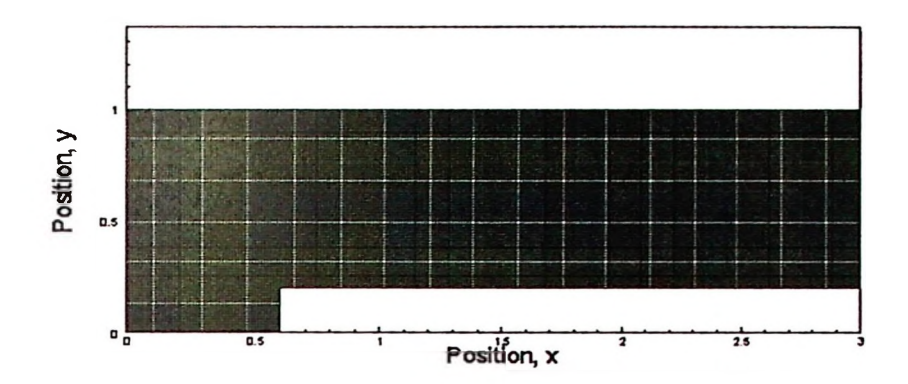
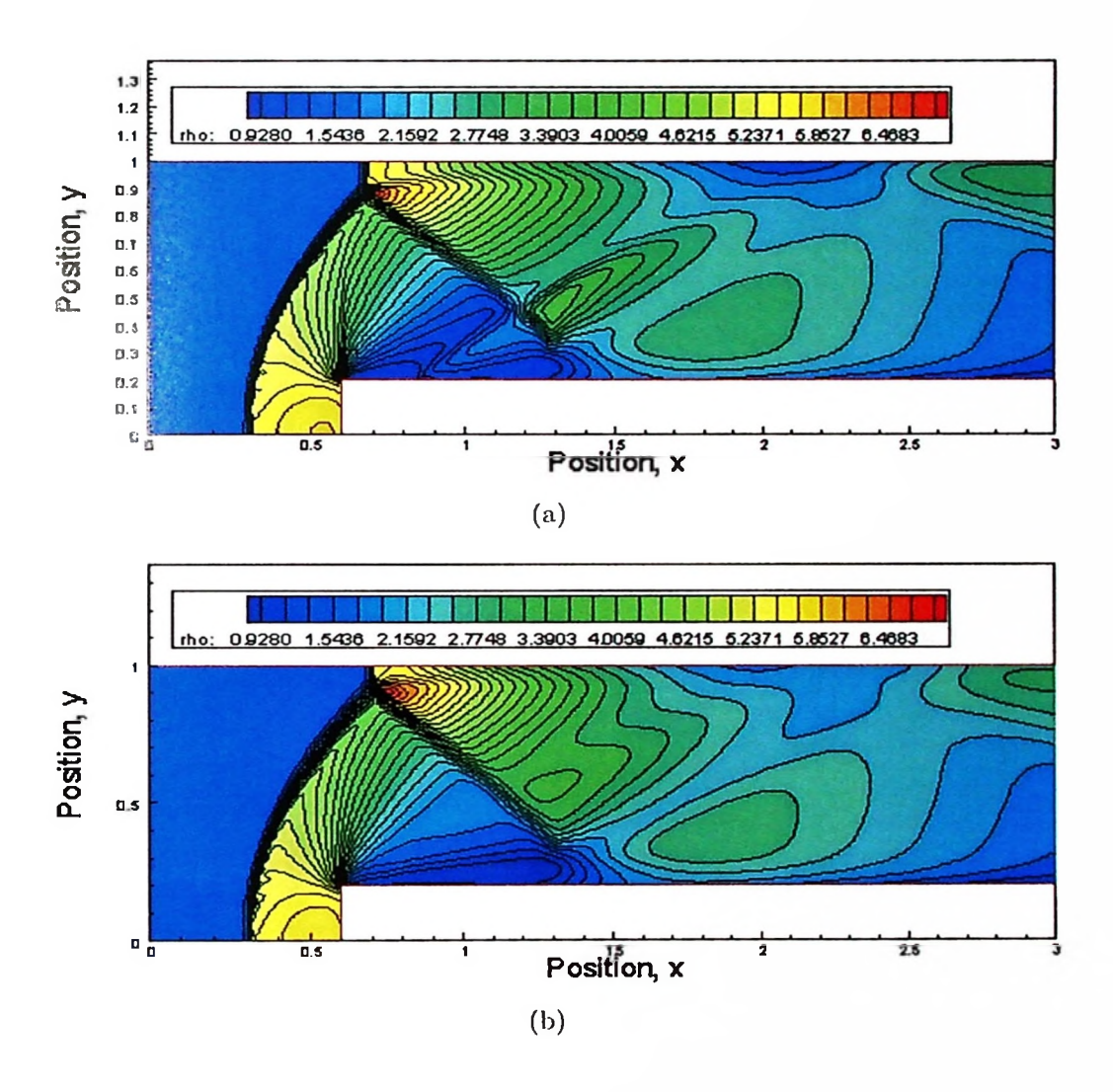


Figure 5.13: Sample grid of the forward facing step.

## 5.4.2 Flow over a forward facing step

The ECS flux is then tested using the problem of a Mach 3 flow over a forward facing step in a channel of infinite width. This problem was introduced by Colella and Woodward (1984), and has been widely used as a proving ground for shock capturing schemes ever since. A sample grid of this test case is shown in Figure 5.13. The major challenge of simulating flow for this problem is the existence of several intersecting shocks.

From Figure 5.14, it is seen that the ECS flux produced a qualitative result that is closer to the Roe flux than to the EC1 and the EC2 fluxes. The location of the initial shock is closer to being parallel to the step as compared to the other entropy consistent fluxes, and the oblique shocks downstream are thinner and more defined. This shows that the ECS flux is less diffusive that the other fluxes compared here, and less susceptible to the problem of smearing in the shock profile. Whilst the EC1 and EC2 fluxes have been shown to produce acceptable results in Roslan and Ismail (2012) as compared to the PPMLR scheme in Colella and Woodward (1984), the ECS flux represents further improvement with regards to this test case from its predecessors.



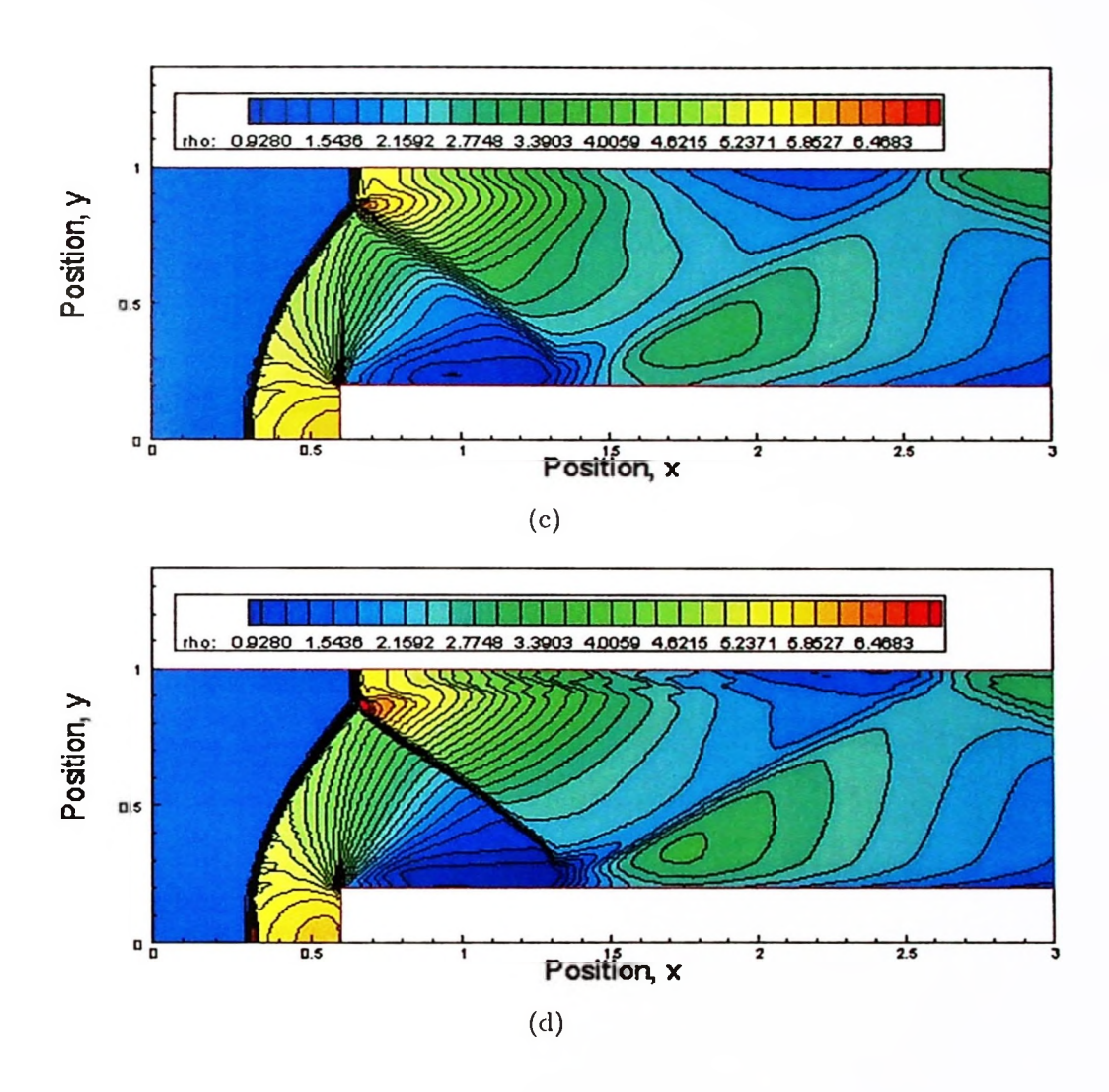


Figure 5.14: Results for flow over forward facing step using (a) EC1, (b) EC2, and (c) Roe, (d) ECS.

Table 5.3: Initial conditions for flow over a cylinder

Parameter	Case: Low Ma	Case: Medium Ma	Case: High Ma
Density	1.4	1.4	1.4
Velocity (x)	$0.006 \sim 0.03$	$0.2 \sim 0.8$	$1.5 \sim 3.0$
Velocity (y)	0.0	0.0	0.0
Pressure	1.0	1.0	1.0
Temperature	400	400	400
Viscosity	0.00021	$2.1 \times 10^{-4}$	$2.1\times10^{-4}$

### 5.4.3 Flow over a cylinder

The evaluation of two-dimensional Navier-Stokes solution is continued with simulations of flow over a circular cylinder of assumed infinite length in the third dimension. This test is notoriously difficult for flux functions that are based on the inviscid flow formulation, or any numerical methods for that matter, and the problem is still extensively studied today after over a century of investigation (Rajani et al., 2009). A compendium of data from experiments, simulations, and analytical calculations is available in a systematically organized book by Zdravkovich (1997). Some of the flow characteristic that usually occur under select conditions in this problem require special treatment that is beyond the scope of this thesis. Therefore, the aim of the ECS flux for this particular test is not to compete with sophisticated high-order schemes that utilize turbulence models in terms of flow accuracy. Rather, this test case could hopefully illustrate the difference between the ECS flux and it predecessor the entropy consistent flux of Ismail and Roe (2009), based on the inviscid Euler equations. The initial condition for this problem is defined in Table 5.3.

A few test grids were created in order to perform the grid independence test, as shown in Figure 5.15. From amongst these, three mesh configurations have been selected to demonstrate the independence of results from the possible variance due to the grid size. The first one in 5.15(a) is the grid deemed as the coarse mesh with a node count of 160 around the perimeter of the cylinder, and 80 nodes of equal distance between each other from the cylinder wall to the domain outer boundary. The second one in 5.15(b) also has 160 nodes around the cylinder edge and 160 nodes in the radial direction; the nodes heading outwards from the cylinder are spaced such that they have a growth or stretch factor of 3.7. The third mesh has the same node count as in (b), but the stretch has been increased to 5.0. This means that the mesh closer to the center has a finer resolution, getting progressively coarser as it gets to the outer region.

Table 5.4.3 summarizes the L-1, L-2, and L-infinity norms for the variable residuals of the considered fluxes from first and second-order simulations. The numbers reported are obtained after 30000 iterations, and are at a scale of 10<sup>-7</sup>. The norms of the first two cases are relatively similar to one another be it for the first or the second order results. Even though the norms generally decrease with the reduction in grid intervals, the marginal difference between the norms of different mesh sizes become less and less significant the finer the mesh becomes. However, the stretch factor associated with each mesh is also an important parameter to be considered. In the third case, even though the node count is the same as the second case, a stretch factor that is too high would bring about an adverse effect towards the ability of the flux to converge towards a stable solution. This may be due to the high skewness of the stretched grid, which would distort the result of the conserved variables.

In Figure 5.16, the EC1 flux in (a) is compared with the system flux in (b) for the case of flow at Mach number 0.3. At first glance, the results for both fluxes look very similar to each other, but under closer scrutiny, one particular difference stands out. In subfigures (c) and (d), a zoomed-in view of the near wall region

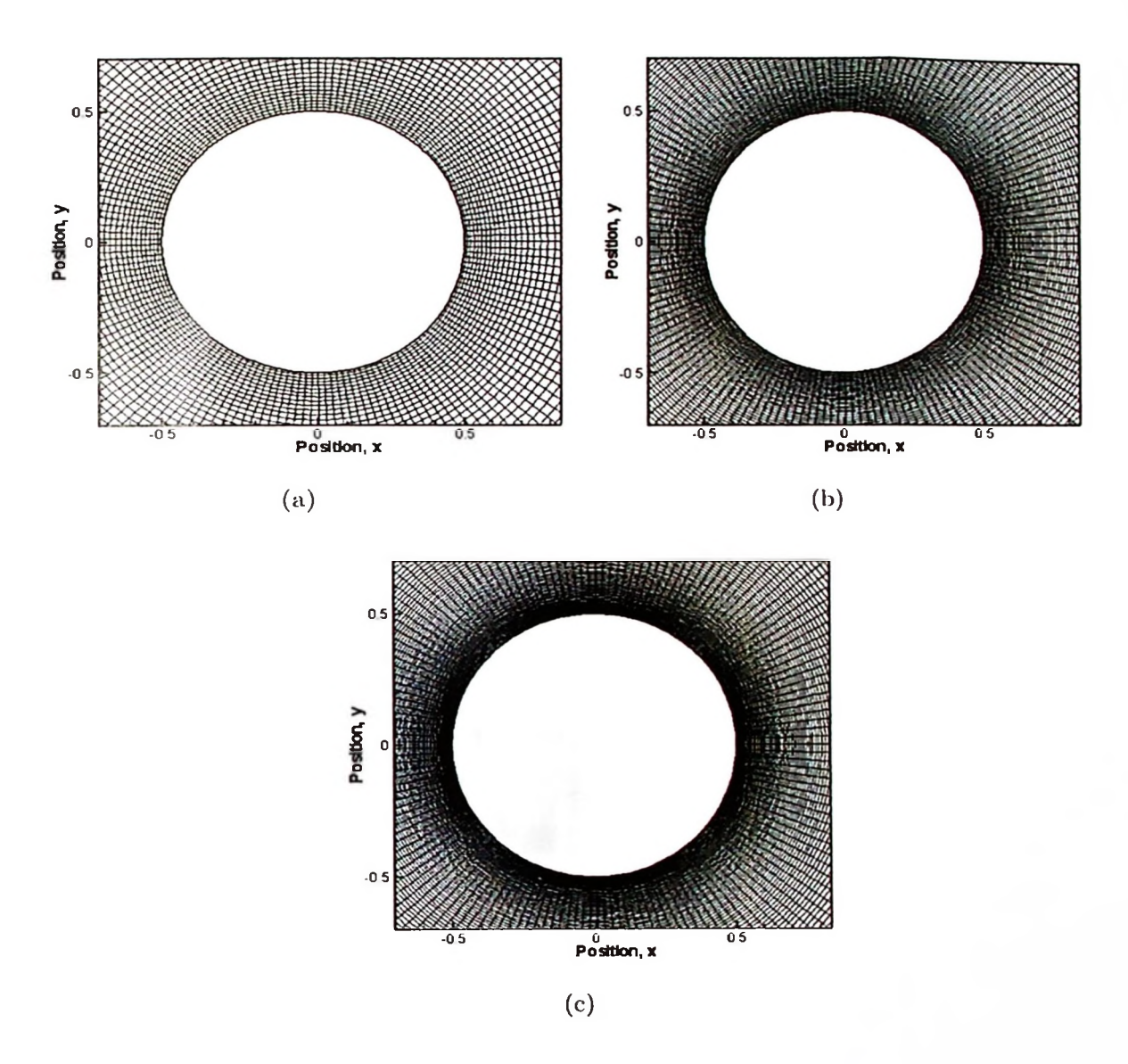


Figure 5.15: Grid used for flow over cylinder with node counts of (a)  $80 \times 160$ , (b)  $161 \times 160$  with growth factor 3.2, and (c)  $161 \times 160$  with growth factor 5.0.

Table 5.4: Comparison of L1, L2 and infinity norms between different grid sizes for the ECS flux a

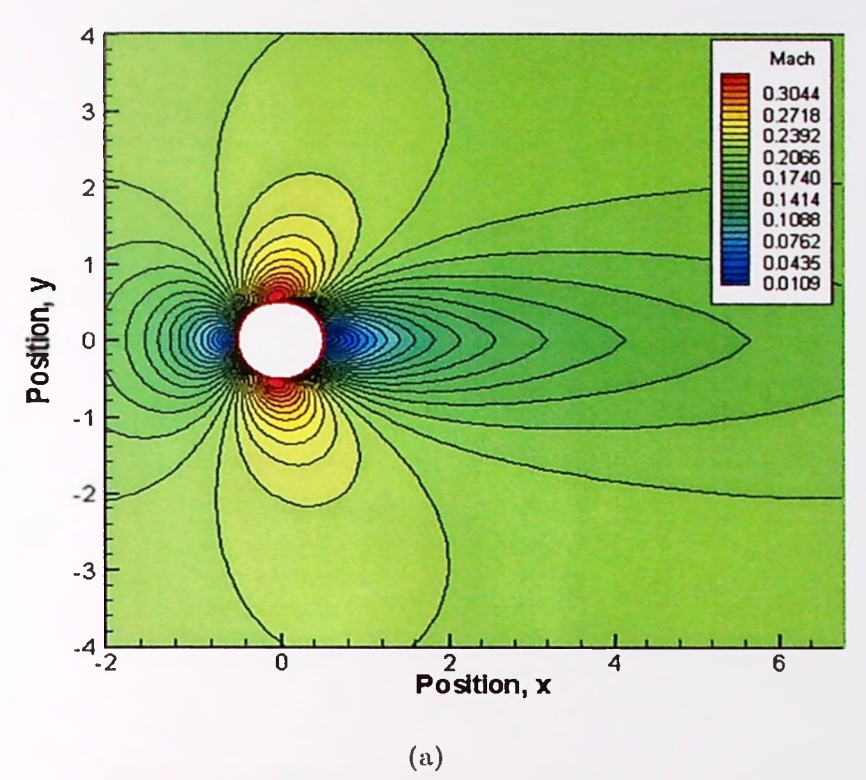
	Grid	81 x 160		161 - 160		161 - 160	
				161 x 160		161 x 160	
Flux	Stretch	1.0		3.7		5.0	
	Order	1st	2nd	1st	2nd	1st	2nd
Mass	L1	1.0268	4.3084	1.0268	3.2503	1.0268	6.1745
	L2	1.0379	4.8533	1.0379	4.0045	1.0379	7.6002
	$L_{inf}$	1.0626	10.254	1.0626	10.846	1.0626	16.941
X-Momentum	L1	1.0000	3.4890	1.0000	3.4636	1.0000	6.4967
	L2	1.1000	4.5630	1.1000	4.3622	1.1000	8.2327
	$L_{inf}$	1.0667	32.424	1.0499	20.243	1.0499	30.443
Y-Momentum	L1	1.0567	2.7186	1.0499	3.4813	1.0379	6.6731
	L2	1.1266	3.9692	1.1000	4.2243	1.1000	8.1970
	$L_{inf}$	1.0982	11.234	1.0805	9.9909	1.0769	19.688
Energy	L1	1.0000	10.967	1.0000	8.0496	1.0000	15.122
	L2	1.0000	12.333	1.0000	9.7409	1.0000	18.382
	$L_{inf}$	1.1000	24.366	1.1000	20.554	1.0921	38.086

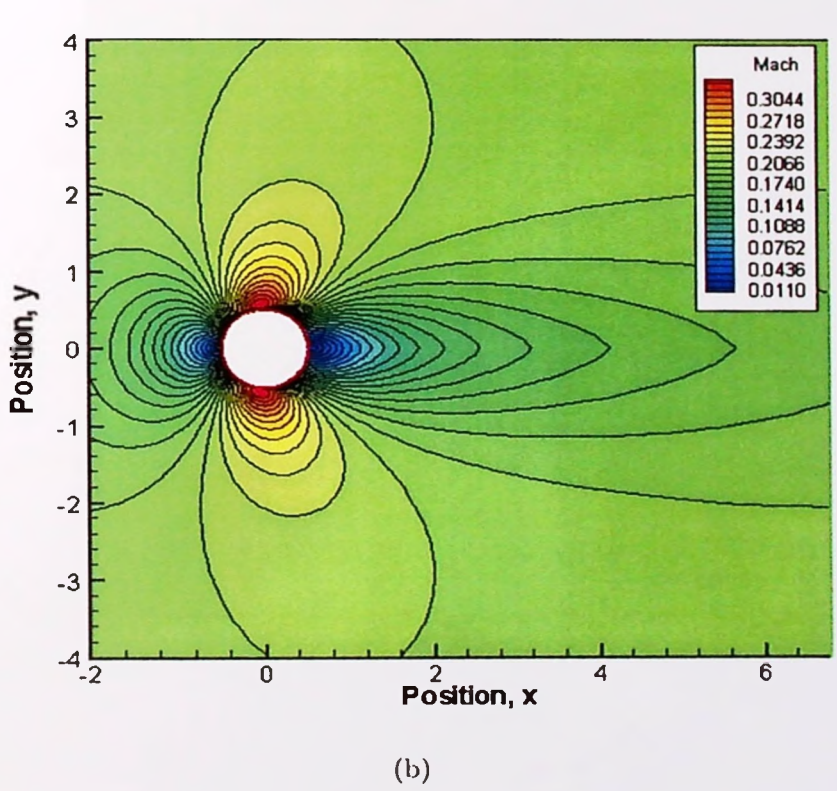
<sup>&</sup>lt;sup>a</sup> Numbers reported are at a scale of  $1 \times 10^{-7}$ 

is provided, to show how the boundary layer of the flow is characterized by each flux. In the near wall region, the EC1 flux displays the boundary effect only at the cell immediately adjacent to the wall, with the velocity almost immediately increasing close to the free stream condition the next cells up. Conversely, the ECS flux displays a more gradual increase in velocity as we move outwards from the cylinder wall, consistent with the boundary layer result demonstrated in the flat plate simulation.

In Figure 5.17, x-axis velocity contours for the system flux is shown for the case of flow at Reynolds number 40 in (a), and at Reynolds number 2000 in (b). These values correspond to a x-velocity values of 0.03 and 0.3 respectively for set constants of density and viscosity coefficient. Conversely for sub-figures (c) and (d), results for the same cases are shown as produced by the commercial software Fluent. Results from Fluent are obtained using laminar settings for the same grid setup as the ECS case, without any turbulence model added on.

The plots show a slight discrepancy between ECS and Fluent at Re = 40, but





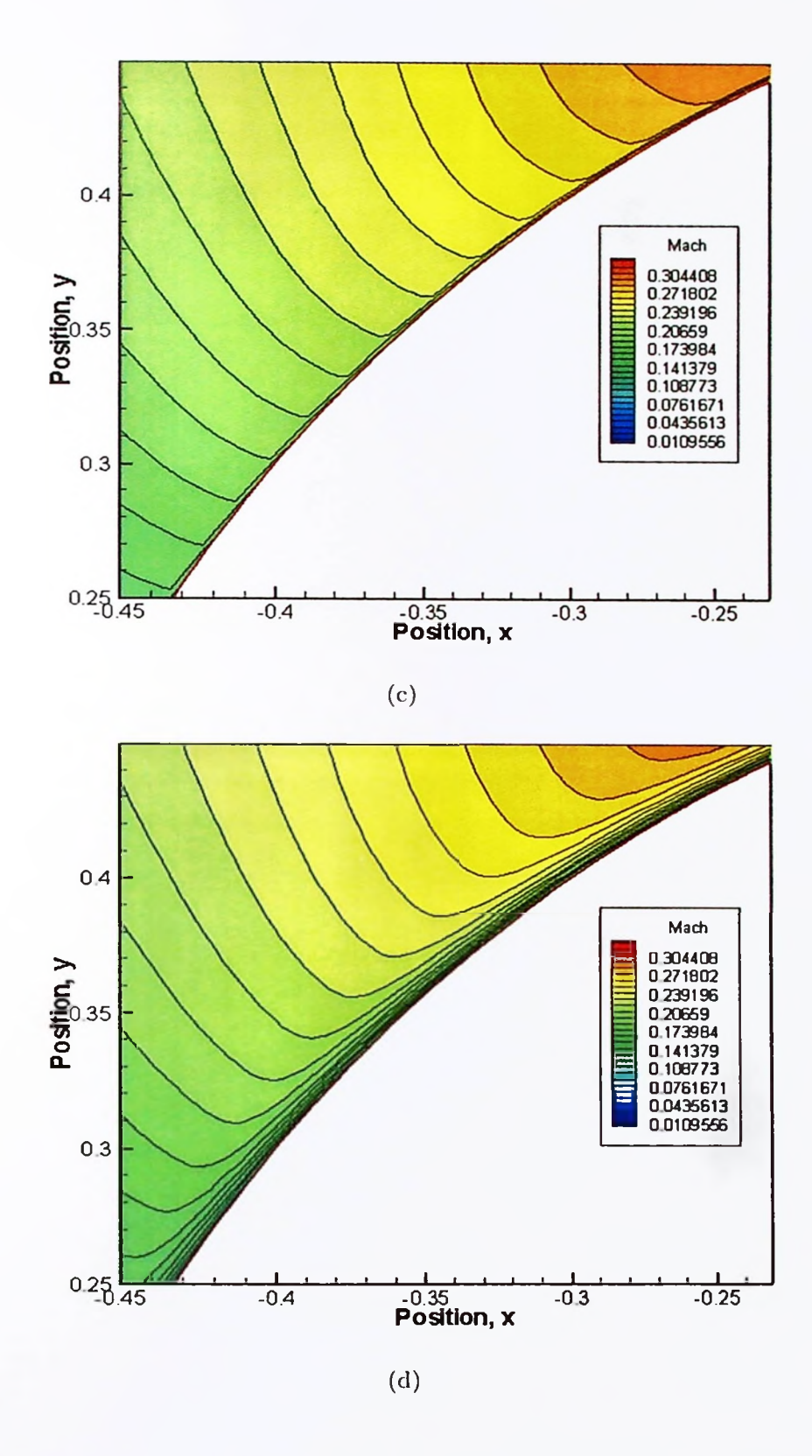
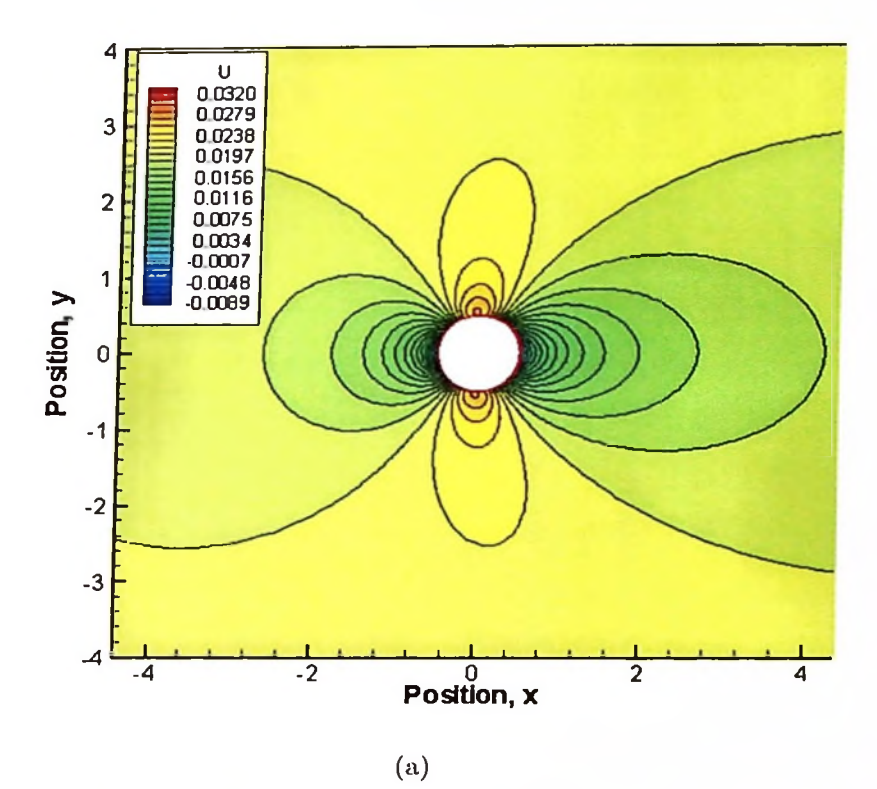
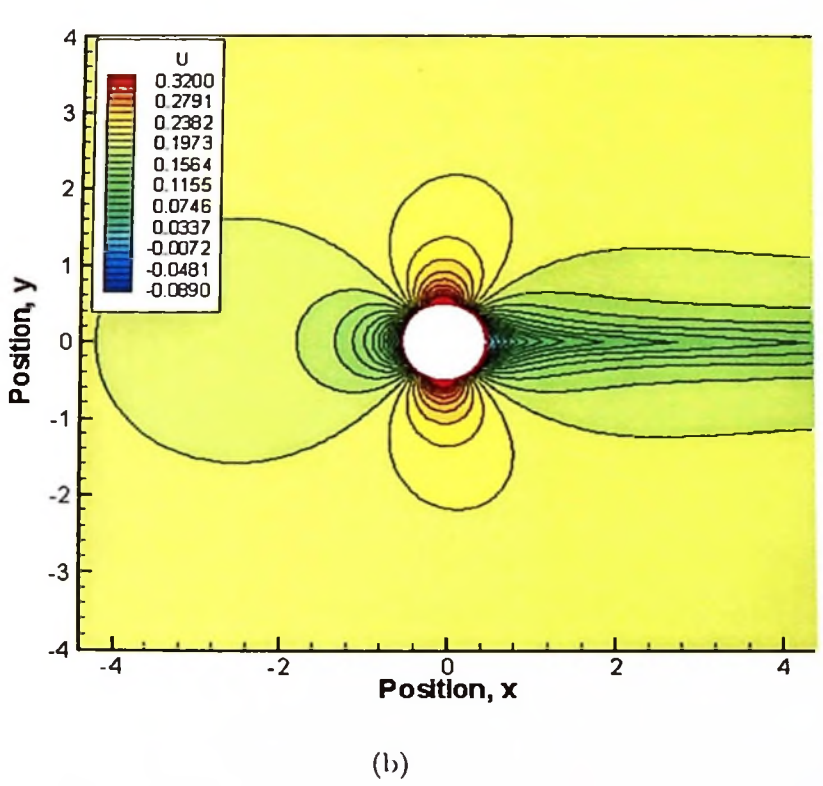


Figure 5.16: Flow over cylinder at Mach numbers 0.3 for fluxes of (a) EC1, (b) ECS, (c) EC1 zoomed in, and (d) ECS zoomed in.





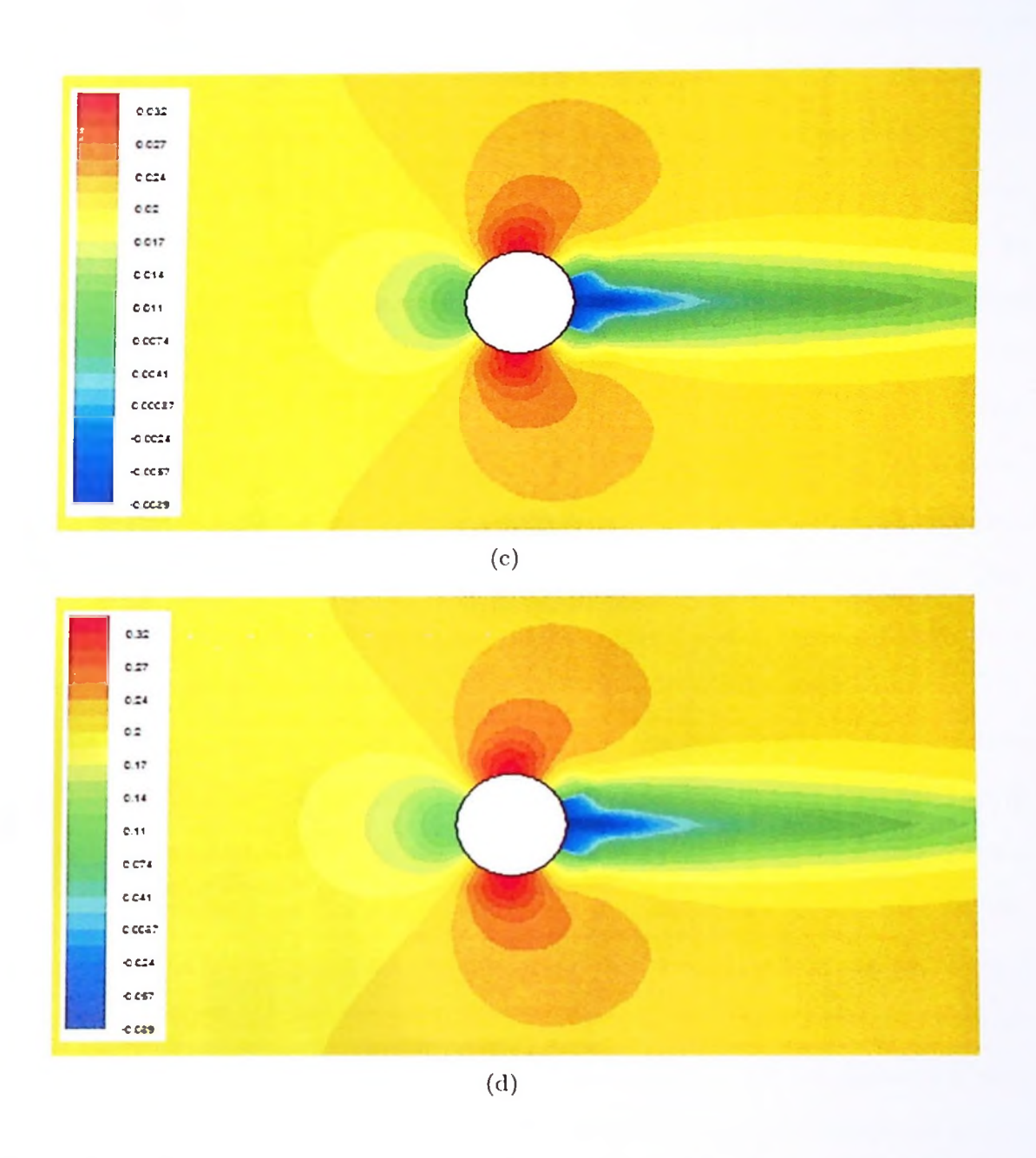


Figure 5.17: X-Velocity contour at low Reynolds number for (a) ECS flux at Re = 40, (b) ECS flux at Re = 2000, (c) Fluent result at Re = 40, (d) Fluent result at Re = 2000.

a good agreement between the two at Re = 2000. Having said that, the Fluent results do not show a significant difference between the two Reynolds numbers cases. In theory, flow separation does indeed occur even at Re = 40, but the wake behind the cylinder is not expected to be as developed as the Fluent result shown here. However, at Re = 2000, the flow is supposed to be on the verge of turbulence, with a qualitative profile closer to the one shown by Fluent as opposed to the ECS flux. This result demonstrates the limitation of the ECS flux in simulating complex flow behavior such as the case of flow over a cylinder. For one, the ECS flux is developed based on the laminar assumption, and even with the added viscosity term, the scheme cannot yet be considered as a full Navier-Stokes flux as it lacks additional terms accounting for thermal diffusion and heat transfer. This lack of thermal diffusion is probably the main reason why flow separation did not occur for the ECS flux in the case of Re = 40, and also why the separation is less pronounced for ECS in Re = 2000 compared to Fluent. The absence of a heat component in the flux means that the dissipation in the flow is less than it should be, making the simulation results appear less developed. Additionally, the ECS flux has not yet been augmented by turbulence models that would obviously help in getting a better result especially in the wake region. In Figure 5.18(a), the pressure coefficient  $(C_p)$  distribution along the top half of the cylinder wall is shown for the ECS flux at Re = 40 in comparison with available experimental data from Grove at Re = 40, Thom at Re = 40, and Dennis-Chang at Re = 100, all compiled in Droge (2007) for the laminar to transition region of free flow. On the other side in 5.18(b), the  $C_p$  distribution from the ECS flux at Re=2000 is compared with data from Dennis-Chang at Re=100 and from Norberg at Re = 3900, both also available in Droge (2007), and Werle-Gallon at Re = 2000, extracted from Werle and Gallon (1972). It can be seen that overall,

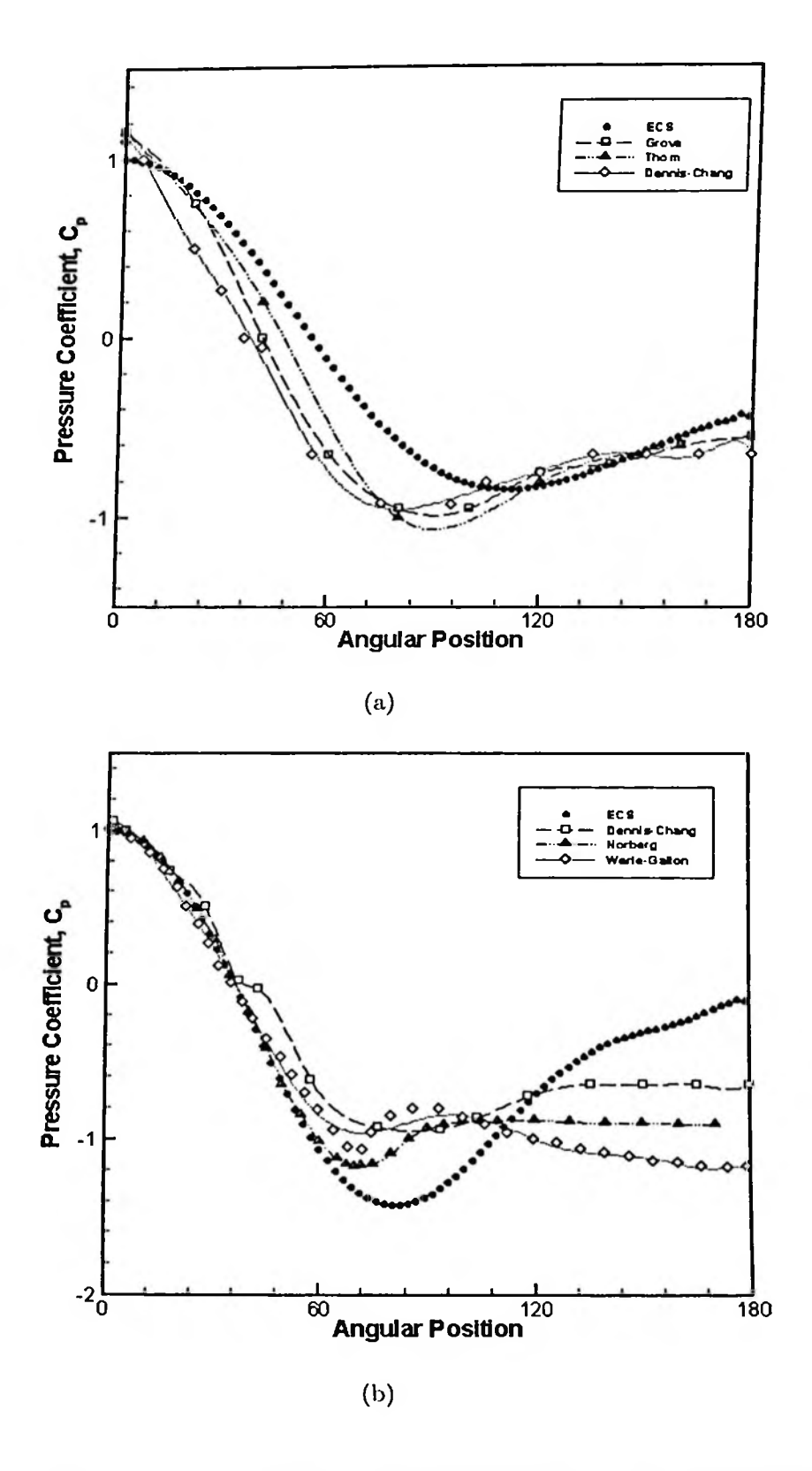


Figure 5.18: Pressure data for the ECS flux showing pressure coefficient  $(C_p)$  distribution at (a) Re=40, and (b) Re=2000, compared to available experimental data.

the ECS flux prediction of the pressure coefficient is within the acceptable range of values as compared to experimental results. However, the minima of the  $C_p$  curve produced by the ECS flux is consistently situated further back of the cylinder as compared to the experimental results. Additionally, the ECS flux overestimates the pressure levels at the back of the cylinder, minimally at Re = 200, and by a significant margin at Re = 2000. These characteristics are suspected to be due to the same reasons as discussed above.

In Figure 5.19, Mach number contours are shown for the EC1 and ECS fluxes respectively at Mach number 3.0. Results show that even with the diffusive nature of the viscosity term, the ECS flux still maintain a bow shock profile that is consistent with the established EC1 flux. Therefore we can say that the ECS flux maintains the shock capturing capability of its predecessors the Roe, EC1, and EC2 fluxes, whilst having an added advantage of being able to reasonably predict the near wall regions of the flow.

#### 5.4.4 Flow over an airfoil

Last but not least, the two-dimensional Navier-Stokes system flux is tested in the problem of flow over a NACA0012 airfoil. The profile of this airfoil, along with the mesh of the flow domain in its vicinity is shown in figure 5.20. This mesh has 161 nodes around the profile of the airfoil and 160 nodes between the airfoil surface to the outer boundary. The nodes around the airfoil are evenly spaced, whilst the spacing of nodes starting at the object surface grows outwards gradually at a factor of 5. Other configurations were also tested, but this mesh was found to give the best balance between grid independency and iteration speed. Free stream Reynolds number is  $Re = 9.7 \times 10^4$  for all cases unless stated otherwise.

Figure 5.21 shows the Mach number profile of flow over the NACA0012 airfoil at

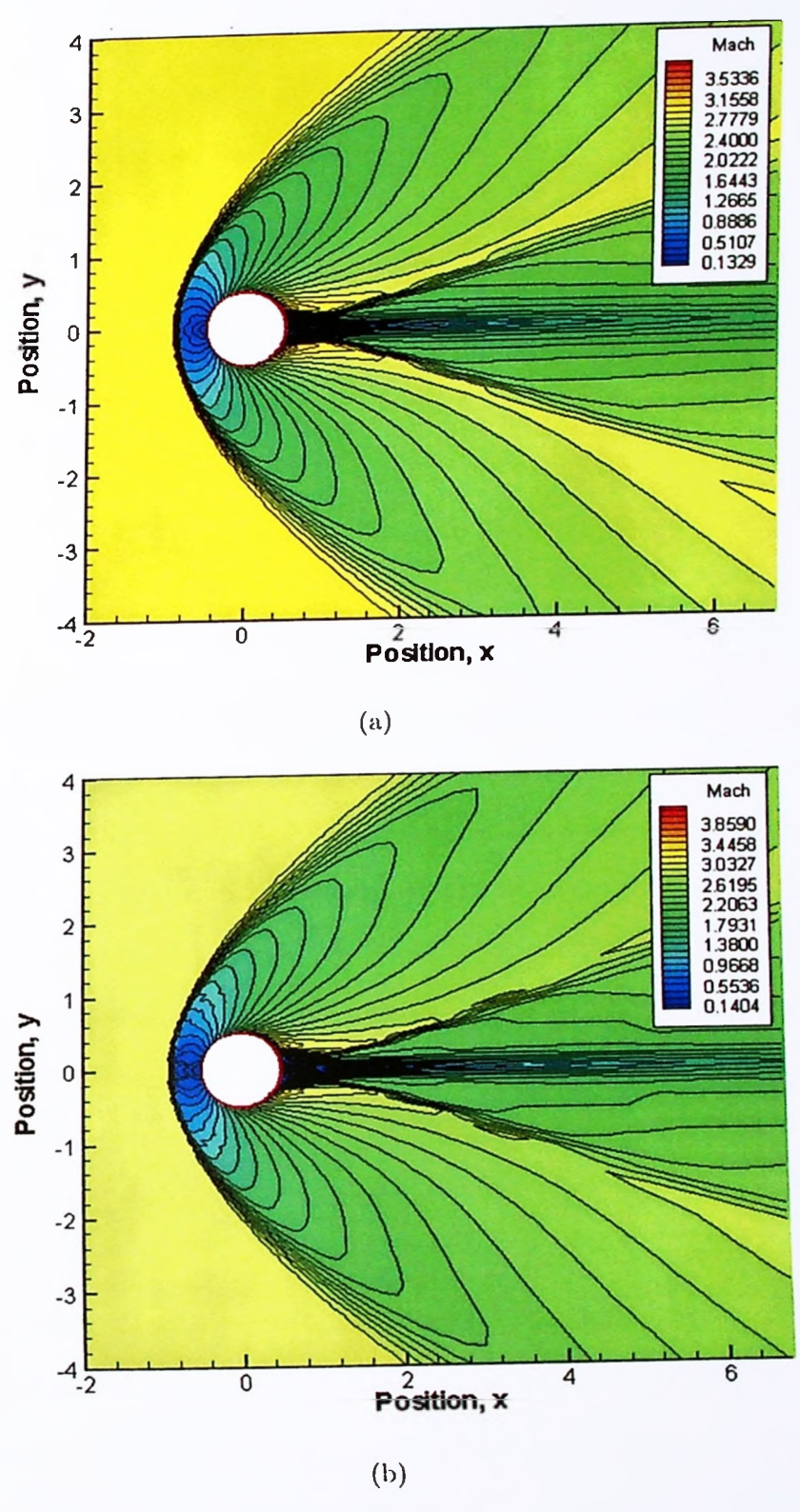


Figure 5.19: Contour plot at Mach 3.0 for (a) EC1 flux, (b) ECS flux.

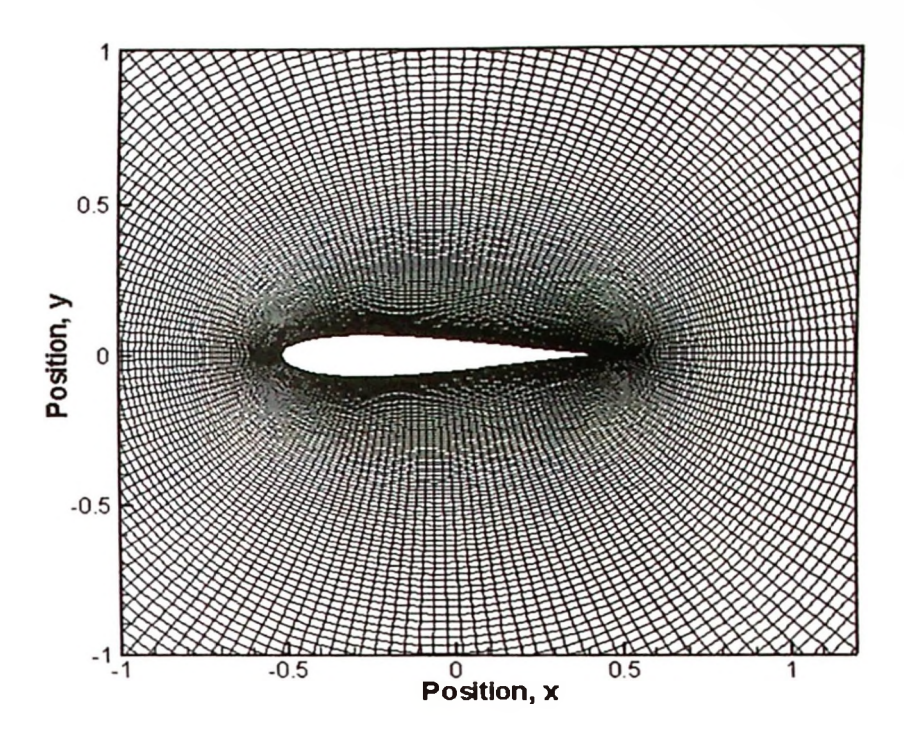


Figure 5.20: Mesh of NACA0012 airfoil using quadrilateral cells.

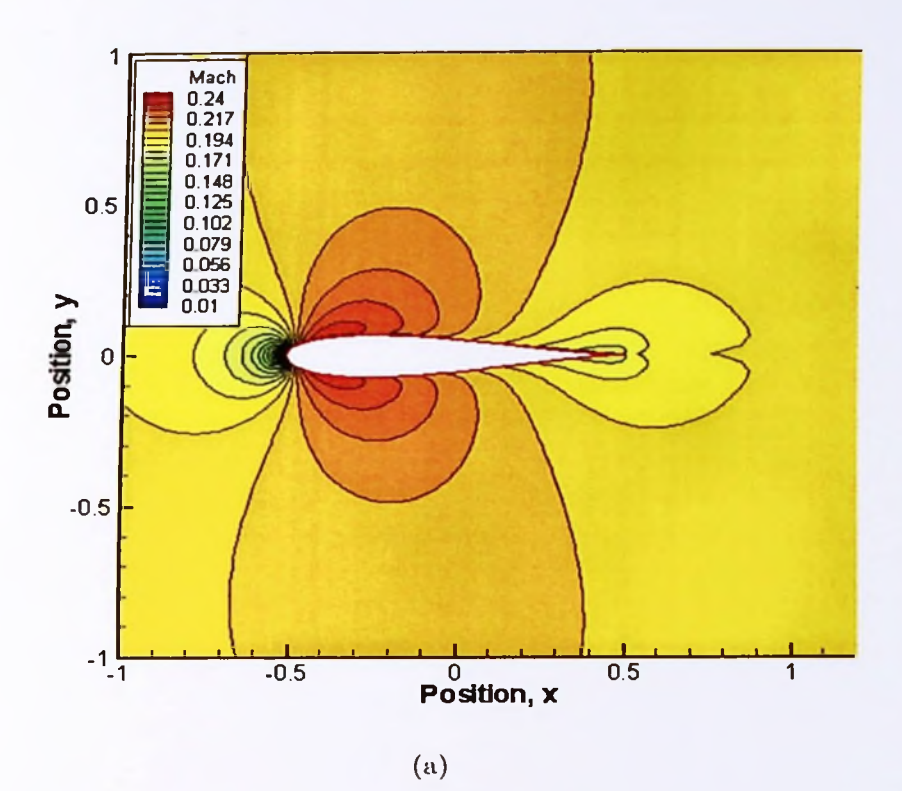
a Mach number of 0.2 for the Roe flux, EC1 flux and the system flux in (a), (b), and (c) respectively. Figure 5.22 also shows the Mach number profile of flow over the NACA0012 airfoil at a low Mach number of 0.2 for the Roe flux, EC1 flux and the system flux in (a), (b), and (c) respectively. However, in these figures the view has been zoomed in close to the walls of the airfoil to show the flow behavior of each flux near solid bodies. This is followed by Figure 5.23, which shows the Mach number profile of flow over the NACA0012 airfoil at subsonic Mach number of 0.63 for the Roe flux, EC1 flux and the system flux in (a), (b), and (c) respectively. Next, Figure 5.24 shows the Mach number profile of flow over the NACA0012 airfoil at a transonic Mach number region of 0.9 for the Roe flux, EC1 flux and the system flux in (a), (b), and (c) respectively. Last but not least, Figure 5.25 shows the Mach number profile of flow over the NACA0012 airfoil at a supersonic Mach value of 1.5 for the Roe flux, EC1 flux and the system flux in

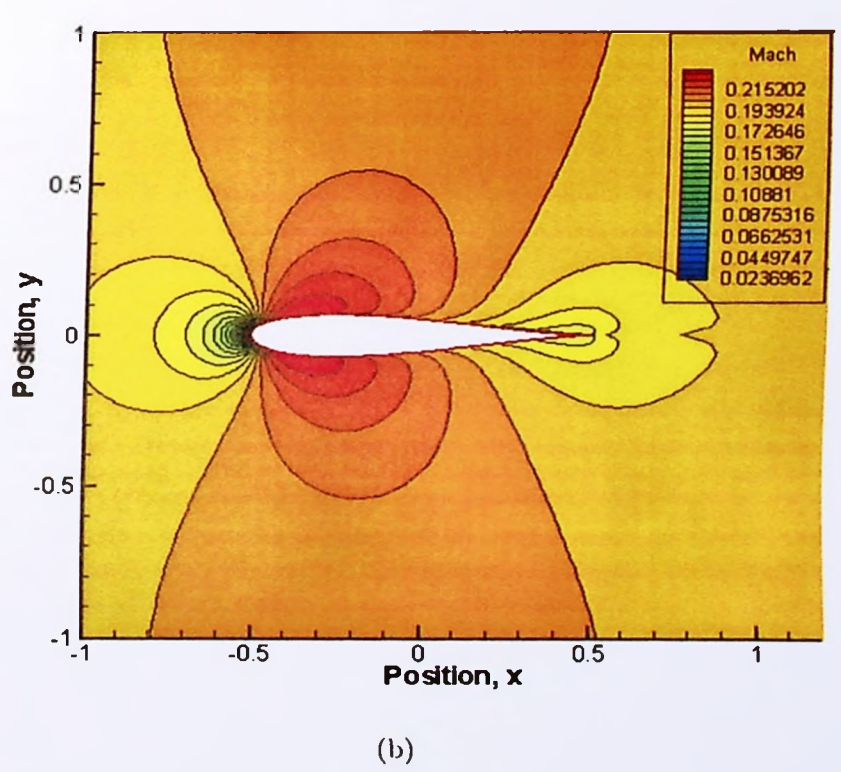
# (a), (b), and (c) respectively.

From the series of plots, it can be seen that the ECS flux is able to produce a slightly improved flow prediction at the aft of the airfoil as compared to the other fluxes. Furthermore, the ECS flux is able to provide a slightly more developed boundary layer profile in the near wall region in Figure 5.22. In terms of pressure, Figure 5.25(d) shows the pressure coefficient distribution of flow over the NACA0012 airfoil the system flux at  $Re = 9.7 \times 10^4$ . The low Reynolds number result shows that the ECS flux is able to provide a good representation of the  $C_p$  around the airfoil as compared to the experimental result. The flux seem to overestimate the pressure coefficient at the fore of the airfoil, but underestimates  $C_p$  from the point of x/C = 0.15 all the way to the aft, with the largest error occurring at the trailing edge. However, this result is still within acceptable limits, and is already expected based on the results of earlier test cases.

## 5.5 Summary

A number of test cases has been done in one and two dimensions to demonstrate the performance of the ECS flux compared to both other established fluxes and also select experimental results. It has been shown that the ECS flux is generally able to produce acceptable results, and in some cases such as the one-dimensional simulations, good to excellent results. This is despite the fact that the ECS flux is still not a fully fledged Navier-Stokes scheme.





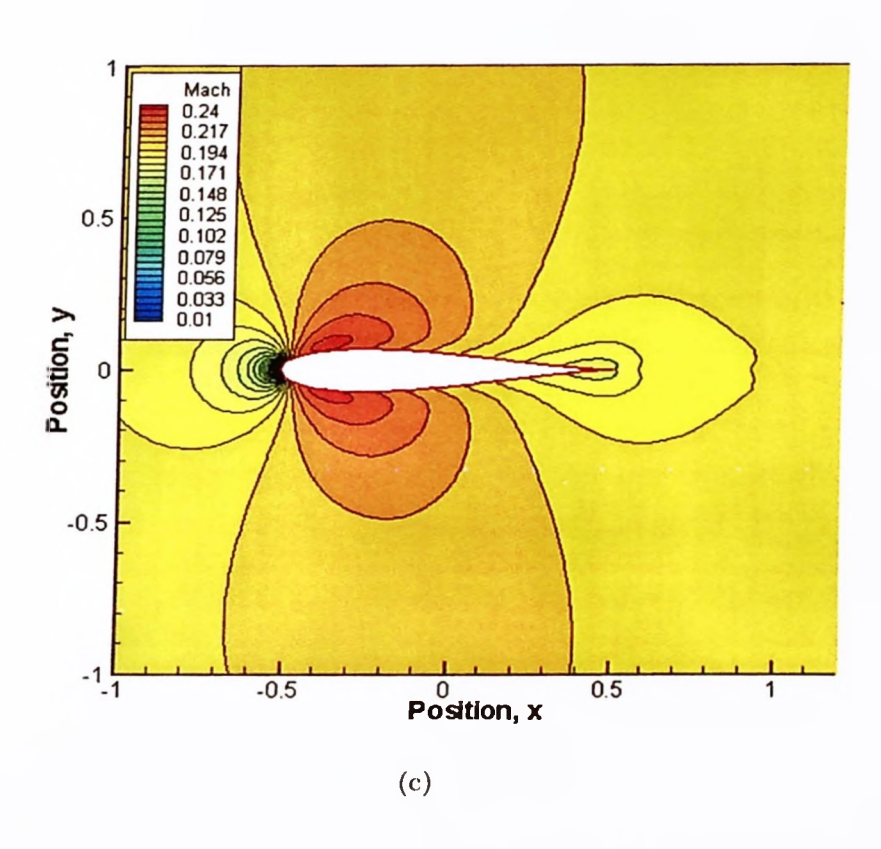
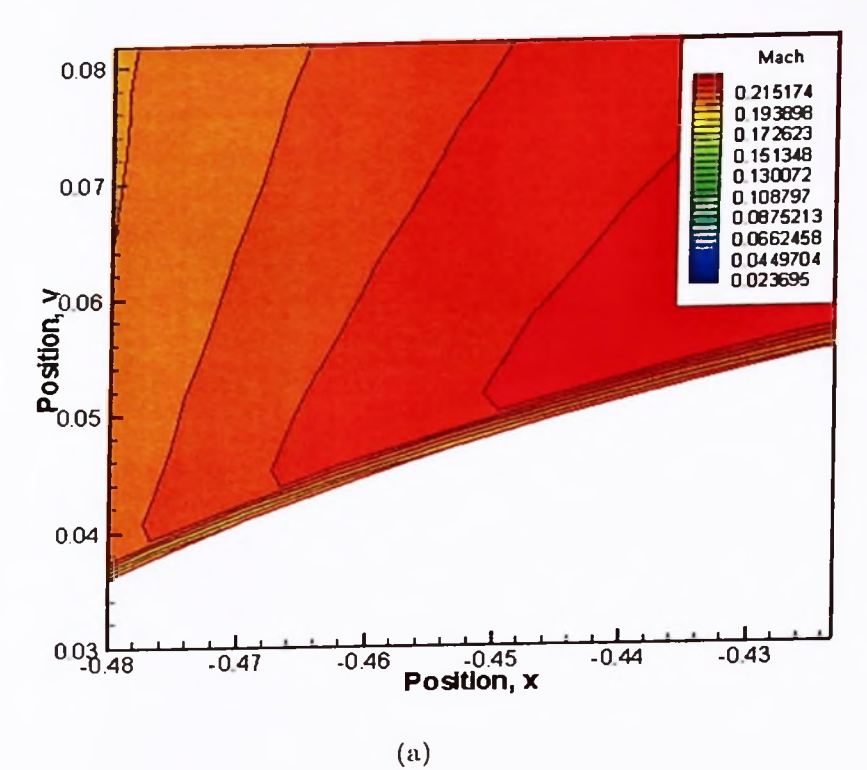
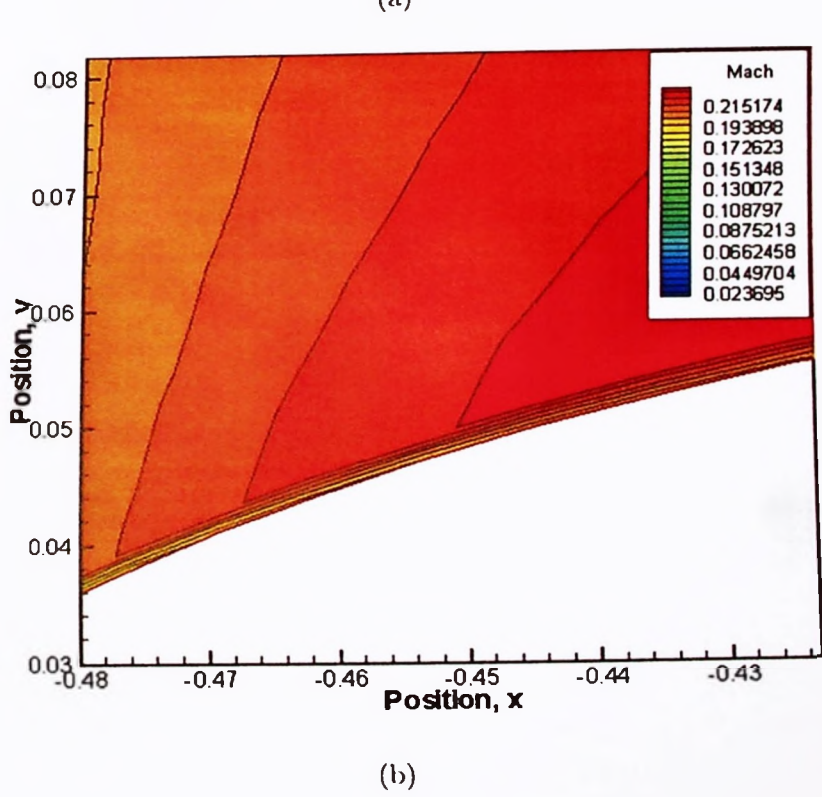


Figure 5.21: Flow over airfoil at Mach numbers 0.2 for fluxes of (a) Roe, (b) EC1, and (c) ECS.





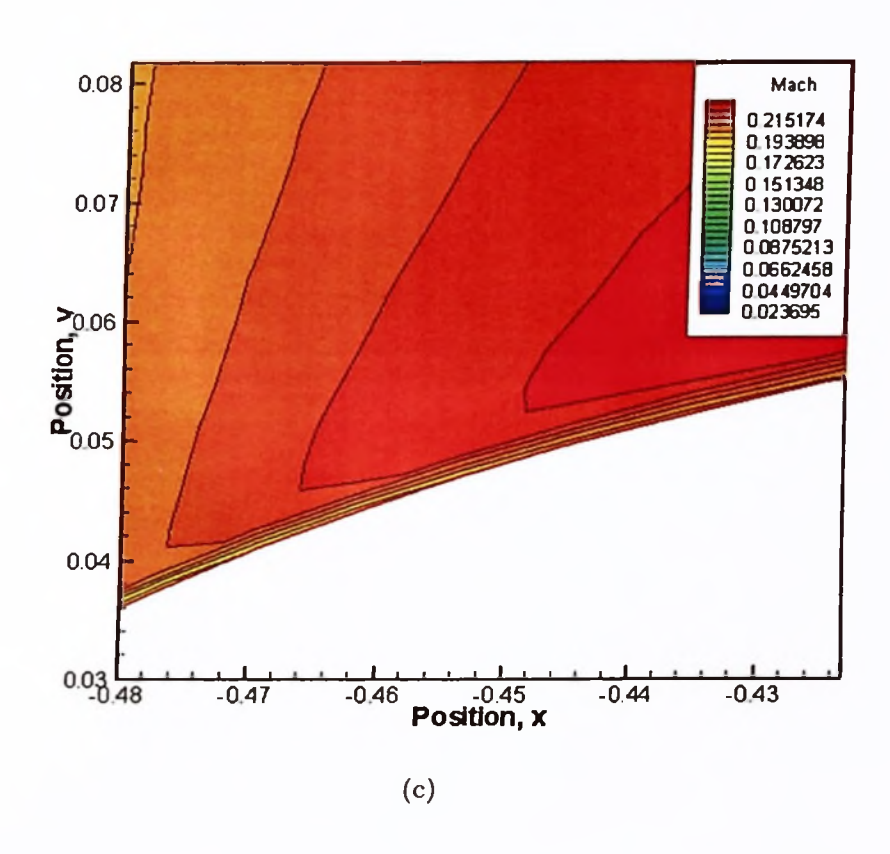
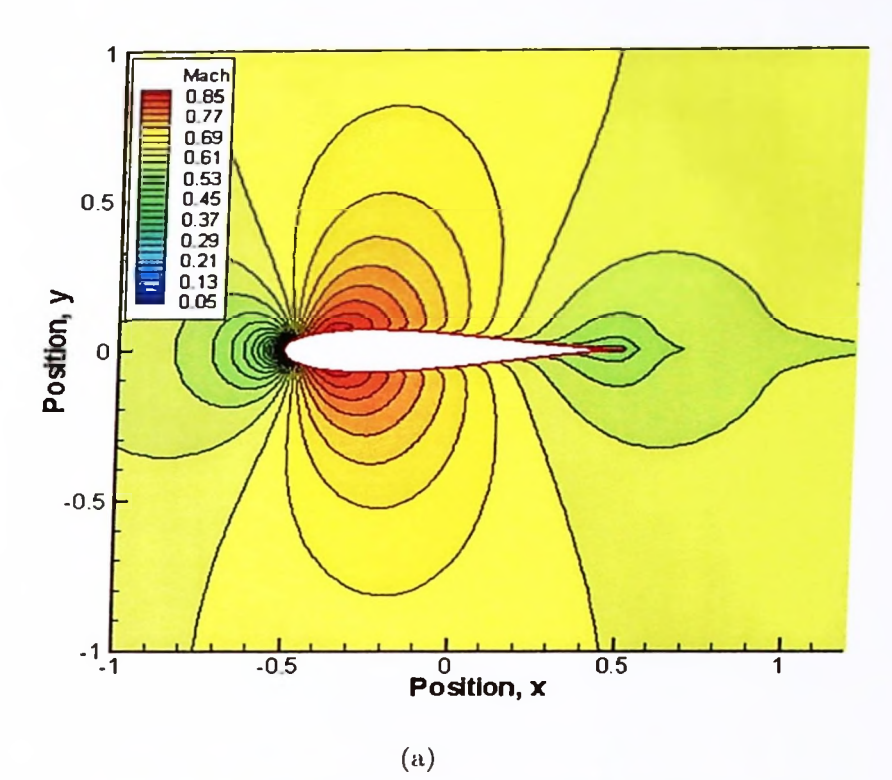
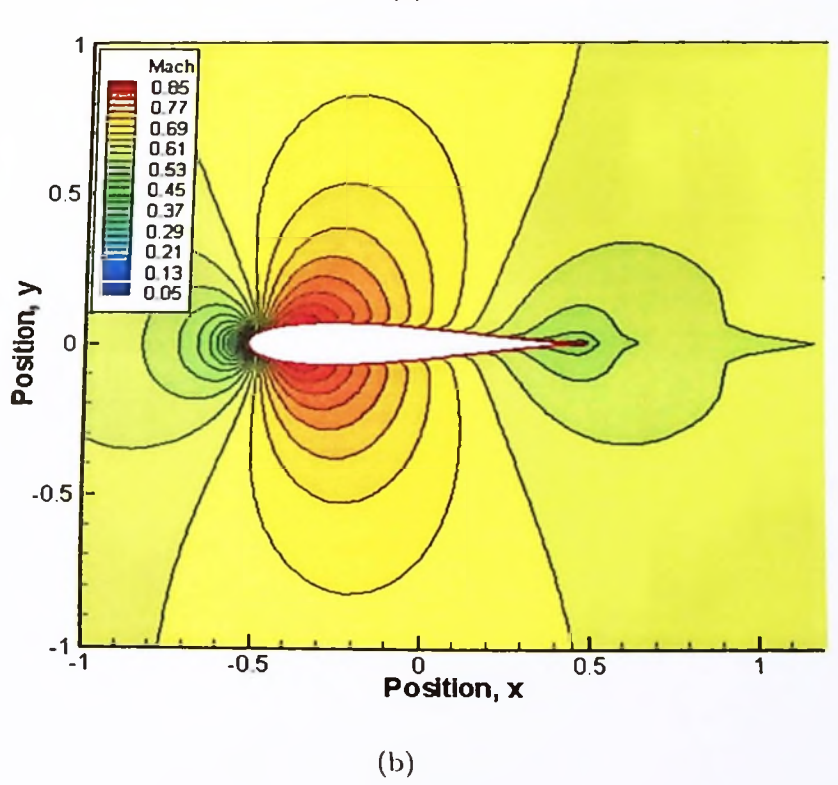


Figure 5.22: Zoomed in view of flow over airfoil at Mach numbers 0.2 for fluxes of (a) Roe, (b) EC1, and (c) ECS.





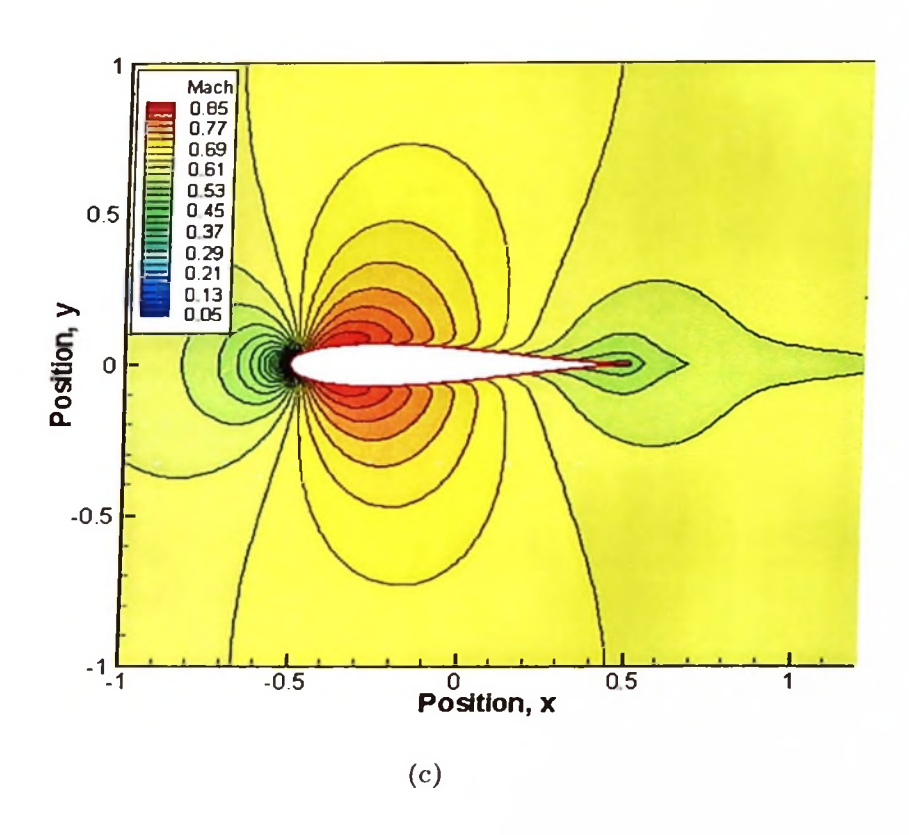
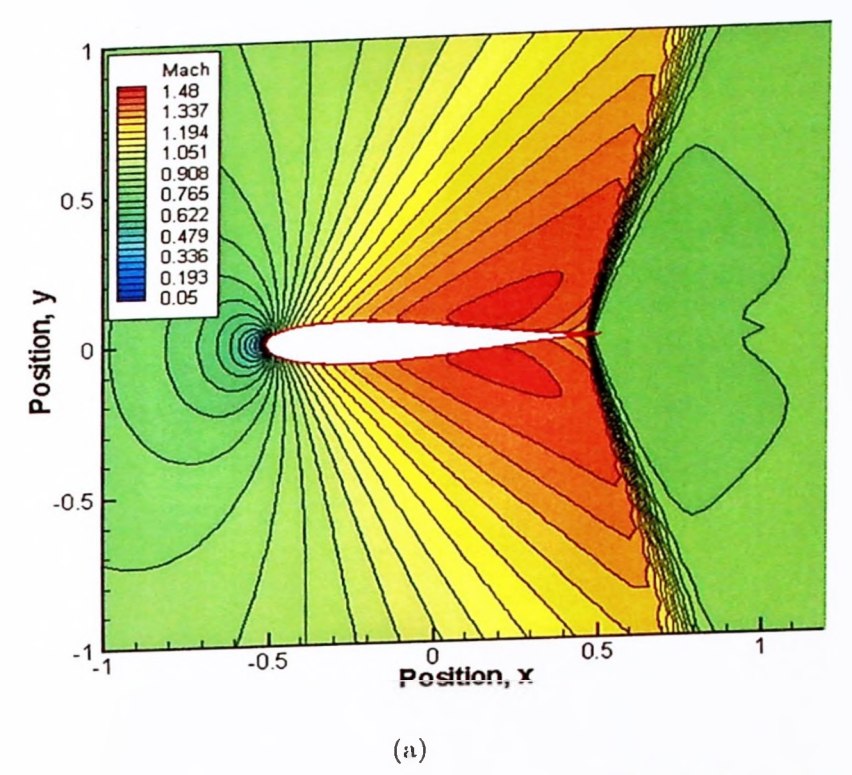
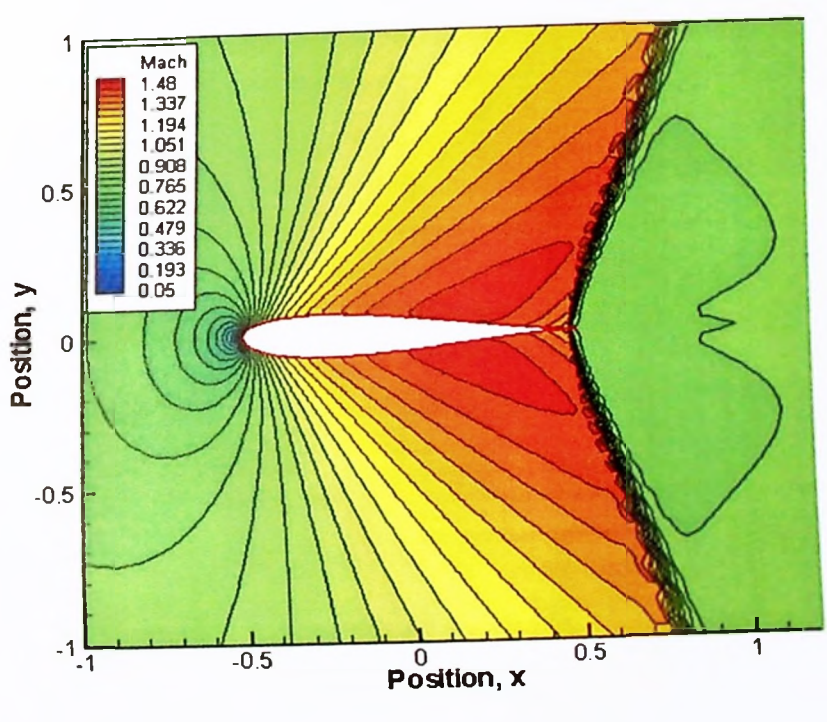


Figure 5.23: Flow over airfoil at Mach numbers 0.63 for fluxes of (a) Roe, (b) EC1, and (c) ECS.





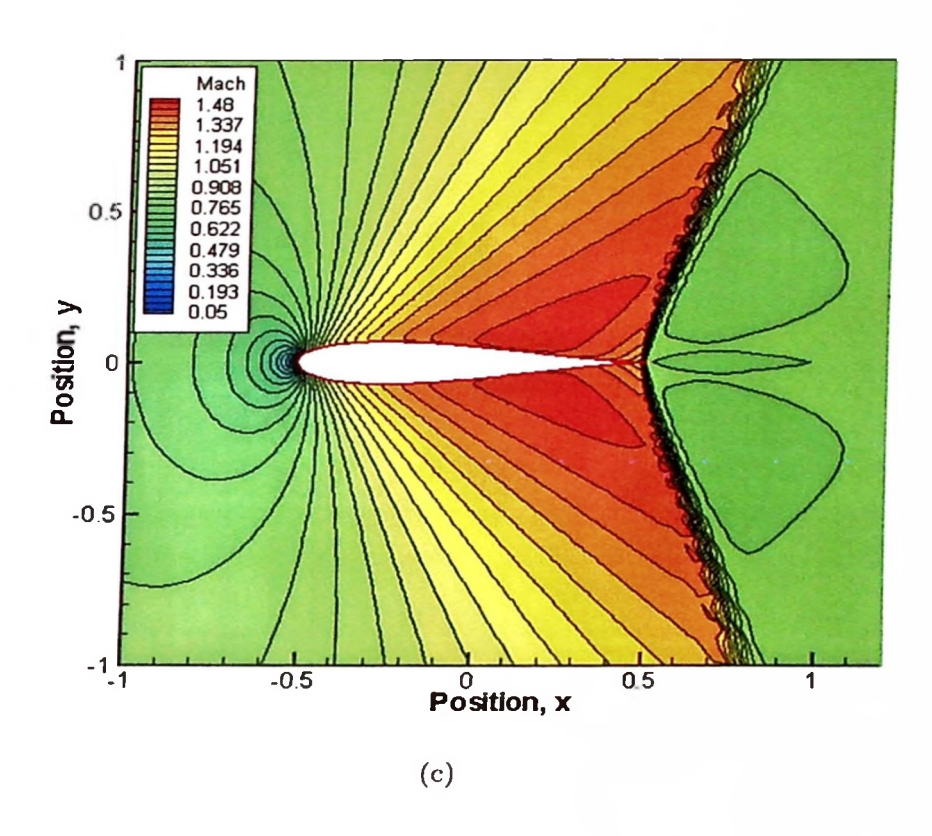
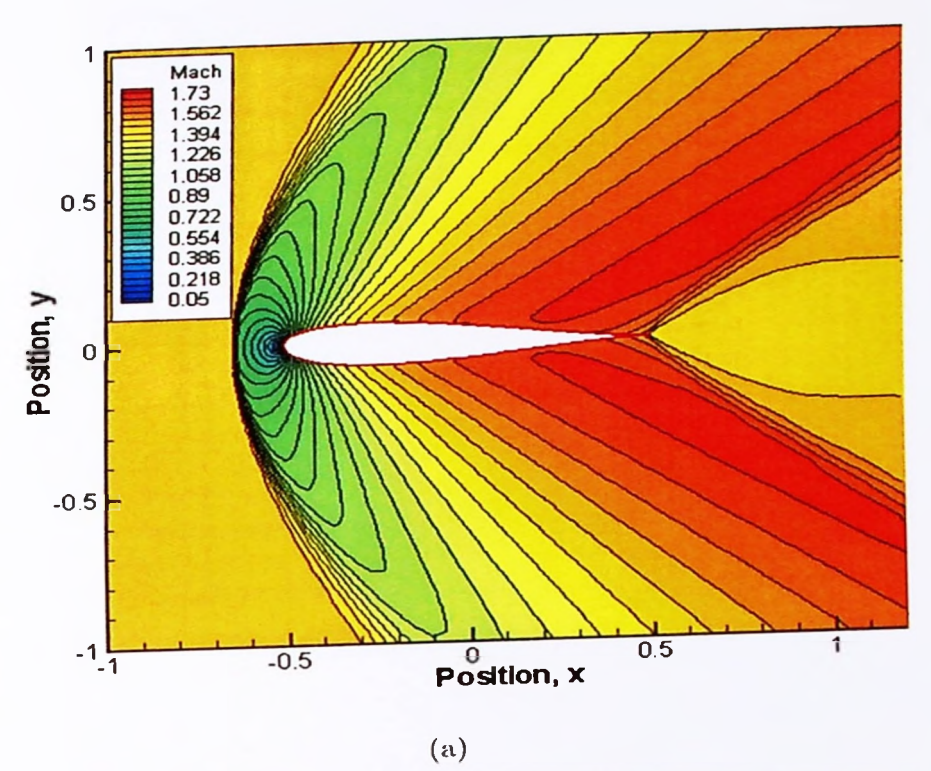
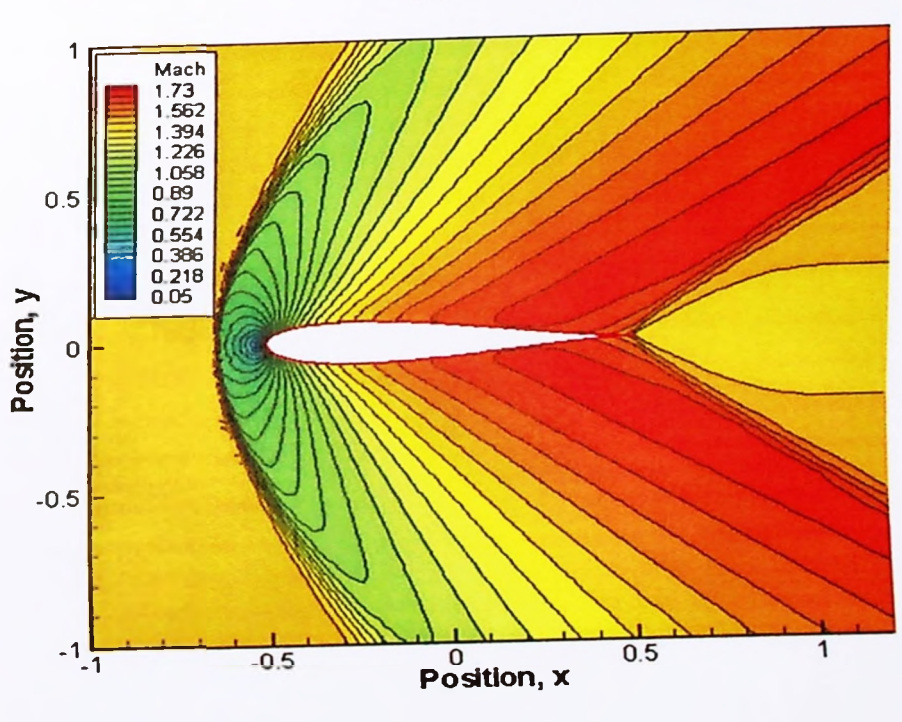


Figure 5.24: Flow over airfoil at Mach numbers 0.9 for fluxes of (a) Roe, (b) EC1, and (c) ECS.





(b)

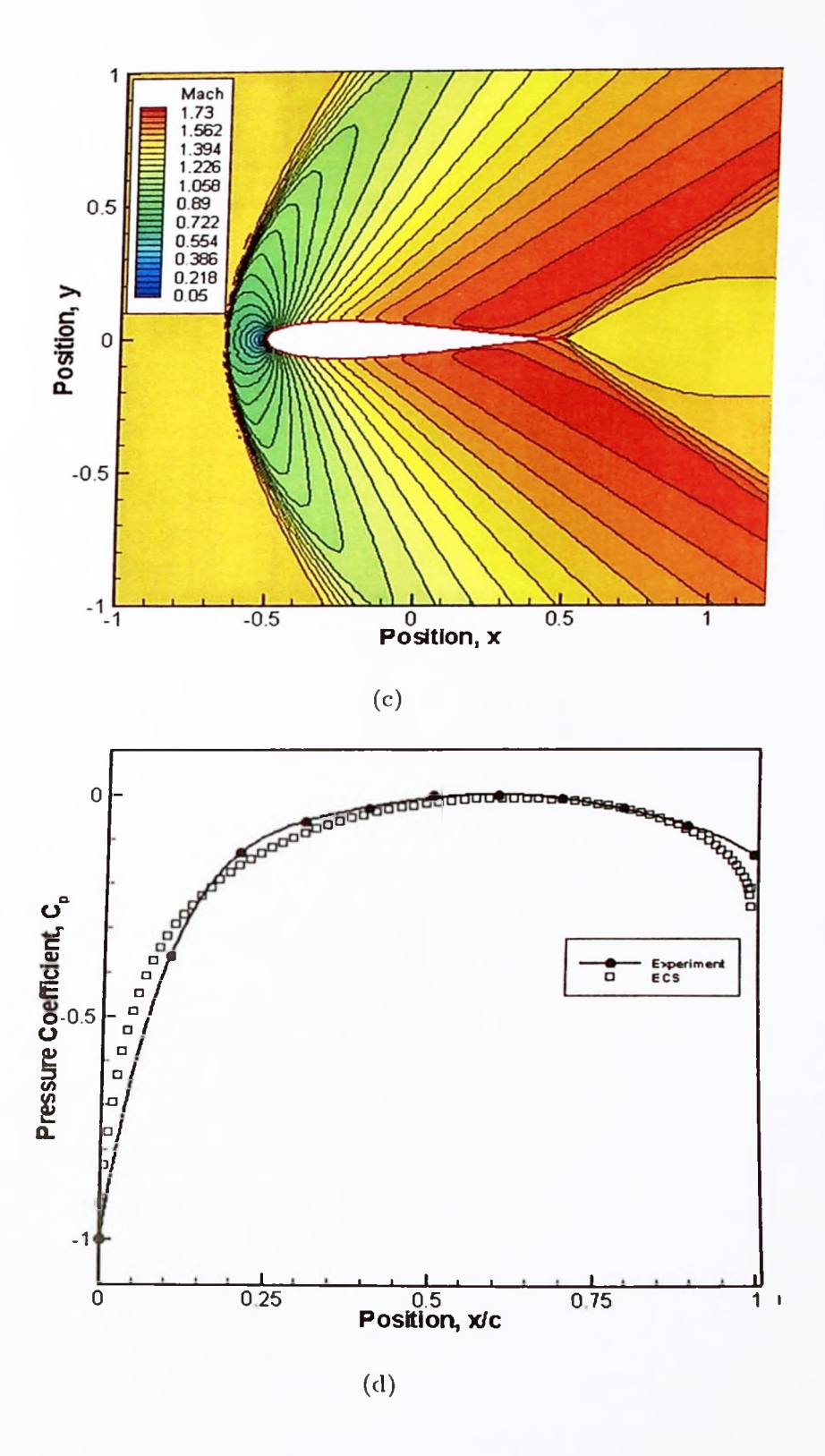


Figure 5.25: Flow over airfoil at Mach numbers 1.5 for fluxes of (a) Roe, (b) EC1, (c) ECS, and coefficients of pressure for  $Re = 9.7 \times 10^4$ .

# CHAPTER 6 CONCLUSIONS AND FUTURE WORK

#### 6.1 Conclusion

The work encapsulated in this thesis centers around the development of a new approach in constructing flux functions for the purpose of simulating high speed fluid flow, particularly in the presence of discontinuities and shock. The approach builds on the efforts of past researchers who developed discrete conservation equations that are tied to the concept of entropy control and its consistency with the second law of thermodynamics. Previously, the mechanism for control is in the form of carefully designed numerical entropy production, based on numerous empirical observations. Despite the excellent results obtainable from these entropy-consistent functions, a knowledge gap still remains in the fact that any entropy production term is essentially artificial in nature, and is not strongly linked to the actual physics of flow. Hence, a more natural means is sought, with the prime candidate being the insertion of a viscosity component in the inviscid based model which would naturally provide diffusion and the generation of entropy.

Coincidentally, a new development in the field of source terms, of which viscosity is an example, has been made recently. Viscosity is parabolic in nature, and is traditionally treated differently from the advection part of conservation equations that are fundamentally hyperbolic. The new development provides a solution for this compatibility issue by resolving the higher-order source terms in a set of first-order equations. Thus, there would no longer be a need to utilize two different numerical schemes for the advection and diffusion parts of the governing laws; both can be stated in hyperbolic form and discretized in a uniform manner. This approach provides an avenue for the concept of entropy control to be expanded

into the realm of viscosity, which would hopefully eliminate the need for any form of artificial dissipation.

Therefore, a new concept that combined the philosophy of entropy consistency and the approach of using first-order hyperbolic systems into one scheme was developed. This method firstly maps the conservative variables of the hyperbolic system into its entropy variables. These variables are then used to construct entropy conservative fluxes, and augmented with its diagonalized matrix of eigenvectors that provide stability and consistency. The fluxes are divided into its inviscid and viscous components; this is so that each component can be controlled individually and conveniently. The concept was firstly applied to the linear Burgers' equation, in which a new entropy pair has been chosen to include both inviscid and viscous terms. The same strategy is then expanded into the Navier-Stokes governing equations via the Euler equations. In this case, the hyperbolic discretization of viscosity terms is done separately from inviscid terms so that the physical (or mathematical) entropy still remains a dominant feature for the overall entropy-stability and entropy-consistency control. The additional entropy function for the viscous terms are created to ensure some form of entropy-stabillity is also achieved for hyperbolic discretization of the physical viscosity. Subsequently, the Navier-Stokes system is upgraded into its two-dimensional version. As such, the creation of these fluxes complete the first objective of this research.

With the completion of the system fluxes, they are then put through several tests to evaluate their performance. Overall, the new fluxes have been shown to provide comparable results to older methods and experimental results for a range of viscosity levels at low Reynolds number. This satisfied the second objective of this research. However, the Navier-Stokes fluxes are still incomplete due to the omission of heat transfer effects. Due to their respective signs, the entropy

generation from heat transfer would oppose that of the rest of the system, affecting the entropy stability and consistency of the system as a whole. Thus, considerable work is still required to realize the full potential of this approach.

## 6.2 Future Work

To expand on the work in this thesis, a number of potential research avenues has been identified. The most obvious of this is to extend the Navier-Stokes flux to the full three dimensions. Work on previous finite-volume entropy consistent schemes by others has shown that this extension is possible without a high degree of difficulty. The three-dimensional configuration will allow the entropy-consistent system flux to be employed in real-world applications for practical use.

Additionally, a big milestone for us to achieve is to include heat transfer considerations into the system flux. The framework for this has already been established by Dr Nishikawa in his series of papers, but the key problem to solve now is to find entropy pairs or other methods that would allow the heat transfer term itself to remain entropy stable, thus ensuring stability and consistency for the whole flux.

Last but not least, the long term goal for this endeavor would be to generalize the flux so that it encompasses the whole flow regime. Currently, the entropy-consistent system flux has only been proven to work well in inviscid or laminar conditions of low Reynolds number. In the future, it is hoped that the system flux can be augmented with vorticity capturing and suitable turbulence models so that it can cater for turbulent flow applications.

#### REFERENCES

- Anderson, J. D. 2004. *Modern Compressible Flow with Historical Perspective*. 3rd edn. McGraw-Hill.
- Arora, M. 1996. Explicit Characteristic Based High-Resolution Algorithms for Hyperbolic Conservation Laws with Stiff Source Terms. PhD thesis, The University of Michigan.
- Babuska, I. and Guo, B. Q. 1992. The h, p and h-p version of the finite element method: basis theory and applications. *Advances in Engineering Software* 15, Issue 3-4: 159–174.
- Barth, T. J. 1999. Numerical methods for gasdynamic systems on unstructured meshes. In An Introduction to Recent Developments in Theory and Numerics for Conservation Laws (eds. M. O. D. Kroner and C. Rhode), 195–285. Springer-Verlag, Lect. Notes Comput. Sci. Eng. 5.
- Bressan, A. 2009, Hyperbolic conservation laws an illustrated tutorial, Notes and Tutorials, Department of Mathematics, Penn State University.
- Chen, G. Q., Levermore, C. D. and Liu, T. P. 1994. Hyperbolic conservation laws with stiff relaxation terms and entropy. *Commun. Pur. Appl. Math.* 47: 787–830.
- Colella, P. and Woodward, P. 1984. The piecewise parabolic method (PPM) for gas dynamical simulations. *J. Comp. Physics* 54: 174–201.
- Courant, R., Friedrich, K., and Lewy, H. 1967. On the partial difference equations of mathematical physics. *IBM Journal* 11: 215–234.
- Courant, R., Isaacson, E. and Reese, M. 1952. On the solution of nonlinear hyperbolic differential equations by finite differences. *Comm. Pure and Applied Mathematics* 5: 243–255.
- Donat, R., Higueras, I. and Martinez-Gavara, A. 2009. Numerical schemes for scalar conservation laws with stiff source terms. In XXI Congreso de Ecuaciones Diferenciales y Aplicaciones, 1–8. Universitat Jaume I, Ciudad Real, Spain.
- Droge, M. 2007. Cartesian Grid Methods for Turbulent Flow Simulation in Complex Geometries. PhD thesis, Groningen University.
- Einfeldt, B. 1988. On Godunov type methods for gas dynamics. *J. Comp. Physics* 25: 294–318.
- Evans, L. C. 2010. Partial Differential Equations. 2nd edn. American Mathematical Society.

- Fisher, T. C. and Carpenter, M. H. 2013, High-order entropy stable finite difference schemes for nonlinear conservation laws: finite domains, NASA TM-2013-217971, Langley Research Center.
- Fjordholm, U. S., Mishra., S. and Tadmor, E. 2008. Energy preserving and energy stable schemes for the shallow water equations. In *Foundations of Computational Mathematics Hong Kong 2008*, 93–139. Cambridge University Press, London Mathematical Society Lecture Note Series 363.
- Fjordholm, U. S., Mishra., S. and Tadmor, E. 2011. Energy stable schemes well-balanced schemes for the shallow water equations with bottom topography. *J. Comput. Physics* 230: 5587–5609.
- Fjordholm, U. S., Mishra., S. and Tadmor, E. 2013. ENO reconstruction and ENO interpolation are stable. *Found. Comput. Math* 13: 139-159.
- Friedrich, K. O. 1954. Symmetric hyperbolic linear differential equations. Comm. Pure and Applied Mathematics 7: 345-392.
- Godunov, S. K. 1959. Finite difference method for numerical computation of discontinuous solutions of the equations of fluid dynamics. *Math Sb.* 47: 271–306.
- Gustaffson, B. 1987. Unsymmetric hyperbolic systems and the Euler equations at low Mach numbers. J. Sci. Comput. 2, No. 2: 123–136.
- Harten, A. 1983a. High resolution schemes for hyperbolic conservation laws. J. Comp. Physics 49: 357–393.
- Harten, A. 1983b. On the symmetric form of systems of conservation laws with entropy. J. Comp. Physics 49: 151–164.
- Harten, A. and Hyman, J. M. 1983. Self-adjusting grid method for one-dimensional hyperbolic conservation laws. *J. Comp. Physics* 50: 235–269.
- Hirsch, C. 2000. Numerical Computation of Internal and External Flows, Vol. 1 and 2. Reprint edn. Wiley.
- Hittinger, J. A. 2000. Foundations for the Generalization of the Gudonov Method to Hyperbolic Systems with Stiff Relaxation Source Terms. PhD thesis, The University of Michigan.
- Hou, T. Y. and Lefloch, P. 1994. Why non-conservative schemes converge to the wrong solutions: error analysis. *Math. of Comput.* 62: 497–530.
- Hughes, T., Franca, L. and Mallet, M. 1986. A new finite element formulation for compressible fluid dynamics I: symmetric forms of the compressible Euler and Navier Stokes equations and the second law of thermodynamics. Comp. Meth. App. Mech. Eng. 54: 223-234.

- Ismail, F. 2006. Toward a Reliable Prediction of Shocks in Hypersonic Flow: Resolving Carbuncles with Entropy and Vorticity Control. PhD thesis, The University of Michigan.
- Ismail, F. and Roe, P. L. 2009. Affordable, entropy consistent Euler flux functions II: entropy production at shocks. J. Comp. Phys 228: 5410-5436.
- Jin, S. and Levermore, C. D. 1996. Numerical schemes for hyperbolic conservation laws with stiff relaxation terms. *J. Comp. Physics* 126: 449-467.
- Kitamura, K., Roe, P. L. and Ismail, F. 2009. Evaluation of Euler fluxes for hypersonic flow computations. *AIAA Journal* 47, No. 1: 44-53.
- Laney, C. 1998. Computational Gasdynamics. Cambridge University Press.
- Lax, P. D. 1954. Weak solutions of nonlinear hyperbolic equations and their numerical computation. Comm. Pure and Applied Mathematics 7: 159-193.
- Lax, P. D. 1957. Hyperbolic systems of conservation laws II. Comm. Pure and Applied Mathematics 10: 537-566.
- Lax, P. D. and Wendroff, B. 1960. System of conservation laws. Comm. Pure Applied Math 13, Issue 2: 217–237.
- Lefloch, P., Mercier, J. and Rohde, C. 2002. Full discrete entropy conservative schemes of arbitrary order. SIAM J. Num. Anal. 40: 1968–1992.
- LeVeque, R. J. 2002. Finite Volume Methods for Hyperbolic Problems. 1st edn. Cambridge Text in Applied Mathematics.
- LeVeque, R. J. and Yee, H. C. 1988, A study of numerical methods for hyperbolic conservation laws with stiff source terms, NASA TM-100075, Ames Research Center.
- Liou, M. S. and Steffen, C. 1993. A new flux splitting scheme. J. Comp. Physics 107: 23–39.
- Lowrie, R. B. and Morel, J. E. 2000. Methods for hyperbolic systems with stiff relaxation. *Int. J. Num. Meth. Fluids* 40: 413-423.
- MacCormack, R. 2003. The effects of viscosity in hypervelocity impact cratering. J. of Spacecraft and Rockets 40, No. 5: AIAA Paper 69-354.
- Masatsuka, K. 2009. I do like CFD, VOL. 1. Governing Equations and Exact Solutions. 1st edn. Katate Masatsuka.
- Mos, N., Dolbow, J. and Belytschko, T. 1999. A finite element method for crack growth without remeshing. *Int. J. Num. Meth. Eng.* 46: 131-150.

- Neumann, J. V. and Richtmayer, R. D. 1950. A method for numerical calculation of hydrodynamic shocks. J. Appl Phys. 21: 232-237.
- Nishikawa, H. 2007. A first-order system approach for diffusion equation I: second-order residual-distribution schemes. J. Comp. Physics 227: 315–352.
- Nishikawa, H. 2010a. Beyond interface gradient: A general principle for constructing diffusion schemes. In 40th Fluid Dynamics Conference and Exhibit, AIAA Paper 2010–5093. AIAA Conferences, Chicago.
- Nishikawa, H. 2010b. A first-order system approach for diffusion equation II: unification of advection and diffusion. J. Comp. Physics 229: 3989-4016.
- Nishikawa, H. 2011a. New-generation hyperbolic Navier-Stokes schemes: O(1/h) speed-up and accurate viscous/heat fluxes. In 20th AIAA CFD Conference, AIAA Paper 2011–3043. AIAA Conferences, Hawaii.
- Nishikawa, H. 2011b. Two ways to extend diffusion schemes to Navier-Stokes schemes: Gradient formula or upwind flux. In 20th AIAA CFD Conference, AIAA Paper 2011–3044. AIAA Conferences, Hawaii.
- Nishikawa, H. 2012. Divergence formulation of source term. J. Comp. Physics 231: 6393–6400.
- Nishikawa, H. 2013a. First, second, and third order finite-volume schemes for advection-diffusion. In 21st AIAA CFD Conference, AIAA Paper 2013–2568. AIAA Conferences, San Diego, California.
- Nishikawa, H. 2013b. First, second, and third order finite-volume schemes for diffusion. In 51st AIAA Aerospace Sciences Meeting, AIAA Paper 2013-1125. AIAA Conferences, Grapevine, Texas.
- Nishikawa, H. and Kitamura, K. 2008. Very simple, carbuncle-free, boundary-layer-resolving, rotated-hybrid Riemann solvers. *J. Comp. Physics* 227: 2560–2581.
- Nishikawa, H. and Roe, P. L. 2004. On high-order fluctuation-splitting schemes for Navier-Stokes equations. In *Computational Fluid Dynamics* 2004, 799–804. Springer-Verlag.
- Osher, S. 1984. Riemann solvers, entropy conditions and difference approximations. SIAM J. Num. Anal. 21: 217-235.
- Patera, A. T. 1984. A spectral element method for fluid dynamics laminar flow in a channel expansion. J. Comp. Physics 54: 468-488.

- Rajani, B., Kandasamy, A. and Majumdar, S. 2009. Numerical simulation of laminar flow past a circular cylinder. *Applied Mathematical Modelling* 33: 1228-1247.
- Reed, W. H. and Hill, T. R. 1973, Triangular mesh methods for the neutron transport equation, Tech. Report LA-UR-73-479, Los Alamos Scientific Laboratory.
- Roe, P. L. 1981. Approximate Riemann solvers, parameter vectors and difference schemes. J. Comp. Physics 43: 357–372.
- Roe, P. L. unpublished. Affordable, entropy-consistent, Euler flux functions I: analytical results. unpublished.
- Roe, P. L. and Arora, M. 1993. Characteristic-based schemes for dispersive waves I: the method of characteristics for smooth solutions. *Num. Meth. PDE* 9: 459–505.
- Roslan, N. K. H. and Ismail, F. 2012. Evaluation of the entropy consistent euler flux on 1D and 2D test problems. In 4th Int. Meeting Adv. Thermofluids. AIP Conf. Proc. 1440, 671, Melaka, Malaysia.
- Sod, G. A. 1978. A survey of several finite difference schemes for hyperbolic conservation laws. J. Comp. Physics 27: 1–31.
- Sweby, P. 1984. High resolution schemes using flux limiters for hyperbolic conservation laws. SIAM J. Num. Anal. 21: 995–1011.
- Tadmor, E. 1984. Numerical viscosity and the entropy condition for conservation difference schemes. *Math. Comp.* 43: 369–381.
- Tadmor, E. 1987. The numerical viscosity of entropy stable schemes for systems of conservation laws. *Math. Comp.* 49: 91–103.
- Tadmor, E. 2003. Entropy stability theory for difference approximations of non-linear conservation laws and related time dependent problems. *Acta Numerica* (2003) 451–512.
- Tadmor, E. and Zhong, W. 2006. Entropy stable approximations of Navier-Stokes equations with no artificial numerical viscosity. J. of Hyperbolic DE 3: 529-559.
- Toro, E. F. 1999. Riemann Solvers and Numerical Methods for Fluid Dynamics: A Practical Introduction. 2nd edn. Springer-Verlag.
- Van Leer, B. 1979. Toward the ultimate conservative difference scheme V: a second order sequel to Godunov's method. J. Comp. Physics 32: 101–136.

- Van Leer, B. 2001. Computational fluid dynamics: science or toolbox? In 15th AIAA CFD Conference, AIAA Paper 2001–2520. AIAA Conferences, Anaheim, California.
- Werle, H. and Gallon, M. 1972. Controle d'ecoulements par jet transversal. Aeronaut. Astronaut. 34: 21-33.
- Wong, J. S., Darmofal, D. L. and Peraire, J. 2001. The solution of the compressible Euler equations at low Mach numbers using a stabilized finite element algorithm. *Comput. Methods Appl. Mech. Engrg.* 190: 5719-5737.
- Xu, K. 2000. Gas kinetic schemes for fluid simulations. In 1st International Conference on Computational Fluid Dynamics (ed. N. Satofuka), 14–23. Kyoto, Japan.
- Yu, S. T. and Chang, S. C. 1997. Treatments of stiff source terms in conservation laws by the method of space-time conservation element/solution element. In 35th Aerospace Sci. Meet. and Exhibit, AIAA Paper 97-0435. AIAA Conferences, Reno, Nevada.
- Zdravkovich, M. 1997. Flow Around Circular Cylinders, vol. 1. Oxford Science Publication.

## APPENDIX A

## FLUX AVERAGING

## A.1 (Entropy Conserving Flux)

The entropy conserving flux  $f_i$  from equation 4.55 satisfies

$$\mathbf{v}^{\mathbf{T}}\mathbf{f}_{i} = [\rho\mathbf{u}] \tag{A.1}$$

and is calculated based on averaged quantities of

$$\mathbf{f}_{i}(\mathbf{u}_{L}, \mathbf{u}_{R}) = \begin{bmatrix} \hat{\rho}\hat{u} \\ \hat{\rho}\hat{u}^{2} + \hat{p_{1}} \\ \hat{\rho}\hat{u}\hat{H} \end{bmatrix}$$
(A.2)

To determine the averaged quantities, we firstly define positive definite quantities

$$z_1 = \sqrt{\frac{\rho}{p}}, \quad z_2 = \sqrt{\frac{\rho}{p}u}, \quad z_3 = \sqrt{\rho p}$$
 (A.3)

The averaged quantities are composed from functions of arithmetic mean  $\bar{a} = \frac{a_L + a_R}{2}$  and logarithmic mean as defined in the next section. Based on equation A.1, the quantities used in the flux are as follows

$$\hat{u} = \frac{\bar{z}_2}{\bar{z}_1}, \quad \hat{\rho} = \bar{z}_1 z_3^{ln}, \quad \hat{p}_1 = \frac{\bar{z}_3}{\bar{z}_1}, \quad \hat{p}_2 = \frac{\gamma + 1}{2\gamma} \frac{z_3^{ln}}{z_1^{ln}} + \frac{\gamma - 1}{2\gamma} \frac{\bar{z}_3}{\bar{z}_1}$$
(A.4)

$$\hat{a} = (\frac{\gamma \hat{p_2}}{\hat{\rho}})^{\frac{1}{2}}, \quad \hat{H} = \frac{\hat{a}^2}{\gamma - 1} + \frac{\hat{u}^2}{2}$$
 (A.5)

## A.1 (Logarithmic Mean)

Let us define

$$\zeta = \frac{a_L}{a_R} \tag{A.6}$$

We also define

$$a^{ln}(L,R) = \frac{a_L + a_R}{ln(\zeta)} \frac{\zeta - 1}{\zeta + 1} \tag{A.7}$$

Here, the quantity  $ln(\zeta)$  is

$$ln(\zeta) = 2\left(\frac{1-\zeta}{1+\zeta} + \frac{1}{3}\frac{(1-\zeta)^3}{(1+\zeta)^3} + \frac{1}{5}\frac{(1-\zeta)^5}{(1+\zeta)^5} + \frac{1}{7}\frac{(1-\zeta)^7}{(1+\zeta)^7} + O(\zeta^9)\right)$$
(A.8)

To calculate the logarithmic mean we use the following subroutine:

1. Set the following: 
$$\zeta = \frac{a_L}{a_R}, \quad f = \frac{\zeta - 1}{\zeta + 1}, \quad u = f * f$$

2. If 
$$(u < \epsilon)$$

$$F = 1.0 + u/3.0 + u * u/5.0 + u * u * u/7.0$$

3. Else

$$F = ln(\zeta)/2.0/(f)$$

thus

$$a^{ln}(L,R) = \frac{a_L + a_R}{2F}, \quad \epsilon = 10^{-2}$$

# APPENDIX B

## ALGORITHM

# B.1 (Flow Chart)

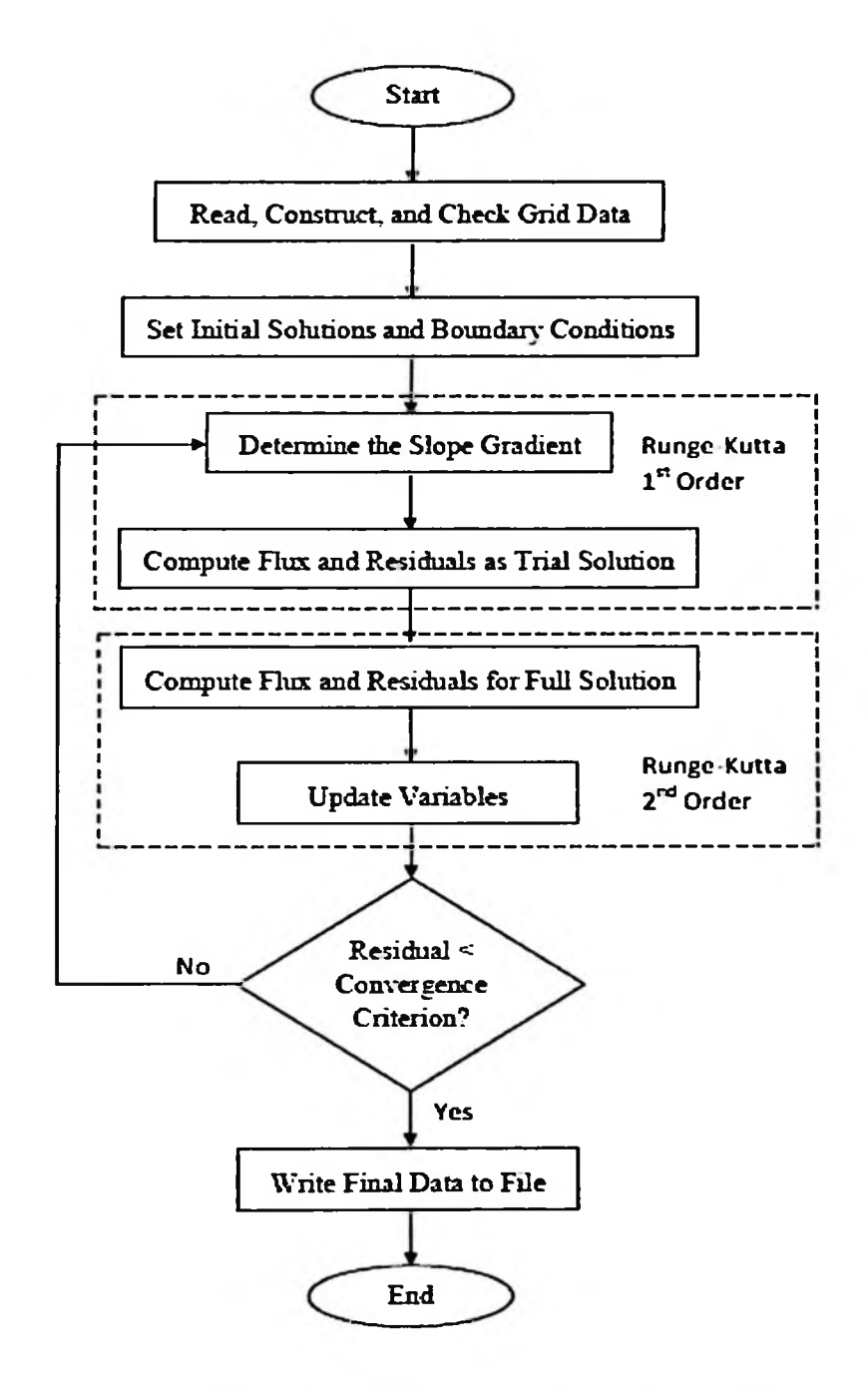


Figure B.1: Flow chart of the solver algorithm.

## BIODATA OF THE STUDENT

The author of this thesis has been a USM student and PhD candidate since April 2010. He is a scholarship holder from the Ministry of Higher Education of Malaysia under the Public Institution of Higher Education (IPTA) Academic Training Scheme (SLAI). He is also a staff contracted to Universiti Tun Hussein Onn Malaysia (UTHM), at the Faculty of Mechanical and Manufacturing Engineering (FKMP).

The author is happily married and is blessed with a son.

### LIST OF PUBLICATIONS

Publications that arise from the study:

Mohammed, A. N. and Ismail, F. 2011. Development of entropy-consistent flux function: Incorporating viscous terms. In 2nd Mechanical and Aerospace Postgraduate Research Colloquium, USM Engineering Campus, Pulau Pinang.

Mohammed, A. N. and Ismail, F. 2011. Entropy-consistent flux function in CFD: Integrating viscous effects. In *International Conference on Mechanical and Manufacturing Engineering 2011*, Putrajaya.

Mohammed, A. N. and Ismail, F. 2013. Study of an entropy-consistent Navier-Stokes flux. In *International Journal of Computational Fluid Dynamics*, Volume 27, Issue 1, January 2013, pages 1-14. (Impact Factor 0.87, Quarter 2/Quarter 3) http://dx.doi.org/10.1080/10618562.2012.752573

Mohammed, A. N. and Ismail, F. 2014. Entropy Consistent Methods for the Navier-Stokes Equations: A first-order systems approach. Under review for *Journal of Scientific Computing* (Impact Factor 1.7, Quarter 1).